nature materials

SUPPLEMENTARY INFORMATION

DOI: 10.1038/NMAT3944

Scalable production of large quantities of defect-free few-layer graphene by shear-exfoliation in liquids

Authors: Keith R Paton[1,2], Eswaraiah Varrla[1,3], Claudia Backes[1,3], Ronan J Smith[1,3], Umar Khan[1,3], Arlene O'Neill[1,3], Conor Boland[1,3], Mustafa Lotya[1,3], Oana M Istrate[1,3], Paul King[1,3], Tom Higgins[1,3], Sebastian Barwich[1,3], Peter May[1,3], Pawel Puczkarski[1,3], Iftikhar Ahmed[3], Matthias Moebius[3], Henrik Pettersson[1,3], Edmund Long[1,3], João Coelho[1,4], Sean E O'Brien[1,3], Eva K McGuire[1,3], Beatriz Mendoza Sanchez[1,4], Georg S Duesberg[1,4], Niall McEvoy[1,4], Timothy J. Pennycook[5], Clive Downing[1], Alison Crossley[6], Valeria Nicolosi[1,3,4] and Jonathan N Coleman[1,3]*

*colemaj@tcd.ie

[1]*Centre for Research on Adaptive Nanostructures and Nanodevices (CRANN), Trinity College Dublin, Dublin 2, Ireland.*

[2]*Thomas Swan & Co. Ltd., Rotary Way, Consett, County Durham, DH8 7ND, United Kingdom.*

[3]*School of Physics, Trinity College Dublin, Dublin 2, Ireland.*

[4]*School of Chemistry, Trinity College Dublin, Dublin 2, Ireland.*

[5]*SuperSTEM, STFC Daresbury Laboratories, Keckwick Lane, Warrington,WA4 4AD United Kingdom.*

[6]*Department of Materials, University of Oxford, Parks Road, OX1 3PH, Oxford, United Kingdom.*

Contents

DOI: 10.1038/NMAT3944

DOI: 10.1038/NMAT3944

S1 Shear exfoliation of graphene and other layered compounds

S1.1 The mixer and mixing procedure

The mixer used was an L5M high shear laboratory mixer, made by Silverson Machines Ltd., UK. It is fitted with a 250 W motor, providing a maximum rotor speed of 8000 rpm (6000 rpm under full load). It is supplied with a standard mixing assembly, which has an overall outer diameter of 50 mm. The assembly comprises a frame, rotor with four blades, screen and base plate, as shown in figure 1A & B (main paper). The rotor sits within a fixed screen known as the stator. For most of the work in the current study a square-hole high shear screen was used, which has a gap between the rotor and the stator of 135 μm, with 96 square holes, each 2 mm × 2 mm (figure S1.1).

During rotation, the shear mixer acts as a pump, pulling both liquid and solids into the mixing head where centrifugal forces drive them towards the edge of the rotor/stator (figure S1.1, right). This is accompanied by intense shear as the materials are driven at high velocity between the rotor and screen and then out through the perforations in the stator and into the main volume of the fluid.

Silverson provide a considerable amount of information on their website including descriptions of mixer operation (http://www.silverson.com/us/lab-mixer-how-it-works.html) and videos showing it in operation (http://www.silverson.com/us/component/videos/).

Figure S1.1: Close up view of the D=32 mm rotor/stator used in this work and (right) a schematic illustrating the operation of the rotor stator. The top arrow indicates the direction of rotation while the other arrows illustrate the direction of liquid (and associated solids) flow.

As well as the standard mixing assembly, experiments were also carried out using tubular assemblies, with overall outer diameter of 19 mm and 16 mm. The 19 mm assembly has a rotor

diameter of 15.6 mm, and is fitted with a square-hole high shear screen (48 holes, 2 mm × 2 mm) with a gap of 100 μm. The 16 mm assembly has a 12.4 mm diameter rotor fitted with a general purpose disintegrating screen (6 circular holes, 6 mm diameter) with a gap of 115 μm. In addition, large scale trials were performed with rotors of diameter 70, 98 and 110 mm (see below).

For mixing, the mixing head is lowered to its lowest position (30 mm from base plate) and positioned approximately half a vessel radius from the centre of the mixing vessel. This asymmetry is to prevent the formation of a vortex during mixing and ensure bulk circulation of the liquid in the vessel. In a typical experiment, the graphite is weighed into the mixing vessel, and then the solvent is added. The mixer head is then lowered into the vessel and positioned, and the speed increased gradually until the desired speed is reached. The mixer is then run at this speed for a predetermined mixing time. The mixing vessel is positioned in a water bath connected to a recirculating chiller set at 15 ^{o}C to prevent heating of the solvent. In a typical mix with a 32 mm rotor running at 4500 rpm in a 500 mL vial of solvent, temperature typically rises by <1 ^{o}C over 60 minutes.

To assess the resultant dispersion, the required volume was removed and centrifuged to remove any unexfoliated graphite (1500 rpm for 150 min, Thermo scientific, Model: Heraeus Megafuge 16 Centrifuge, Rotor: TX-400 Swinging Bucket Rotor (Max:5000 rpm) with auto lock system). The supernatant could then be collected for further study.

S1.2 Processing parameters

When mixing, the user has direct control of 5 main processing parameters:

Mixing time, t: The time for which the chosen rotation rate was applied;

Mixing speed, N: The rotor speed, usually expressed in rpm but converted to s^{-1} for calculations;

Mixing Volume, V: The volume of liquid being mixed. In this work, we varied the volume by varying the liquid height in beakers of a range of capacities from 250 mL to 5 L;

Rotor diameter, D: The diameter of the rotor in the rotor/stator combination. In the labscale work, three rotor/stator combinations were used (D=12, 16 and 32 mm) while a larger rotor/stator combination (D=100 mm) was used in the large scale trial;

DOI: 10.1038/NMAT3944

Graphite concentration: The mass of graphite (or other layered material) to be mixed divided by the volume of liquid being mixed.

A range of other parameters could conceivably be studied, but were kept constant in this work e.g. rotor/stator gap (always close to 0.11 mm), rotor/stator position in tank, presence/number/configuration of baffles (none), pre-treatment of graphite (none used), the graphite type (three types tested) etc.

S1.3 Mixing liquids and stabilisation mechanisms

In this work we have mixed only in liquids that are known to stabilise exfoliated graphene (and other layered compounds). In general, when exfoliated, graphene can be stabilised in three types of liquid (see figure S1.2),[1]:

Suitable organic solvents: When graphene (or other exfoliated layered material) is mixed with solvents with surface energy (or solubility parameter) close to that of graphene itself, the energy of mixing is very low. This results in the stabilisation of the exfoliated nanosheets against reaggregation.[1-9] Solvents used in this study are N-methyl-2-pyrrolidone and N-cyclohexyl-2-pyrrolidone. N-Methyl-2-pyrrolidone (NMP) with an assay of 99.5 % was obtained from VWR. N-cyclohexyl-2-pyrrolidone (CHP) with an assay of 99 % was obtained from Sigma-Aldrich.

Aqueous surfactant solutions: Graphene (or other exfoliated layered materials) can be stabilised by exfoliating in water in the presence of surfactant molecules. In this case, the tail groups adsorb onto the graphitic surface. The head groups interact with the water, becoming largely dissociated (for ionic surfactants). The resulting double layer of bound surfactant ions and mobile counter ions acts as a multipole. As a result nearby surfactant coated nanosheets are repelled by electrostatic effects resulting in stabilisation against aggregation.[10-14] The most commonly used surfactant for nanotube and graphene stabilisation is sodium cholate which was used in this study (Sigma-Aldrich).

Polymer solutions: Graphene (or other exfoliated layered materials) can be stabilised by exfoliating in solvents, in the presence of dissolved polymers. Under the right circumstances, the polymer chains partially adsorb on the nanosheets' surface, such that extended sections protrude into the solvent. This results in inter-flake repulsions due to entropy based steric effects.[15,16] Any solvent-polymer combination can be used to stabilise a given type of nanosheets so long as the

Hildebrand solubility parameters of all three components are reasonably close.[16] In this work, we studied exfoliation in aqueous solutions of polyvinylalcohol (Fluka, M.W. ~72 000).

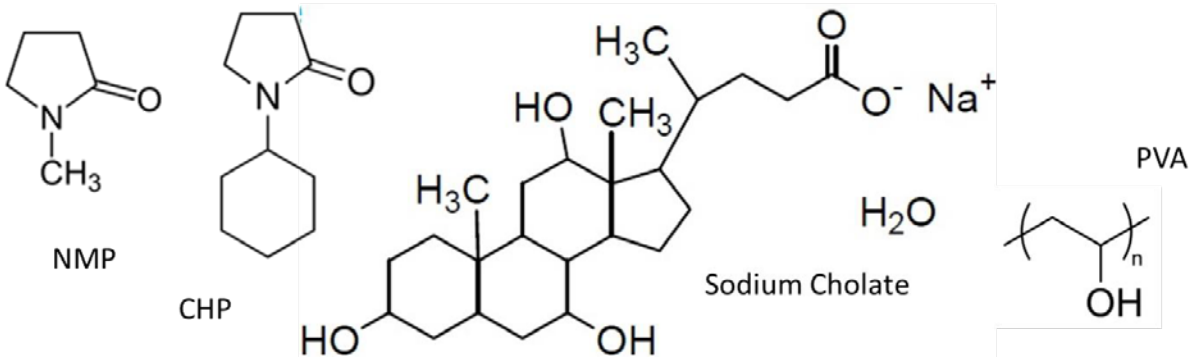

Figure S1.2: Structures of the solvents, surfactant and polymer used in this work.

DOI: 10.1038/NMAT3944

S2 Materials: Graphite powder

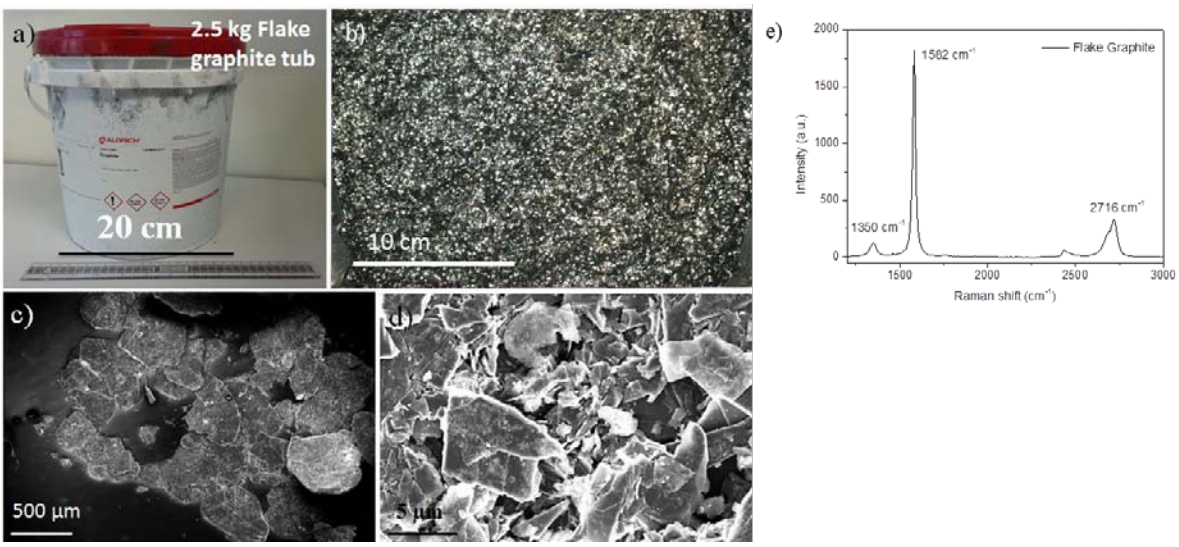

Figure S2.1: Image of A) 2.5 kg graphite flakes tub (Sigma Aldrich) and B) top view of bulk graphite flakes; C) low and D) high magnification FESEM image of graphite flakes; E) raman spectrum of as received graphite flakes.

Graphite flakes were purchased from Sigma-Aldrich (Product number 332461) and used without any further treatments (Figures S2.1 A & B). This graphite particle size is quoted as +100 mesh, i.e. >150 µm particles (min ≥ 75 %). The assay of graphite flakes are ~90 % as per the supplier and confirmed by us. Typical micrographs of graphite flakes in platelet structures can be seen in figures S2.1 C & D. As seen in figure S2.1-D, the purchased material also contains small graphite flakes with typical dimensions of approximately 1-10 μm. Raman spectroscopy showed features at: 1350 cm^{-1} (D-band) which corresponds to the breathing mode of sp^2 carbon atoms, and is absent without the presence of defects (including graphite edges); 1582 cm^{-1} (G-band), associated with the doubly degenerate (iTO and LO) phonon mode at the Brillouin zone centre, which are associated with in-phase vibrations of the graphite lattice; and the relatively wide 2D band at 2716 cm^{-1}, an overtone of the D-band.

We also used graphite powder purchased from FutureCarbon Gmbh (type SGN18). This graphite differs from the Sigma Aldrich graphite in two respects: It has a very low quantity of non-carbon impurities (99.99% C) and the flake size is much smaller, typically <20 µm. finally, we

performed some experiments (Raman) on graphite from Qindao Henglide Graphite Co Ltd (natural flake graphite, 96% carbon, +32 mesh).

A Carl Zeiss Ultra Scanning Electron Microscope was used for secondary electron imaging and elemental analysis has been recorded by Oxford Instruments INCA system with Peltier cooled Si (Li) detector using the same instrument. For imaging, SEM was operated 2-5 kV.

DOI: 10.1038/NMAT3944

S3 Initial characterisation of shear exfoliated graphene

	Processing parameters					Length (NMP, TEM)	Thick-ness (NMP, Raman)	Raman (NMP)	XPS (NMP)	
Code	t (min)	C_i (g/L)	N (rpm)	D (mm)	V (mL)	<L> (nm)	<N>	I_D/I_G	Graphene Fraction	PR scale factor
C_i low	20	1	4500	32	1500	604	-	-	-	0.0022
D low	20	50	4500	12	600	498	-	-	-	0.013
N low	20	80	1500	32	1500	304	5.3	0.27	0.71	0.041
t high	75	50	4500	32	1500	348	4.5	0.36	0.73	0.065
V low	20	50	4500	32	600	333	4.6	0.35	0.75	0.076
D high	20	50	4500	32	2000	400	-	0.26	0.75	0.13
V high	20	50	4500	32	2750	635	5.2	0.30	0.73	0.150
t low	10	50	4500	32	1500	404	4.3	0.25	0.67	0.154
Ci high	20	100	4500	32	1500	301	4.4	0.37	0.71	0.231
N high	20	80	5700	32	1500	382	7.2	0.17	0.763	0.254

Table S3.1: Processing parameters for the samples used in the initial survey. In addition, this table includes some of the flake characterisation data for NMP-exfoliated graphene. Characterisation is described below. Flake length was measured by TEM, while flake thickness was estimated from the Raman 2D band. The Raman data refers to the D:G ratio, a measure of defect content (e.g. edge defects) while the XPS data refers to the fraction of the C1s peak attributed to graphitic carbon. The final column gives the production rate scale factor ($C_i t^{-0.34} N^{1.13} D^{2.28} V^{0.32}$). The overall production scales linearly with this parameter (figure 2H, main paper). NB measurement of thickness by Raman is described in section S3.7.

In order to assess the dependence of flake quality on mixing parameters, we produced a set of dispersions using a range of mixing parameters (table S3.1). This study is described below as the "initial survey". Two sets of mixtures were prepared using the solvent N-methyl-2-pyrrolidone (NMP) and aqueous solutions of the surfactant sodium cholate (NaC). Both NMP and NaC are known to be extremely effective for the exfoliation and stabilisation of graphene.[7,9,12,14]

The NMP dispersions were then characterised using TEM, Raman spectroscopy and XPS to assess the flake length, the defect content and the degree of oxidation (if any). The NaC dispersions were characterised by AFM and Raman spectroscopy to assess the flake thickness, and the defect content. NMP dispersions are unsuitable for AFM characterisation because of difficulties avoiding aggregation during deposition. Surfactant exfoliated flakes are not ideal for XPS characterisation because residual surfactant gives the appearance of oxides.

To explore as much of the available parameter space as possible, in most cases we used a central set of mixing parameters and for each different dispersion, changed one parameter, either to a relatively high value or a relatively low one. The parameters used are shown in table S3.1. Also shown for the NMP exfoliated samples is a summary of the numerical values for lateral flake size, <L>, flakes thickness, <N>, (mean number of monolayers per nanosheet), intensity ratio of D:G Raman bands, I_D/I_G, and the fraction of the C1s contribution to the XPS spectrum due to graphitic carbon. The measurement of these parameters will be described below. The final column shows the numerical value of the production rate scale factor ($C_i t^{0.34} N^{1.13} D^{2.28} V^{0.32}$). The data have been arranged in order of increasing PR scale factor. This is equivalent to ordering the data with increasing production rate.

S3.1 Electron microscopy of mixer-exfoliated graphene

The NMP dispersions prepared during the initial mixing study were analysed using TEM. All TEM samples were drop-casted onto Agar Scientific finder holey carbon grids and allowed to dry at 60 ^{o}C for 72 h under vacuum. Bright field and energy filtered TEM micrographs were taken at random locations across the grids, to ensure a non-biased representation of the level of exfoliation.

TEM analysis was carried out at two levels of detail.

DOI: 10.1038/NMAT3944

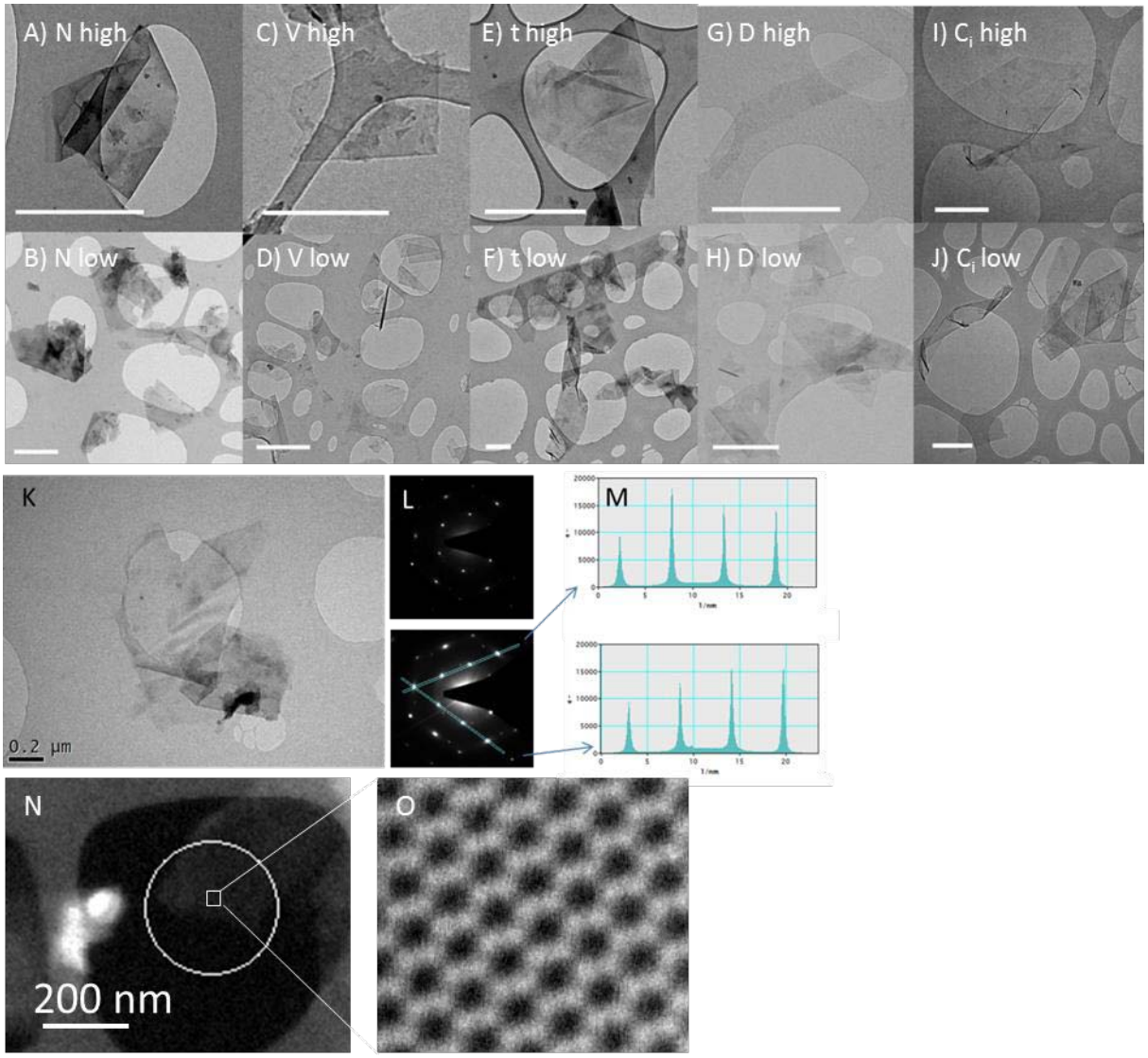

Figure S3.1: A selection of TEM images (collected from samples prepared with a range of processing parameters) of representative graphene flakes. In all cases, the scalebar is 500 nm. Processing parameters are given in table S3.1. K-M) Evidence for monolayer production. Some of the flakes observed in the survey are clearly monolayers. The flakes observed in K had a diffraction pattern (L) which had more intense inner spots (M). This is a clear fingerprint of a graphene monolayer.[7] N) A STEM image of a graphene monolayer. O) Zoomed image showing atomic positions (this image is the same as that in main paper, figure 1H).

Low resolution TEM:

The samples listed in table S3.1 (and a range of other dispersions with controllably varied mixing parameters) were characterised using low resolution TEM. The aim of this was twofold: to assess the nature and quality of the exfoliated flakes; and in some cases (see below and main paper) to measure the lateral flake dimensions. Samples were prepared by drop-casting and imaging the grids in a LaB_6 Jeol 2100 operated at 200 kV in bright field TEM mode.

High resolution scanning TEM:

Some samples were characterised at the SuperSTEM facility in Daresbury, UK using an aberration-corrected Nion Ultrastem100 operated at 60 kV. The aim of this study was to investigate the atomic structure of the mixer-exfoliated graphene.

A selection of TEM images of flakes observed in the low resolution TEM study are shown in figure S3.1 In general, thin multilayers are most commonly observed. Interestingly, ~50 % of these are folded. Also shown is a HR STEM image.

S3.2 Flake length measurements (TEM)

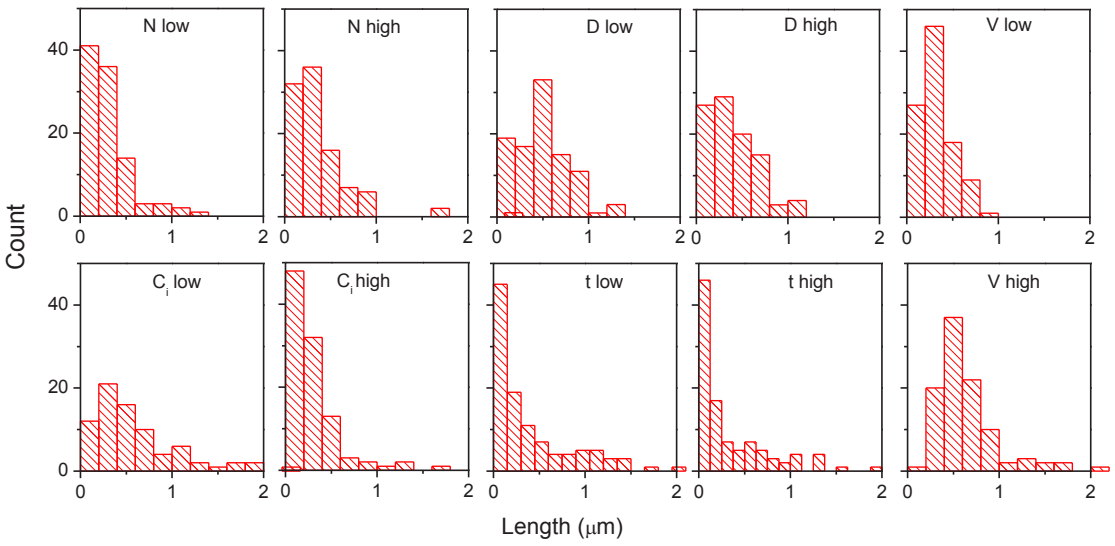

Figure S3.2: Flake length histograms for NMP exfoliated graphene. Processing parameters are given in table S3.1.

DOI: 10.1038/NMAT3944

The TEM measurements made on the samples prepared for the initial survey were used to measure the mean flake length (i.e. the longest dimension). This data is given in table S3.1. Histograms and mean values are shown in figures S3.2-3.

We note that there is no apparent trend to the data in figure S3.3. However, below (section S8) we will explore the dependence of length on processing parameters in more detail.

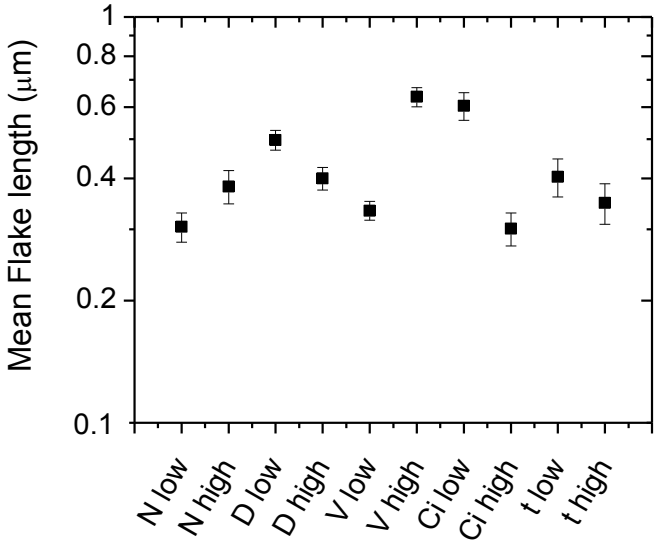

Figure S3.3: Mean flake length for samples measured in the initial survey of NMP exfoliated graphene. The dependence of length of processing parameters is explored in more detail in figure S8.1. Processing parameters are given in table S3.1.

S3.3 Flake thickness measurements (AFM)

In order to demonstrate the efficacy of shear exfoliation, it is critical to show that the exfoliated graphene flakes are relatively thin. To do this, we determined the number of monolayers per flake, N_G, by atomic force microscopy. However, nanosheet height measurement by AFM requires the ability to deposit nanosheets from dispersion, onto substrates without aggregation occurring. This is challenging when depositing from solvents such as NMP because, due to their high boiling point, evaporation is slow, allowing reaggregation to occur. As a result, we have chosen to measure nanosheet thickness on surfactant-exfoliated nanosheets as these can be readily deposited with minimal reaggregation.

To minimise reaggregation during deposition, a 10 μL drop of the dispersion was drop-casted on preheated (150 ºC) Si/SiO_2 wafers (0.5×0.5 cm, 300 nm oxide). We found heating of the wafers to a temperature greater than the boiling point of the solvent to give the most homogenous coverage of nanosheets, as the solvent quickly evaporates. Furthermore, if possible, the surfactant-exfoliated graphene dispersions were diluted with distilled water (rather than surfactant) to optical densities of ~0.05 (at 600 nm). This dilution is beneficial in two ways. Firstly, it reduces the concentration of free surfactant, which is important as this is hard to remove completely from the wafer by washing. Secondly, the resultant coverage of nanosheets on the wafer tends to be dense, but yet not dense enough to lead to pronounced aggregation. After deposition, the wafers were rinsed with 5 mL of distilled water and isopropanol prior to the AFM measurements. For flake thickness measurements, only flakes were considered that were clearly not re-aggregated as assessed from phase contrast images which were recorded in parallel.

However, height analysis of surfactant-exfoliated graphene is nonetheless not without challenges. The conversion of measured AFM height (histogram figure S3.4) to number of layers can be difficult in surfactant-exfoliated samples, as the surfactant is not completely removed from the nanomaterial, thus potentially contributing to its height. In addition, the apparent AFM height in tapping mode strongly depends on the scanning parameters. For our AFM imaging, we have chosen very robust scanning parameters involving high setpoints, i.e. a low interaction between tip and substrate. These parameters were chosen to maximise throughput, an important consideration in a study such as this which measures the height of 1700 nanosheets. However, such parameters do not necessarily give the accurate height, rather an apparent height that is proportional to the real height.[17] To resolve this, we utilised the fact that incompletely exfoliated nanosheets often display terraces separated by steps which are associated with flake edges (as clearly discernible in case of the flake depicted in figure S3.4 inset). We analysed the AFM height on a large number of steps over many flakes and plotted the step height in ascending order (figure S3.4) revealing that the step height is always a multiple of 0.95 nm.

The thinnest flakes we have observed have an AFM height of close to 2 nm (approximately 7 % of all nanosheets), which would be consistent with a monolayer height of 0.95 nm plus approximately 1 nm surfactant coating at the bottom of the flakes also contributing to the overall

DOI: 10.1038/NMAT3944

AFM height measured. To definitively conclude that the 2 nm nanosheets are indeed monolayered graphene, we relocated the same sample area previously analysed by AFM in a Raman microscope (figure S3.5 A and B). An example of such a graphene nanosheet and its AFM height profile is depicted in figure (S3.5 C and D). The corresponding Raman spectrum (figure S3.5 E and F) is clearly consistent with monolayered graphene displaying a sharp and symmetrical 2D band that can be fitted to one Lorentzian (with a full width at half maximum of 42 cm^{-1}) and a 2D/G band ratio of 1.6. This provides unequivocal spectroscopic evidence that our surfactant graphene nanosheets with an AFM height of around 2 nm are indeed monolayered graphene. With knowledge of the monolayer height and the step heights, the measured height can be converted to the actual number of monolayers per flake as presented in the main manuscript and below. Examples of flakes counted in this way are shown in figure S3.6.

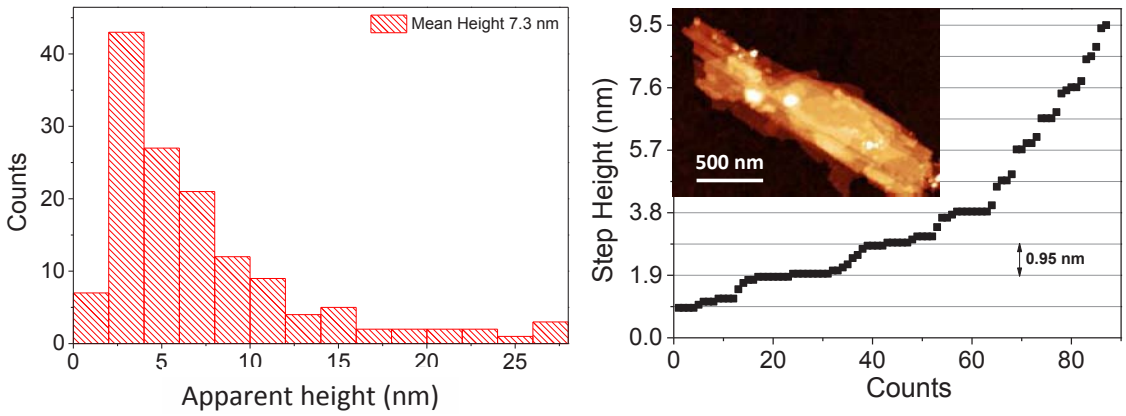

Figure S3.4: (Left) AFM height histogram after deposition of surfactant-exfoliated graphene Si/SiO_2 wafers. NB these heights do not reflect the real thickness of the nanosheets as described in the text.) (Right) Analysis of AFM step heights on deposited graphene nanosheets with clearly distinguishable layers as the one displayed as inset. The step height is found to be a multiple 0.95 nm with strongly suggesting that one layer of surfactant-exfoliated graphene contributes 0.95 nm to the overall height.

Experimental details for AFM

Atomic force microscopy (AFM) was carried out on a Veeco Nanoscope-IIIa (Digital Instruments) system equipped with a E-head (13 μm scanner) in tapping mode after depositing a drop of the dispersion (10 μL) on a pre-heated (150 °C) Si/SiO_2 wafer with an oxide layer of 300 nm. Typical image sizes were 2.5-5 μm at scan rates of 0.4-0.6 Hz. The setpoint was chosen as high as possible.

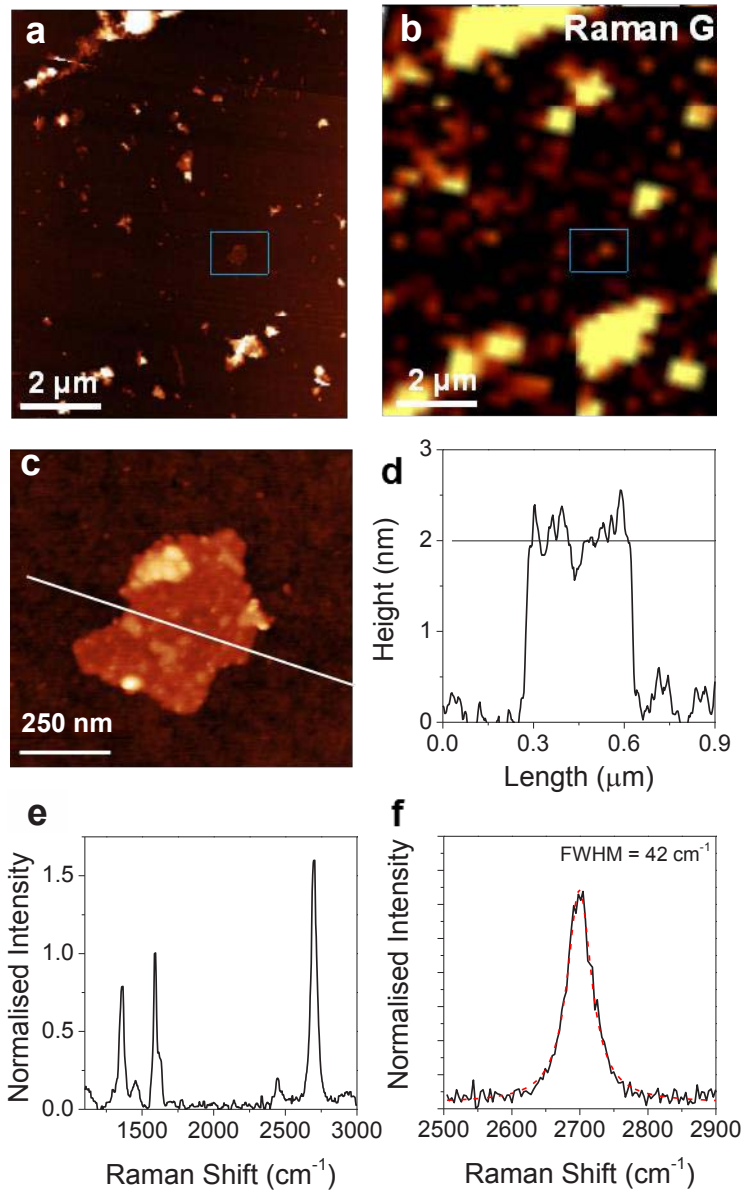

Figure S3.5: A) AFM overview image of surfactant-exfoliated graphene on Si/SiO_2, B) corresponding Raman map plotting the G-band intensity (532 nm excitation), C) AFM image of

DOI: 10.1038/NMAT3944

a suspected monolayer graphene sheet and D) corresponding height histogram displaying a height of close to 2 nm, E and F) Raman spectrum (532 nm excitation) of the flake in C evidencing its monolayered nature.

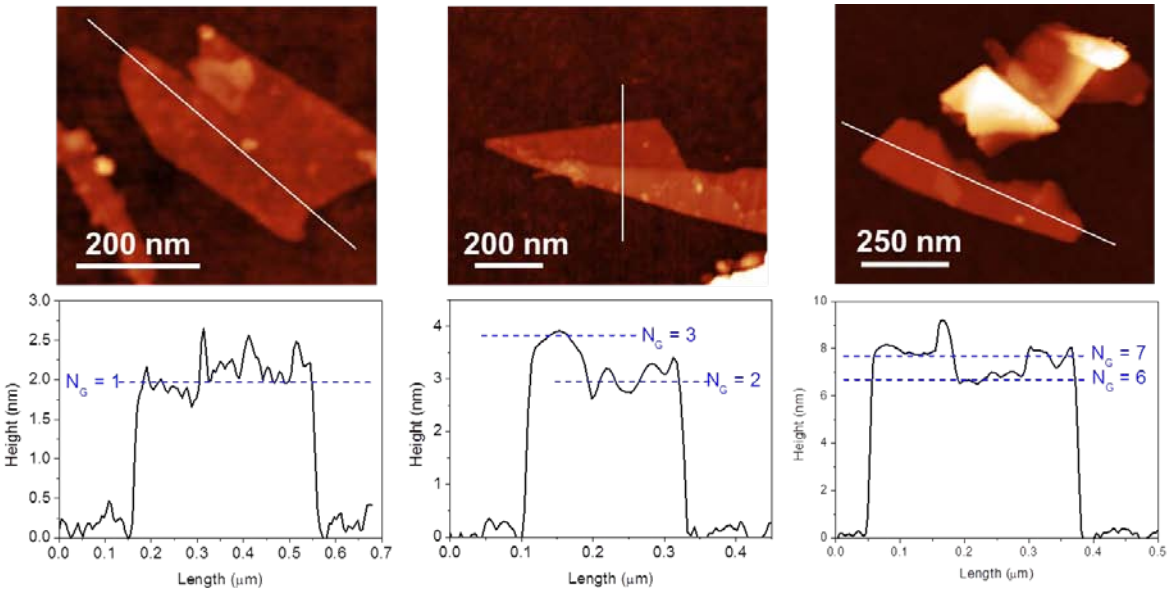

Figure S3.6: AFM images and corresponding height profiles of (left to right): monolayer, bi/trilayer and few layer graphene.

The analysis described above allows us to extract the real number of layers per flakes from the apparent nanosheet height. We have performed this analysis for the surfactant-exfoliated samples produced in the initial survey as shown in figure S3.7 (production parameters given in table S3.1). In all cases the vast majority of nanosheets had <10 monolayers. The mean number of monolayers per flakes is given in figure S3.8 (left) for each set of processing parameters. With the exception of the N low sample, all samples had mean N_G between 7 and 8. Interestingly the N low flakes were slightly thicker, suggesting poorer exfoliation at lower rotor speed. We note that in all cases ~30% of flakes had 1, 2 or 3 layers (figure S3.8 (right)).

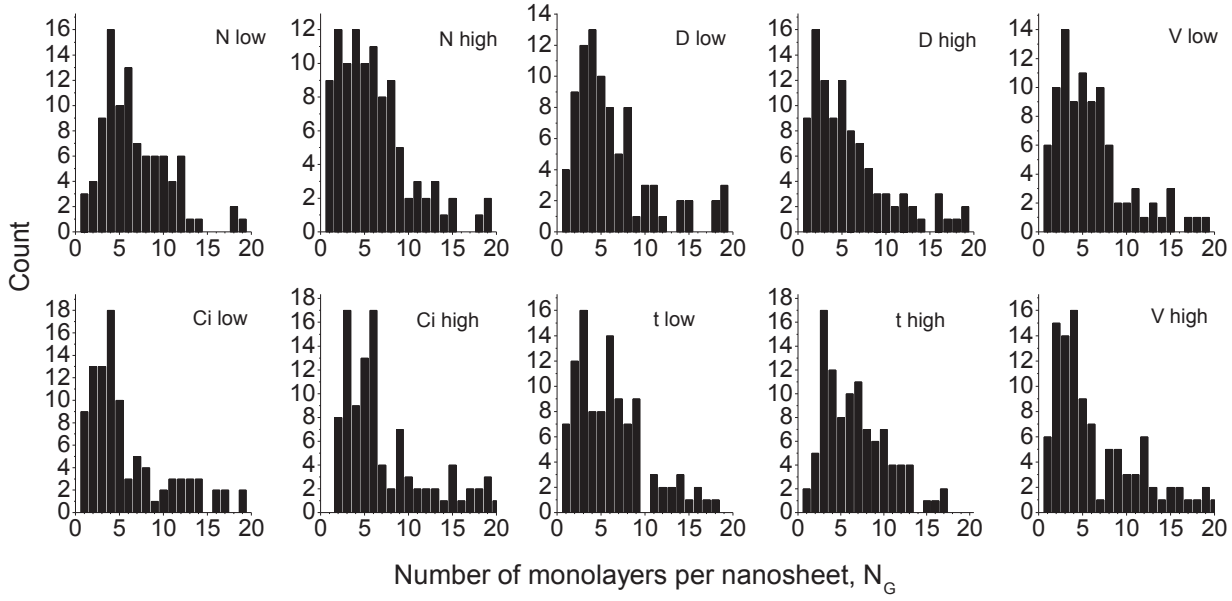

Figure S3.7: Flake length histograms for surfactant-exfoliated graphene. Processing parameters are given in table S3.1. In all cases 100-110 flakes were counted.

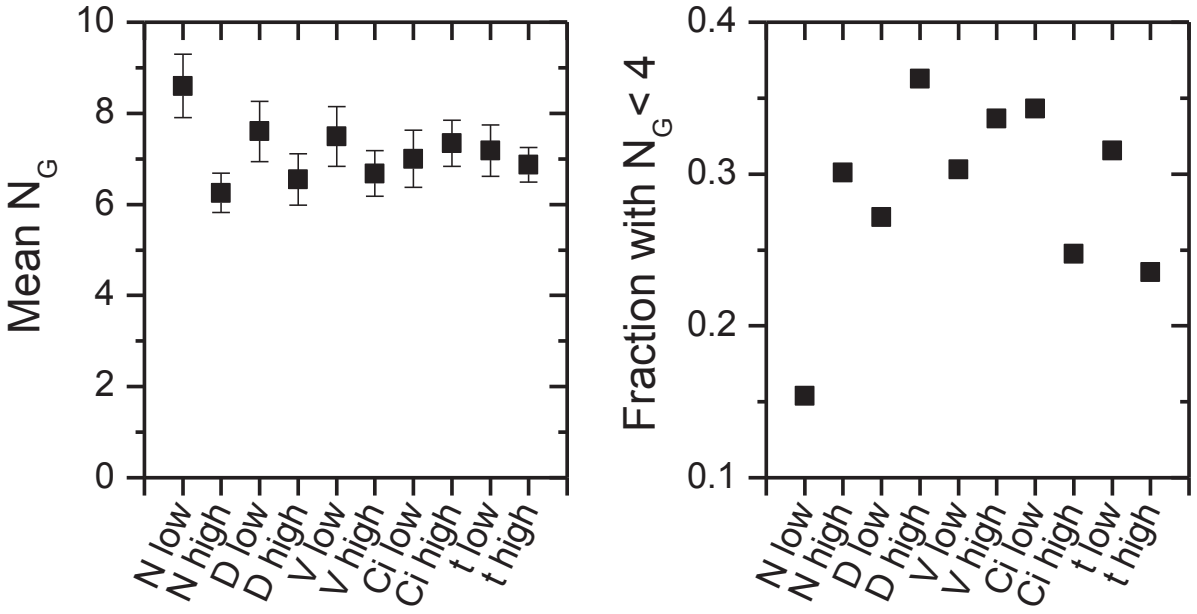

Figure S3.8: (Left) Mean flake thickness (number of monolayers) for samples measured in the initial survey of surfactant-exfoliated graphene. (Right) Fraction of nanosheets with 1-3 monolayers. Processing parameters are given in table S3.1.

DOI: 10.1038/NMAT3944

S3.4 Vacuum filtration of thin films

Dispersions of graphene exfoliated in both NMP and NaC, using the parameters listed in table S3.1, were used to prepare thin films for further characterisation. Thin films were prepared by vacuum filtration of dispersions onto unsupported alumina membranes resting on fritted glass holders. The alumina membranes had pore size 0.2 μm and each film was subsequently rinsed with isopropanol. The films were dried at 60 °C under vacuum over a weekend. Optical microscopy and SEM was carried out on a set of 8 films. The films were found to be of high quality with good uniformity. SEM showed that the films were composed of a disordered network of flakes having similar structure to those imaged in the TEM. A set of typical optical and SEM micrographs is shown in Figure S3.9. Raman analysis showed the films to be highly homogenous spectroscopically (see section S3.6.2, figure S3.14).

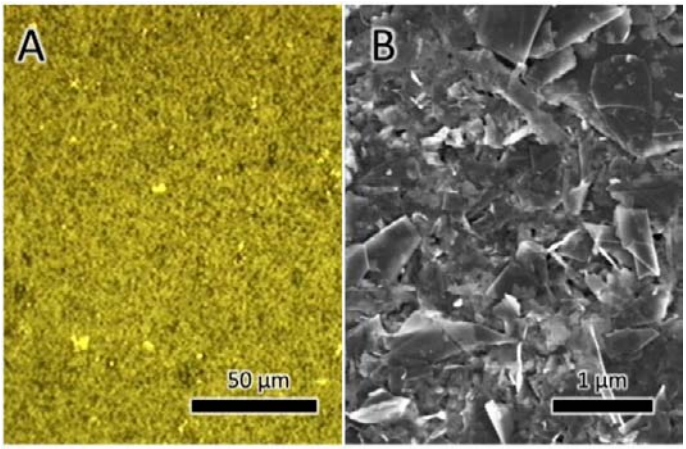

Figure S3.9: A) Optical micrograph of a thin film (V low) of graphene flakes deposited on a porous alumina membrane by vacuum filtration. B) SEM micrograph of the same film shown in A. N=4500 rpm, V=1900 mL, Ci=50 g/L, D=32 mm, t=20 min.

S3.5 Raman spectroscopy on both NMP- and surfactant-exfoliated graphene

Raman characterisation was performed on films prepared from both NMP-and NaC-exfoliated graphene. Raman spectra of the thin films on alumina membranes were acquired using a Horiba Scientific LabRAM-HR Raman microscope. A 532.15 nm excitation laser and a 1800 g/mm grating were used. Spectra were recorded with a 100× lens. For each film, typically 10 spectra were recorded and averaged. Alternatively, The Raman spectra for samples prepared using a

range of mixing parameters are shown in figure S3.10 (NMP-exfoliated) and figure S3.11 (NaC exfoliated). All spectra showed characteristics expected of graphene. In particular they all showed 2D band characteristics typical of few layer graphene.[18,19] In addition, a small D-band was observed in each case with mean D:G band ratios in the range 0.17-0.37 (see table S3.1). As we shall show below, this D band is associated with edge defects.[7,9]

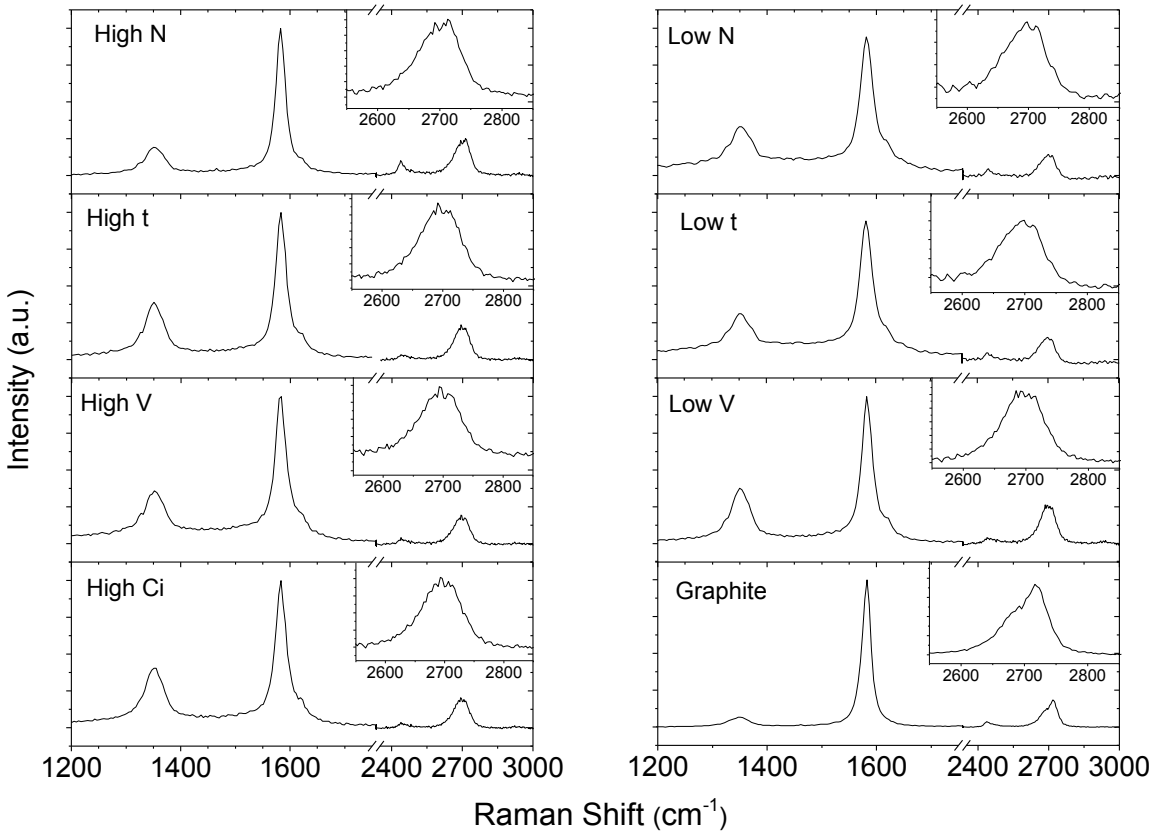

Figure S3.10: Raman spectra for NMP-exfoliated graphene. Normalised and numerically averaged Raman spectra for all graphene thin films tested. The recorded spectra were normalised to the intensity of the G-band and averaged over 10 measurements. Processing parameters are given in table S3.1. The magnified 2D bands are shown as insets.

DOI: 10.1038/NMAT3944

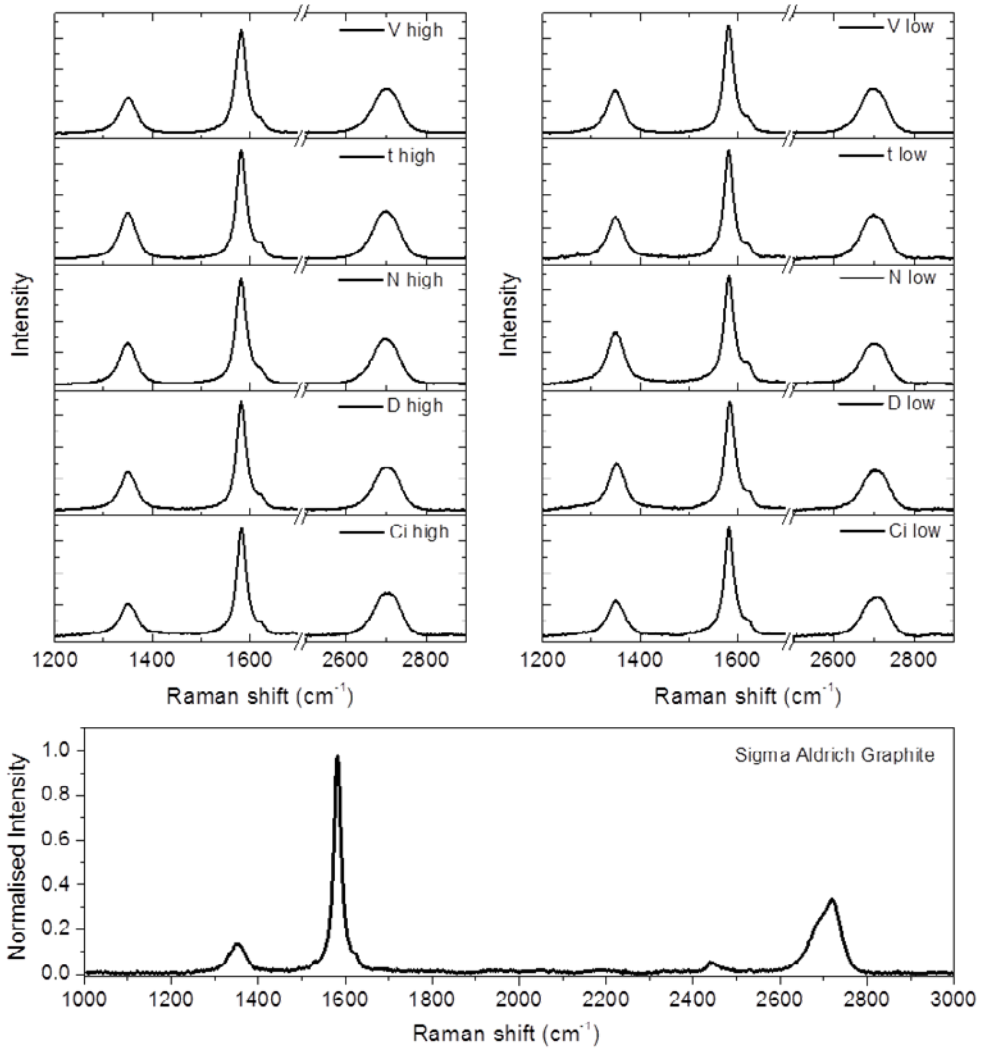

Figure S3.11: Raman spectra for surfactant (NaC)-exfoliated graphene. Normalised and numerically averaged Raman spectra for all graphene thin films tested. The recorded spectra were normalised to the intensity of the G-band and averaged over 10 measurements. Processing parameters are given in table S3.1. The spectrum of the graphite used to prepare these samples is given at the bottom.

S3.6 Size selection and Raman analysis to assess defect type

The data in figure 3.10 and 11 clearly shows the presence of so-called D-bands at ~1350 cm^{-1}. These are associated with the presence of defects in graphene.[18] However, this does not automatically mean the shear-exfoliated nanosheets to contain basal plane defects. By their

very nature, nanosheets contain edges which act as defects. To verify the quality of shear-exfoliated graphene is it critical to identify whether the observed D-bands are due to basal plane defects or nanosheet edges.

It is known that if the only defects present are edge defects, then the D:G band intensity ratio is approximately related to mean lateral flake size, $\langle L \rangle$, by[9,20]

$$I_D / I_G \approx (I_D / I_G)_{powder} + k / \langle L \rangle \qquad [3.2]$$

where $(I_D / I_G)_{powder}$ is the D:G band ratio associated with the starting power and k has been estimated to be ~0.17.[21] To test for this, it is necessary to perform Raman analysis on a set of samples with a range of known nanosheet sizes. To achieve this we perform size selection on a dispersion of shear-exfoliated graphene. We note that a linear relationship between I_D/I_G and $1/\langle L \rangle$ for the graphene samples is not enough to demonstrate the defects to be edge type. The intercept of this straight line must coincide with the measured value of $(I_D / I_G)_{powder}$ (we assume the crystallites in the powder are so large that 1/L~0). This coincidence means that any defects not due to edges represent basal-plane defects which pre-existed in the graphite powder and not new basal-plane defects.

S3.6.1 Size selection procedure

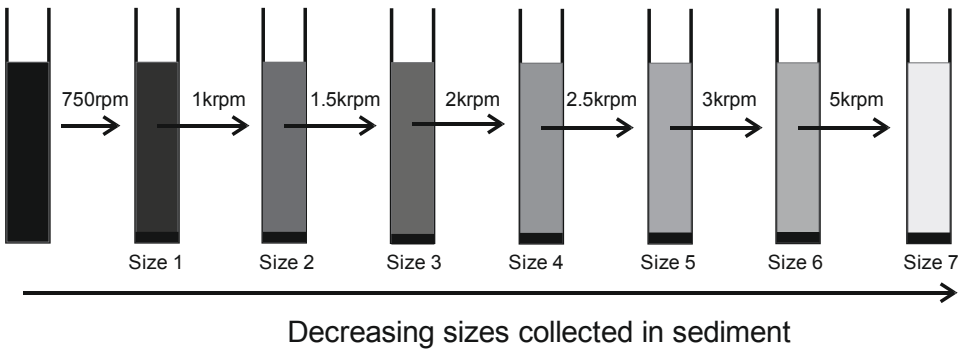

Figure S3.12: Schematic representation of the controlled centrifugation protocol applied to select a broad variation of sizes from a raw dispersion.

DOI: 10.1038/NMAT3944

We achieve size sorting of a shear-exfoliated graphene dispersion in NMP (Sigma graphite, C_i=100g/L, V=500mL, t=60min, D=32mm, N=5000rpm) by a scalable controlled centrifugation procedure. The protocol involves centrifuging the dispersion in consecutive steps each with increased centrifugation speed and is similar to a previously reported method.[21] After each step, the sediment is collected and redispersed (by shaking by hand) in fresh solvent, while the supernatant is subjected to the next centrifugation speed at higher rpm (figure S3.12). This protocol bears a number of advantages over already established techniques: i) basically no material is lost, as both sediment and supernatant is collected, ii) due to redispersing the sediment, the concentration can be adjusted and controlled by the volume of fresh solvent added and iii) it is universal and can be applied to any solvent, surfactant, or polymer system.

The detailed centrifugation conditions are summarised in figure S3.12. Each centrifugation was performed in 10 mL volume per vial (55 mm height) for 100 min in a Hettich Mikro 22R centrifuge equipped with a fixed angle rotor 1016. Prior to the sorting protocol, unexfoliated material was removed by centrifuging for 45 min at 500 rpm.

To confirm the size-selection, statistical length analysis by TEM was performed. We found the aspect ratio to be constant over the number of sizes with a mean of L/w=2.6. The length distribution histograms are shown in figure S3.13 (centrifugation rate is indicated in figure).

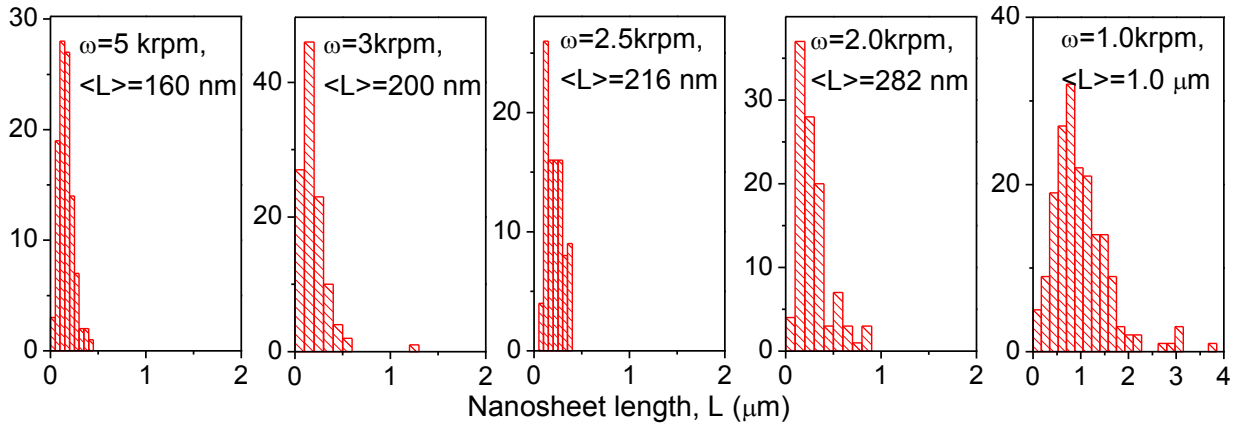

Figure S3.13: TEM length histograms of the size-selected samples. Mean length and centrifugation speed are indicated in figure.

S3.6.2 Raman spectroscopy on size-selected graphene

As described above, graphene nanosheets that are free of basal plane defects should have a D:G band intensity that is related to nanosheet length by equation 3.2. To test whether this is the case for the size selected, shear-exfoliated graphene dispersions, the samples were filtered to form thin films (20 nm pore size alumina membranes) and subjected to Raman spectroscopy. We found the films to be very homogenous with only little variations in the spectra acquired at different laser spot positions (figure S3.14 left). As such, we averaged the Raman spectra over ten individual laser spot positions to give an average spectrum for each size-selected sample (figure S3.14 right). These spectra clearly show the expected increase in I_D/I_G ratios with increasing the centrifugation speed and thus decreasing flake size.

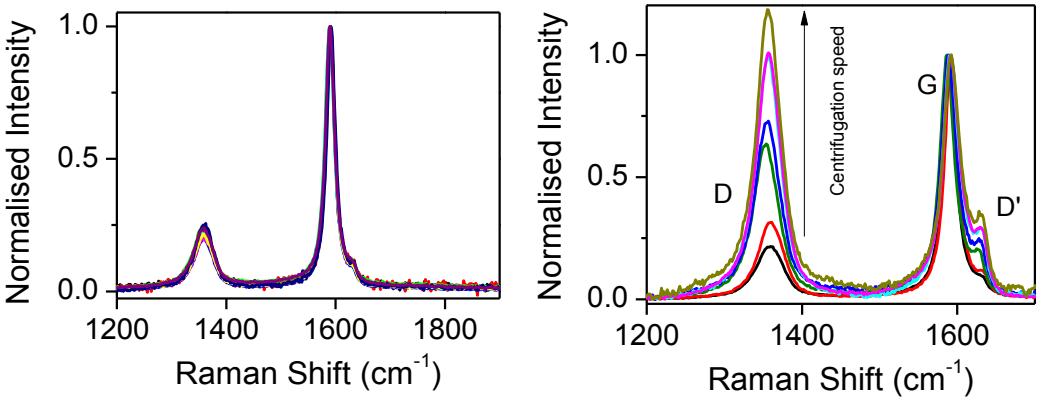

Figure S3.14: (Left) individual Raman spectra (532 nm excitation) at 10 different positions of a film produced from a large nanosheet sample (sediment from 1.5 krpm) demonstrating the homogeneity of the film. (Right) Averaged Raman spectra for the size-selected samples showing the expected increase in the I_D/I_G ratios as the flakes get smaller.

In figure S3.15, we plot the mean I_D/I_G ratio as a function of the mean inverse nanosheet length (measured by TEM) finding very good agreement with equation 3.2, strongly suggesting that no defects are introduced during the exfoliation. The slope of this graph is k=0.17, similar to previously reported values of 0.17 [ref [21]] and 0.26 [ref [20]]. We note that this relationship can be used as a way to estimate graphene nanosheet size from a Raman spectrum:

DOI: 10.1038/NMAT3944

$$L = \frac{0.17}{I_D / I_G - 0.14} \qquad [3.3]$$

However, care must be taken as the 0.14 parameter is essentially set by the D/G ratio of the graphite powder (Aldrich, I_D/I_G=0.14, fig S3.10). Different graphite starting powders will have different values of this parameter which must be determined before eq 3.3 can be used. In addition, while one might expect the k parameter to be independent of graphite type, one cannot assume this be the case (see below).

It is also worth noting the graphite source used here is clearly not perfectly crystalline despite the large crystallite size. We measured a value of I_D/I_G=0.14 for the graphite (fig S3.15). Since the graphite has relatively large grain size, these defects could not come from edges, indicating that some basal plane defects are present in the starting powder.

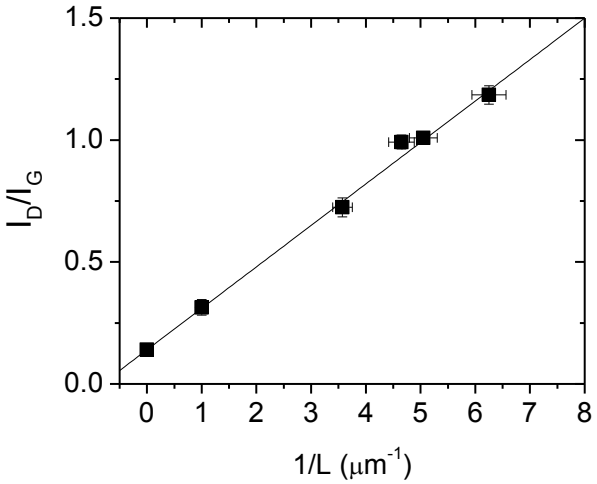

Figure S3.15: Relation of the I_D/I_G ratio as a function of flake size expressed as 1/L. The linear relation strongly suggests that no defects are introduced by the exfoliation procedure.

S3.6.3 Further analysis to confirm defects as edge-type

To further provide evidence that no defects are introduced to the basal plane by the shear-exfoliation method, we use an observation reported recently by Eckmann *et al.*[22] They showed that the nature of defects in graphene can be probed by the ratio of intensities of the D and D' bands (the D' band is a defect related band around 1620 cm^{-1}, that appears as a shoulder on the right side of the G band). The $I_D/I_{D'}$ ratio depends on the nature of defects, with boundary (or

edge) defects being characterised by $I_D/I_{D'}$~3.5, whereas vacancy basal plane point defects giving rise to $I_D/I_{D'}$~7 and sp^3 defects to $I_D/I_{D'}$~13. We note that the data in this paper is somewhat scattered and errors are not given so the ratios given here are approximate.

In figure S3.16A we plot I_D/I_G *versus* $I_{D'}/I_G$ for the size-selected graphene samples prepared from the Aldrich graphite (figure 3.14, right). For completeness, we also include data extracted from the Raman spectra measured during the initial mixing study (fig S3.10). Superimposed on this plot are lines representing the behaviour expected for edge, vacancy and sp^3 defects. The data shows linear behaviour, consistent with $I_D/I_{D'}$~4.6. This is intermediate between that expected for edge and vacancy type defects. However, this is to be expected because the Aldrich graphite contains basal plane defects (I_D/I_G=0.14), even before exfoliation. Measuring $I_D/I_{D'}$ for the graphite powder by fitting gives a value in the range 7.2-8.9, consistent with vacancy defects. Thus, the data in figure 3.16A is consistent with contributions from both vacancy defects (already present in starting graphite) and edge defects. This data is certainly consistent with the hypothesis that no basal plane defects are introduced during shear mixing.

However, because of the importance of this point, we have performed further experiments to remove any doubt that the shear mixing process does not introduce basal plane defects. To do this, we identified a type of graphite powder (Qindao Henglide Graphite Co Ltd, natural flake graphite, +32 mesh) which has a very low population of basal plane defects. This is evidenced by the Raman spectrum in figure S3.16B which shows no observable D or D' band. We exfoliated this graphite by shear mixing in NMP and then performed size selection exactly as described above for the Aldrich graphite. We then measured L by TEM before filtering films and analysing with Raman.

Raman spectra for a range of sizes are shown in figure S3.16C. As expected, the I_D/I_G ratio increases with increasing centrifugation speed (i.e. decreasing nanosheet size), consistent with the D band being associated with edge defects. To confirm this, we plot the D:G band intensity ratios for this Qindao graphene *versus* the inverse nanosheet length as measured by TEM in figure S3.16D. We find a straight line consistent with equation 3.2. *This strongly implies the defects contributing to the D band to be edge type defects only*. Fitting gives

DOI: 10.1038/NMAT3944

$(I_D / I_G)_{powder} \approx 0$ and k=0.12. This k-value is lower than that found above suggesting this parameter to depend on the graphite source.

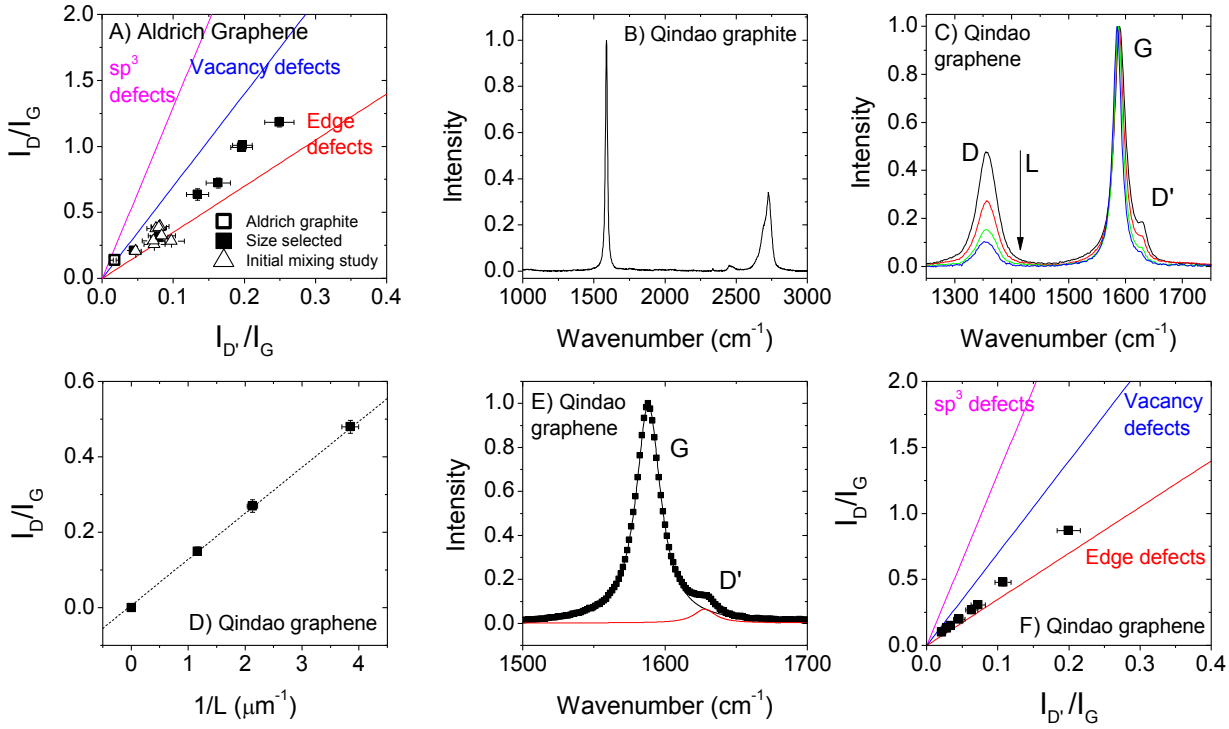

Figure S3.16: A) D:G intensity ratio plotted *versus* D'/G intensity ratio for size-selected graphene prepared from the Aldrich graphite. In addition, we have also included data from the initial mixing study (figure S3.10). Also included is a data point for the Aldrich graphite ($I_D/I_{D'}$=7-8).The lines represent the expected behaviour for the three defect types. B) Raman spectrum for Qindao graphite. C) Raman spectra for size-selected graphene produced from Qindao graphite. D) D:G intensity ratio for size-selected graphene produced from Qindao graphite plotted versus inverse flake length measured by TEM. E) Example of Lorentzian fitting of G and D' band regions for Qindao graphene. F) D:G intensity ratio plotted *versus* D'/G intensity ratio for size-selected graphene prepared from the Qindao graphite.

Critically, we need to determine the D/D' band intensity ratio for graphene produced from this defect-free graphite supply. Because the graphite contained no defects, the nature of the defects in the graphene will determine whether or not shear mixing introduced basal plane defects. We find the D'/G ratio by fitting the G band region to two Lorentzians as shown in

figure S3.16E. In figure S3.16F, we plot I_D/I_G *versus* $I_{D'}/I_G$ for the size-selected graphene samples produced from the Qindao graphite. We find good linearity, consistent with $I_D/I_{D'}$~4.2. This is relatively close to the value of 3.5 quoted by Eckmann *et al*. Given that value is the mean of a data set with some degree of scatter, we feel that $I_D/I_{D'}$~4.2 is indeed consistent with edge defects.

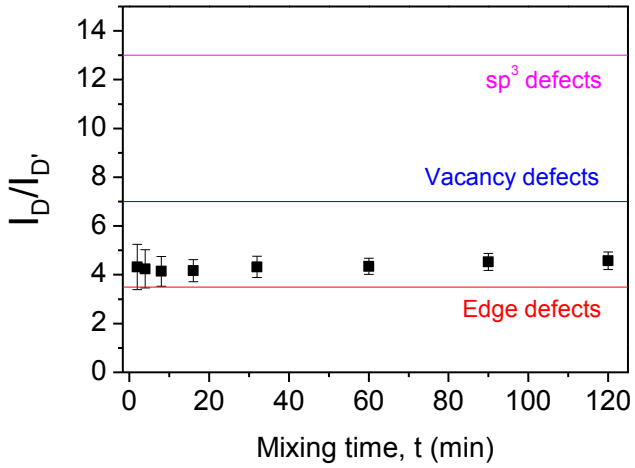

Figure S3.17: D:D' intensity ratio (by fitting) for graphene prepared from Qindao Graphite plotted as a function of mixing time.

However, because the value of $I_D/I_{D'}$~3.5 quoted by Eckmann *et al* contains no error range, it is necessary to perform more experiments to be completely certain that the values of $I_D/I_{D'}$~4.2 found here for Qindao graphene is actually reflective of edges and not vacancies. To do this, we reason that, if vacancies are being formed under shear, then their population should increase with mixing time. This would be reflected in an increase in $I_D/I_{D'}$ with mixing time. However, if the defects are only of the edge type, then $I_D/I_{D'}$ should not change with mixing time. To test this we produced SEG by mixing Qindao graphite in NMP (C_i=50g/L, V=500mL, N=5000rpm, D=32mm, total time=120min). After different mixing times, 15mL samples were removed, centrifuged at 1500rpm for 150min and the top 10mL decanted for analysis. Then 8mL were filtered onto 0.45μm nylon membranes and analysed using Raman spectroscopy. The D/D' ratios were extracted by fitting as before. In figure S3.17, we plot $I_D/I_{D'}$ v mixing time, t. We find $I_D/I_{D'}$ to be invariant with t within error with a value of $I_D/I_{D'}$~4.4. We believe this is strong evidence that the defects observed in the Raman spectra of SEG are edge defects and not shear

DOI: 10.1038/NMAT3944

induced vacancies. *This strongly suggests that shear exfoliation does not introduce defects into the basal plane of the graphene produced*. In addition, we suggest that the value of $I_D/I_{D'}$~3.5 reported by Eckmann may be slightly low and that perhaps $3 \leq I_D/I_{D'} \leq 4.5$ is more appropriate.

S3.7 Using Raman spectroscopy to measure flake thickness

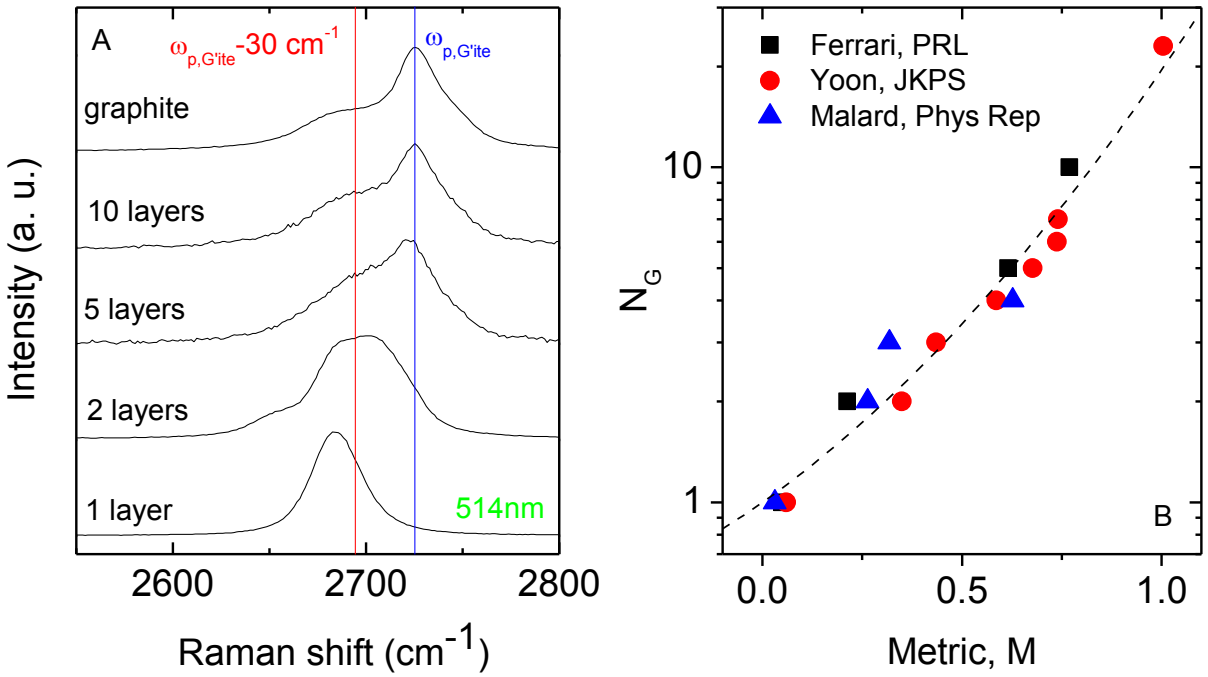

Figure S3.18: A) Raman spectra (originally reported by Ferrari *et al.*) for micromechanically cleaved graphene flakes of different thickness (adapted from [18] with kind permission from Prof Ferrari). The red and blue lines show positions used to generate the thickness metric described in the text. B) Number of monolayers per flake, N_G, plotted *versus* thickness metric, M. This data was extracted from papers by Ferrari,[18] Yoon[19] and Malard.[23] The dashed line is an empirical fit to $N_G = 10^{0.84M+0.45M^2}$. In both panels, the excitation wavelength was 514 nm.

Because of the importance of accurately measuring the thickness of the nanosheets produced by shear exfoliation, it would be highly desirable to have independent confirmation of the thickness data acquired by AFM (section S3.3). It has long been known that the thickness of few-layer graphene nanosheets is reflected in the shapes of their 2D Raman bands (~2700 cm^{-1}).[18] This is

illustrated in figure S3.18A (adapted from [18]). For example, Yoon et al[19] have published spectra of graphene flakes with 1-7 layers. The 2D bands of the spectra in figures S3.10 and S3.11 are similar in shape to the spectra published by Yoon for 4-5 layer graphene.

We propose that the shape of the 2D line can be used to quantitatively estimate the thickness of graphene flakes. We suggest using as a metric, the ratio of the intensity of the 2D band, measured at the wavenumber associated with the peak of the graphite 2D band ($\omega_{p,G'ite}$, i.e. blue line in figure S3.18A), divided by the intensity at the wavelength associated with the low energy shoulder of the graphite 2D band (i.e. red line in figure S3.18A).

Because the peak is well defined, $\omega_{p,G'ite}$ is easy to identify (2725 cm^{-1} in figure S3.18A). However, because the shoulder is poorly defined, care must be taken: we define it as $\omega_{s,G'ite} = \omega_{p,G'ite} - 30\ cm^{-1}$. It is clear from figure S3.18A, that for few-layer graphene, the ratio of Raman intensity at $\omega_{p,G'ite}$ to the intensity at $\omega_{s,G'ite}$ (i.e. $I_{G'ene}(\omega = \omega_{p,G'ite}) / I_{G'ene}(\omega = \omega_{s,G'ite})$) scales with the number of monolayers per flake. However, this ratio alone is not an effective metric because the peak-to-shoulder intensity ratio for graphite (i.e. $I_{G'ite}(\omega = \omega_{p,G'ite}) / I_{G'ite}(\omega = \omega_{s,G'ite})$) varies somewhat from graphite source to graphite source. Because of this, it is necessary to normalise the graphene intensity ratio to that of graphite. This gives a metric, M, which varies with flake thickness:

$$M = \frac{I_{G'ene}(\omega = \omega_{p,G'ite}) / I_{G'ene}(\omega = \omega_{s,G'ite})}{I_{G'ite}(\omega = \omega_{p,G'ite}) / I_{G'ite}(\omega = \omega_{s,G'ite})} \qquad [3.4]$$

A number of papers give the Raman spectra of graphene flakes with well-defined, known thickness. We identified papers by papers by Ferrari *et al*,[18] Yoon *et al* [19] and Malard *et al*,[23] extracted M and plotted N_G *versus* M as shown in table S3.2 and figure S3.18B. We find a well-defined relationship between N_G and M, observed by all three data sets, which can be described empirically by

$$N_G = 10^{0.84M + 0.45M^2} \qquad [3.5]$$

This expression allows the measurement of mean flake thickness directly from the 2D band of a Raman spectrum measured on a graphene flake or an ensemble of flakes so long as a graphite spectrum is also collected. N.B. This graphite spectrum should be measured on the graphite used

DOI: 10.1038/NMAT3944

to produce the graphene. We anticipate that this relationship will be very useful as a simple way to get an estimate of the mean thickness of graphene flakes. We estimate the error is approximately ±1.5 layers.

N_G	1	2	3	4	5	6	7	10	23	40	∞
Ferrari, Physical Review Letters 97, 187401, (2006).											
$\frac{I_{G'ene}(\omega=\omega_{p,G'ite})}{I_{G'ene}(\omega=\omega_{s,G'ite})}$	0.12	0.51			1.49			1.86			2.42
M	0.05	0.21			0.62			0.77			1
Yoon, Journal of the Korean Physical Society 55, 1299-1303, (2009).											
$\frac{I_{G'ene}(\omega=\omega_{p,G'ite})}{I_{G'ene}(\omega=\omega_{s,G'ite})}$	0.10	0.60	0.75	1.01	1.17	1.27	1.28		1.73	1.34	1.73
M	0.06	0.35	0.44	0.59	0.68	0.74	0.74		1	0.77	1
Malard, Physics Reports, 473, 51-87, (2009).											
$\frac{I_{G'ene}(\omega=\omega_{p,G'ite})}{I_{G'ene}(\omega=\omega_{s,G'ite})}$	0.07	0.63	0.76	1.49							2.37
M	0.03	0.26	0.32	0.63							1

Table S 3.2: Metric data as extracted from literature. The data from Ferrari et al and Yoon et al were extracted from the original graphs as kindly supplied by the authors. The data from Malard et al was estimated from the published graph.

However, using this metric requires careful measurement. It is critical that all spectra are collected under the same conditions. In particular, the results will be sensitive to any shifts in the 2D band of the graphene spectrum being analysed relative to the graphite spectrum being used as a standard. Such shifts may occur due to the environment of the graphene flakes under study or simply due to shifts occurring during the acquisition of the spectra when moving the grating. We propose that the strength of this metric is that it can be used as a simple, quick analytic tool to estimate the mean number of layers from liquid-exfoliated graphene. As such, we argue that a recalibration of the spectrometer after every single measurement is not feasible simply because it

is much more time consuming. For example, in the following, we will present the result of the analysis of ~250 individual Raman spectra. Even though peak shifts due to decalibration of the spectrometer can strictly not be corrected after the acquisition due to the nonlinearity of the gratings, we nonetheless shifted the spectra manually so that the G band position matches that of the graphite to crudely account for any occurring shifts.

Here we apply this Raman thickness metric to the surfactant-exfoliated graphene using the spectra given in figure S3.11. Specifically, we start with these samples because we also have AFM data for their mean flake thickness (N_G, figure S3.7-8). We used equation 3.4 to calculate M for the spectra in figure S3.11. In figure S3.19A, we plot the mean number of monolayers per flake, N_G, as measured by AFM (figure S3.7-8) *versus* the Raman thickness metric calculated from the data in figure S3.11 using equation 3.4. This data (closed symbols) sits almost exactly on the empirical N_G-M curve (solid line) plotted using equation 3.5.

However, it is important to show that experimental data for liquid exfoliated graphene matches equation 3.5 for a range of nanosheet thicknesses, not just those around N_G=6-8. To do this, we performed a size selection procedure similar to that described in S3.6.1. In that section we used size selection to control the lateral nanosheet size. However, recent work has shown nanosheet thickness to scale with lateral size for size selected MoO_3 nanosheets.[24] Thus, we expect nanosheet thickness to vary with the centrifugation rate used. Shown in figure S3.19B are Raman spectra collected for the size-selected samples. It is clear from the D band (~1350 cm^{-1}) that the lateral size is changing as before. However, the 2D band (~2700cm^{-1}) clearly shows changes that are due to variations in thickness. We measured the mean nanosheet thickness for the size selected samples using AFM as described in section S3.3. The measured mean nanosheet thickness is plotted *versus* the centrifugation (CF) rate used in the size selection procedure in figure S3.19C. Clearly the thickness falls dramatically with CF rate. To test the applicability of the Raman size metric, we plot N_G (from AFM) *versus* M (calculated from the spectra in figure S3.19B) in figure S3.19A (open symbols). We find very good agreement with the empirical line plotted using equation 3.5.

This is an important result and shows that Raman and AFM data are in perfect agreement. This strongly supports the accuracy of our AFM thickness data and confirms shear-exfoliated graphene nanosheets to be relatively thin.

DOI: 10.1038/NMAT3944

This allows us to calculate N_G from the Raman thickness metric for the surfactant-exfoliated graphene using equation 3.5. We do this for both the initial survey data (figure S3.11) and the size selected data (S3.19B). These data are plotted in figure S3.19D *versus* the AFM thickness data and agree quite well. We plot the same data in figure S3.19E slightly differently: data for N_G calculated both using AFM and Raman are plotted for the various combinations of processing parameters. This shows that the nanosheet thickness is relatively invariant with processing parameters with typical mean values lying in the range $5<N_G<8$.

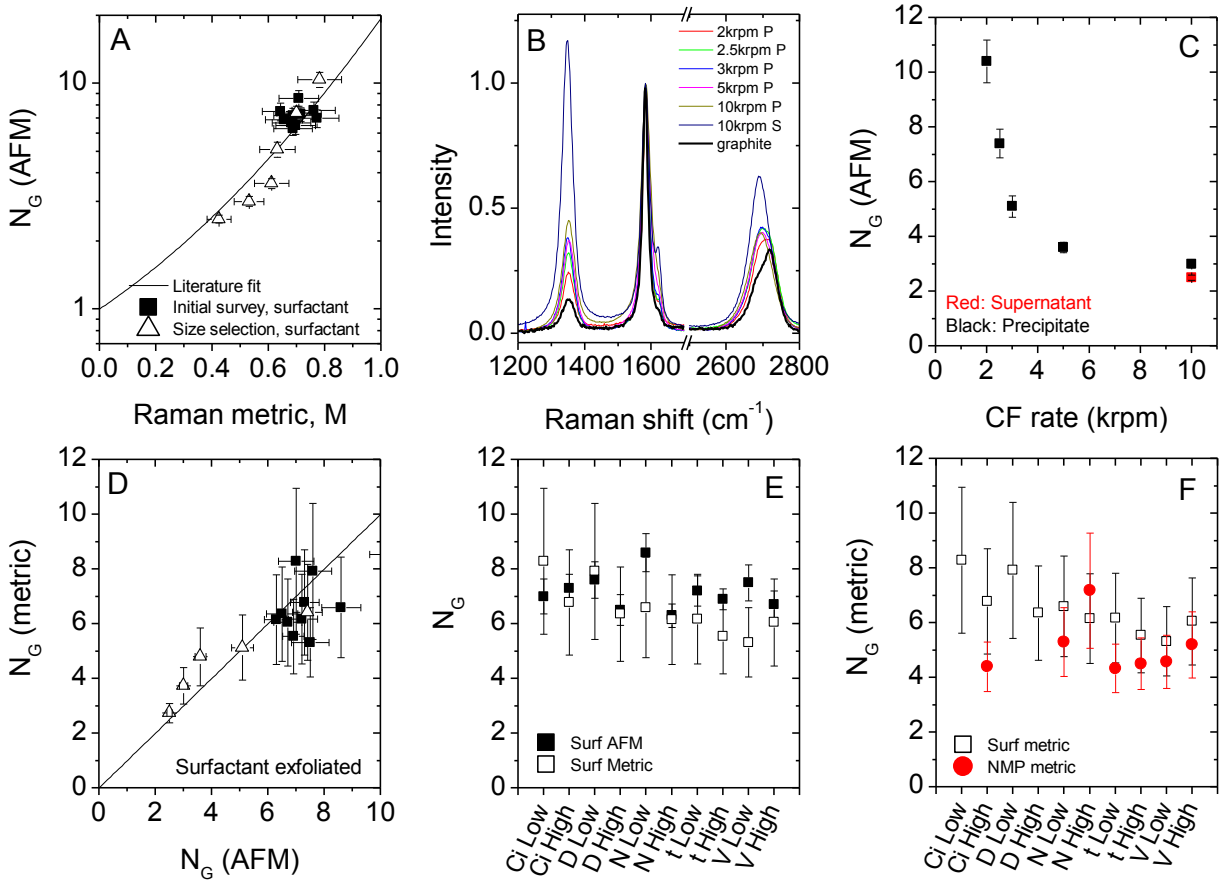

Figure S3.19: A) Mean number of monolayers per flake, N_G, measured by AFM for surfactant-exfoliated graphene plotted *versus* Raman thickness metric, M. The closed symbols represent the initial survey samples (e.g. figure S3.1), while the open symbols represent size-selected samples. The line is a plot of equation 3.5. B) Raman spectra for size-selected graphene. C) Flake thickness, N_G, measured by AFM plotted *versus* centrifugation speed used to select by size. D) Flake thickness, N_G, calculated using equation 3.5 plotted *versus* N_G as measured by AFM.

Symbol codes as in A. E) N_G measured by both AFM and using thickness metric (eq 3.5) plotted for a range of mixing conditions. F) N_G calculated using thickness metric (eq 3.5) plotted for both surfactant-exfoliated and NMP-exfoliated graphene for a range of mixing conditions. The mixing conditions are given in table S3.1.

Finally, we can calculate the Raman thickness metric for the data for NMP-exfoliated graphene shown in figure S3.10. We then use equation 3.5 to estimate N_G for this solvent-exfoliated graphene. This is plotted (with surfactant-exfoliated data for comparison) for a range of processing parameters in figure S3.19F. This data suggests that NMP-exfoliated graphene is typically 4-6 layers thick and may be slightly thinner than surfactant-exfoliated graphene.

S3.8 XPS

X-ray photoelectron spectroscopy characterisation was performed on thin vacuum-filtered films prepared from the dispersions described in table S3.1. The samples were analysed using a VG-Scientific CLAM4 XPS system with a Mg K_α X-ray source. The survey scan was acquired using a constant pass-energy of 100 eV, and the detailed scans were acquired using a constant pass-energy of 20 eV. Carbon 1s core level spectra are shown in figure S3.20.

For graphitic systems such as these we expect to see a large peak at ~284-285 eV representing graphitic carbon (C-C).[7] This is indeed observed. However, a number of smaller features are also observed at higher binding energy. In the case of graphene oxide, peaks are observed in this range representing oxides which are covalently bonded to the graphene carbons.[25] However, this is unlikely to be the case here as such oxides are always accompanied by basal plane defects which have a strong Raman signature. The absence of such a broad, intense D band suggests the absence of covalently bonded oxides. An alternative possibility is that the small peaks are due to residual NMP left over from the exfoliation process. This has been observed previously.[7] We can test this hypothesis by fitting the measured spectra (figure S3.20).

DOI: 10.1038/NMAT3944

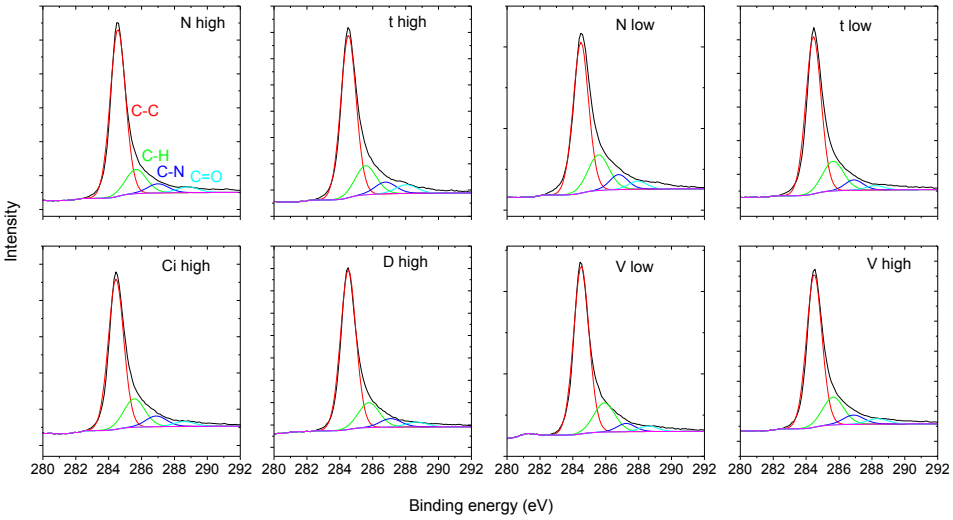

Figure S3.20: XPS spectra for graphene films. The sample code is given in the panel (see table S3.1). Each spectrum was fitted to four lines (and the Shirley background) as shown in the figure. These lines represent (in increasing binding energy) C-C, C-H, C-N and C=O as indicated in the top left panel. Processing parameters are given in table S3.1.

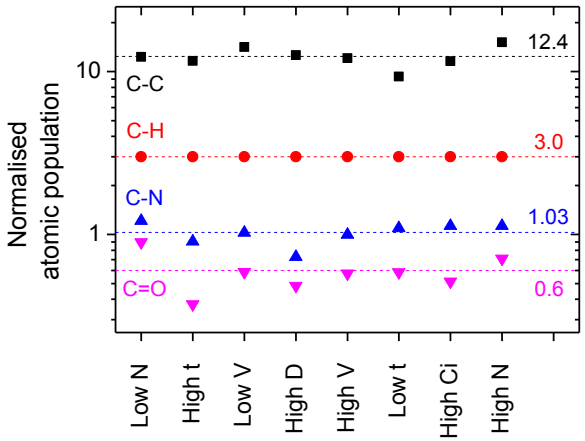

Figure S3.21: Atomic population (normalised to the C-H peak representing 3 C atoms) for a range of samples prepared with different processing parameters (table S3.1).

Fitting was performed using the CASA software. All spectra have been fitted to the following features: graphitic carbon spectrum including a Shirley background and three small features at higher binding energies, representing the carbon atoms in the NMP (C_5H_9NO, see figure S1.2).

These NMP carbons are the carbons that are bonded to H atoms and (i.e. C-H) and the two carbon atoms that are bonded to N (C-N) and the carbonyl carbon (C=O), respectively.

The resultant fits were very good and adequately describe the observed spectra. We note that if the three small high energy peaks represent the presence of residual NMP, then the peak areas (corrected to represent atomic populations) should be in the ratio C-H:C-N:C=O = 3:1:1 (see figure S1.1 for NMP structure).

Shown in figure S3.21 are the relative atomic populations of C-C, C-H, C-N and C=O as derived from fitting the XPS spectra for the samples described in table S3.1. Note that this data has been normalised to C-H=3. This means that these numbers represent the number of each species per NMP molecule. From figure S3.21, the ratio in the ratio C-H:C-N:C=O = 3.0:1.03:0.6, very close to the expected value. This indicates that the XPS spectra can be completely explained by the presence of graphene and residual NMP without the need to assume the presence of oxides. *Coupled with the Raman data this implies shear-exfoliated graphene to be defect and oxide free*.

DOI: 10.1038/NMAT3944

S4 Scale-up study

Once it is known that well exfoliated, defect free, non-oxidised graphene can be produced using shear mixing, it is important to assess how much can be produced. We do this by measuring the dispersed graphene concentration. To measure the concentration, 10 mL aliquots were taken from the dispersion (with the mixer stopped) and centrifuged at 1500 rpm for 150 min. The top 5 mL of the supernatant was decanted from the sediment and characterised by UV-vis absorption spectroscopy (10 mm cuvette). This gave the absorbance per cell length, A/l, (at a given wavelength, 660 nm). From this, the concentration, C, could be calculated from $A/l = \alpha C$, once the absorption coefficient, α, is known.

The value of the absorption coefficient was determined by vacuum filtration of a known volume of dispersion, and weighing the resultant film. By measuring the absorption of the dispersion at a range of dilutions (figure S4.1), a value of $\alpha = 3778 mlmg^{-1}m^{-1}$ was obtained, as shown below. This is in close agreement with the values obtained previously.[7]

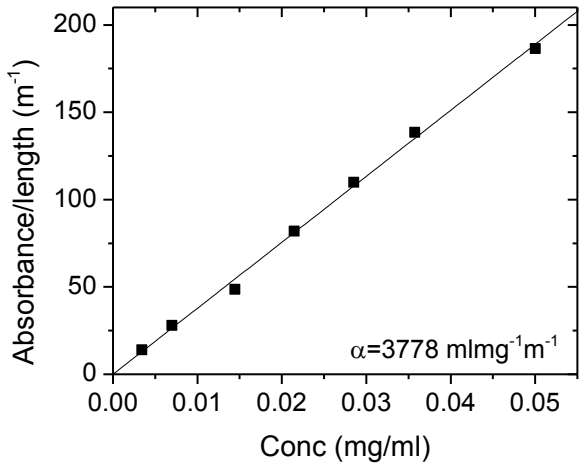

Figure S4.1: Measurement of the absorption coefficient of dispersions of shear-exfoliated graphene. The concentration was measured by vacuum filtration and careful weighing.

S4.1 Time dependence

The most straightforward processing parameter is the mixing time, t. The first experiments performed were measurements of dispersed concentration of graphene *versus* mixing time. These initial experiments showed that the concentration increased with time according to a power law,

with an exponent typically close to 0.5 (figure 4.2-A). Subsequently, a large number of dispersions were made with a range of combinations of processing parameters (i.e. N, V, C_i, D), but in all cases measuring C vs. t. For each combination of parameters, the graphene concentration was measured as a function of mixing time and the data fitted to $C = A \cdot t^{\tau}$. Although the values of τ were always reasonably close to 0.5, the exact values showed a spread, as shown in the histogram in figure 4.2-B. From this histogram we found the average value of the time exponent, $\langle \tau \rangle$=0.66.

Once this was known, each set of *C(t)* data was then re-fitted to $C = At^{0.66}$, and the values of A recorded. This was done to maximise consistency in the measurement of A. Using $C = At^{0.66}$ and the measured values of A for each time dependent data set, the concentration after 1 minute mixing ($C_{1\ min}$) was calculated (numerically identical to A). Values of $C_{1\ min}$ were then plotted against the parameter being varied in a given experiment. For example, Figure 2-C (main paper) shows a graph of $C_{1\ min}$ plotted *versus* C_i. For this set of dispersions, the other parameters (N, V, D) were kept constant.

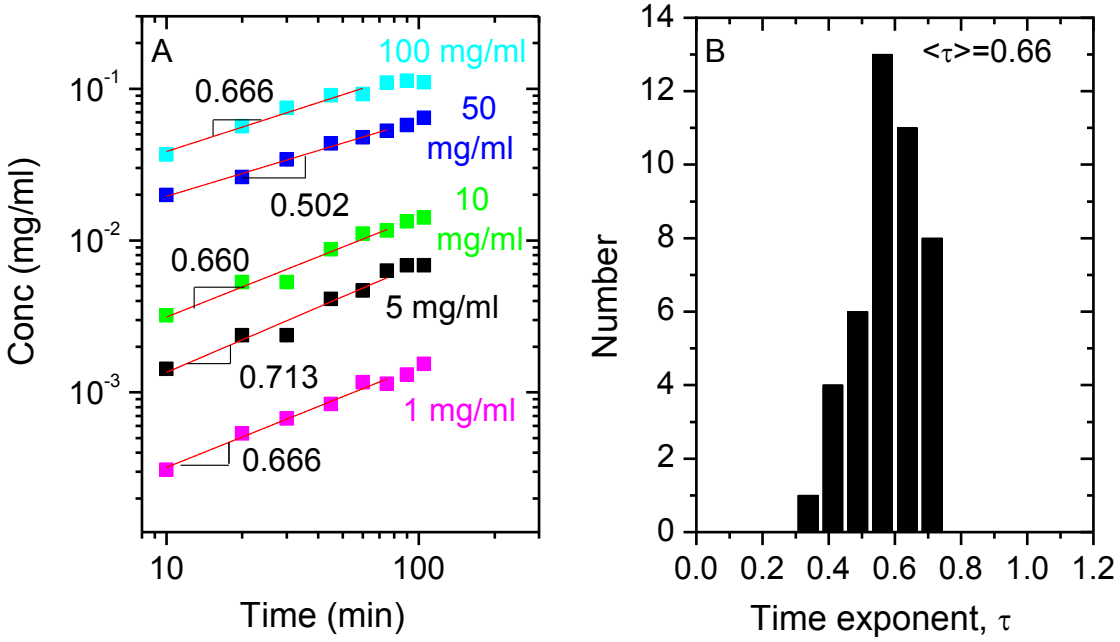

Figure S4.2: A) Dispersed graphene concentration as a function of mixing time. These dispersions were prepared with V=1500 mL, N=4500 rpm and D=32 mm for a range of values of C_i. B) Histogram of all measured values of τ with the mean value of 0.66 shown.

DOI: 10.1038/NMAT3944

S4.2 Volume dependence

To allow as wide a range of volumes as possible to be studied, dispersions were prepared and $C_{1\ min}$ measured using 5 different beakers (table S4.1). For the three largest beakers mixing was performed for 4 liquid volumes with volume controlled by the height of liquid in the beaker. Note that because of this variation in height, the geometry of the liquid was different in each case. Specifically, the ratio of beaker diameter, T, to liquid height, H, was not constant. Because the geometry of the liquid/beaker can be important in mixing experiments,[26] we performed additional experiments where mixing was performed in 5 different beakers (including the three just referred to) where the liquid height, H, was set equal to the beaker diameter, T (i.e. H=T). This scenario is generally referred to as geometrically similarity.[26] In figure 2-E (main paper), the beakers used are labelled as "1 L beaker", "3 L beaker", "5 L beaker" and "Geometrically similar beakers". The first three refer to the beakers where the liquid height was varied while the last term refers to the set of geometrically similar beakers. The volume required to achieve geometric similarity is given in table S4.1 for each beaker.

We note that in figure 2E (main paper), the data for all beakers sit approximately on the same line. This implies that the dispersed concentration is not strongly dependent on beaker shape.

Beaker Capacity	Diameter (mm)	Liquid volume for T=H (mL)
250mL	66	220
800mL	80	490
1000mL	101	800
3000mL	145	2370
5000mL	163	3380

Table 4.1: Properties of the beakers used in the volume study.

S4.3 Calculation of the scalability of shear-exfoliated graphene

It is essential to be able to estimate the degree to which the production of graphene can be scaled up. The relevant quantity to consider is the production rate (i.e the mass of graphene produced per unit time). For scale-up to be viable, it is essential that the production rate increases as the tank volume increases (for a batch process). In this section, we attempt to estimate the scaling of the production rate based on the data described in figure 2 (main paper). In addition, we will estimate the energetic contribution to the financial cost of exfoliation.

The scaling study outlined in figure 2 of the main text shows the exfoliated graphene concentration (after centrifugation) to scale with processing parameters as

$$C = k_1 C_i t^{\tau} N^{n} V^{v} D^{d} \qquad [4.1]$$

where, from figure 2, for graphene exfoliated in NMP: $k_1=1.0\times10^{-6}$ (in SI units), τ=0.66, n=1.13, ν=-0.68 and d=2.28.

The production rate is given by $P_R = VC/t$, so

$$P_R = k_1 C_i t^{\tau-1} N^{n} V^{v+1} D^{d} \qquad [4.2]$$

The maximum achievable concentration and so maximum yield (yield, $Y=C/C_i$) is achieved when the sample is mixed to the saturation time, t_{sat}:

$$t_{sat} = k_2 V N^{-1} D^{-3} \qquad [4.3]$$

Where, for graphene exfoliated in NMP, k_2=7745 (figure 2-B). Thus, we can write

$$P_R = k_1 C_i (k_2 V N^{-1} D^{-3})^{\tau-1} N^{n} V^{v+1} D^{d} = k_1 C_i k_2^{\tau-1} N^{n+1-\tau} V^{v+\tau} D^{d+3-3\tau} \qquad [4.4]$$

During scale-up, it is likely that the rotor diameter will be scaled in proportion to the tank diameter. We assume the tank will be cylindrical with liquid height, H, equal to tank diameter, T. In stirred tanks, the optimum ratio of D/T is thought to be ~0.3. We will assume this value to be applicable to rotor/stator mixing (for example, in a 1000 L tank with T=1.1 m, this would require a stator with D=33 cm). This means that $D = k_3 V^{1/3}$ with k_3=0.325.

We note that this is an example of a scale-up invariant. There are many examples of combinations of parameters being kept constant on scale-up e.g. Reynolds number, Froude number, Weber number etc.[26,27] In this work, the scale-up invariants are $k_3 = DV^{-1/3}$ and $k_2 = t_{sat} V^{-1} N^{1} D^{3}$. [4.5]

DOI: 10.1038/NMAT3944

Applying $D = k_3 V^{1/3}$ gives a production rate of

$$P_R = k_1 C_i k_2^{\tau-1} N^{n+1-\tau} V^{v+\tau} (k_3 V^{1/3})^{d+3-3\tau} = \left(k_1 k_2^{\tau-1} k_3^{d+3-3\tau} C_i\right) N^{n+1-\tau} V^{v+1+d/3} \quad [4.6]$$

which we can express for brevity as

$$P_R(V) = BN^{\alpha} V^{\beta} \quad [4.7]$$

where, taking C_i=100 kg/m^3, and using the numbers quoted for NMP, B=1.17×10^{-7} (SI Units), α=1.47 and β=1.08.

Using this data, we can plot the predicted production rate in NMP as a function of tank volume for a number of values of N (figure S4.3). This data predicts production rates of ~1 kg/h for tanks with V=10 m^3.

However, for purpose built mixers, the maximum available speed may fall off as the rotor gets larger (i.e. D↑). For example, Silverson produces mixers with D=32 mm and D=100 mm which have maximum values of N of 8000 and 3000 rpm. Taking this as a guide to the (engineering limited) scaling of N with D suggests that $N_{max} \approx 5/D$ where D is in meters and N_{max} is in s^{-1}. We note this condition is not quite a scale-up invariant in the normal sense.[26,27] It is more accurately thought of as a limitation associated with the engineering of the mixer. Assuming the mixer is run at its maximum speed results in a modification to the previous equation:

$$P_R = \left(k_1 k_2^{\tau-1} k_3^{d+3-3\tau} C_i\right)(5(k_3 V^{1/3})^{-1})^{n+1-\tau} V^{v+1+d/3} = \left(k_1 k_2^{\tau-1} k_3^{d-n+2(1-\tau)} C_i (5)^{n+1-\tau}\right) V^{v+1+(d-n+\tau-1)/3} \quad [4.8]$$

which we can express for brevity as

$$P_R(V) = B' V^{\kappa} \quad [4.9]$$

where, for NMP, B'=6.48×10^{-6} (SI Units), κ=0.59.

This predicts a slower increase in production rate with V. However, rates of 100 g/h are still achievable at tank volumes of 10 m^3.

For exfoliation in surfactants, scale-up calculations are given below in section 6.

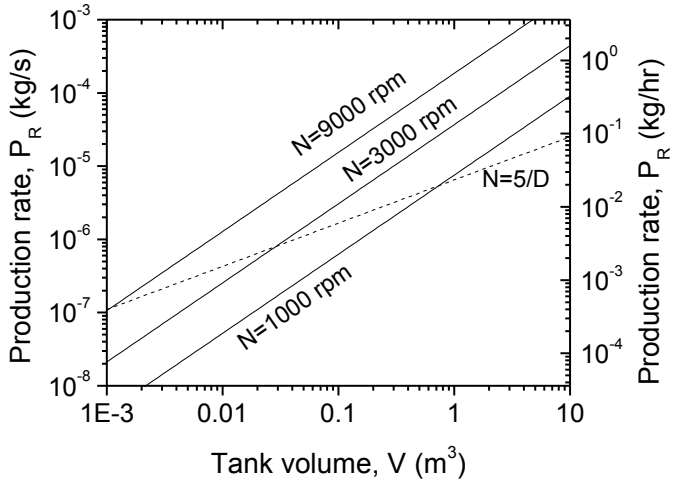

Figure S4.3: Production rate of graphene in NMP plotted against tank volume for three different rotor speeds. Note for N=3000 rpm, the mixing time (t_{sat}) is ~77 minutes (independent of V and D if $k_3 = DV^{-1/3}$ is invariant). This means for a 10 m^3 tank with N=3000 rpm, a single batch run could yield 1.1 kg of graphene.

S4.4 Extrema: Maximising production rate

As each parameter was varied from lowest to highest possible values, every other parameter was kept constant at a medium value (with the exception of D, which was otherwise held at 32mm). In an effort to obtain the highest possible production rate from the current set-up, the parameters were all set to their relevant extreme values. The settings for this experiment are given in table S4.2. This yielded a maximum labscale production rate of 0.4 mg/s (1.4 g/h). This data agrees very well with the scaling observed in figure 2-H (main paper).

C_i (g/L)	N (rpm)	V (mL)	D (mm)	t (min)	Scaling Parameter	PR (mg/s)
100	6000	4500	32	2	0.252	**0.40**

Table S4.2: Parameters used to produce maximise lab-scale production rates.

S4.5 Other solvents

Shear mixing was also performed in other solvents such as N-cyclohexyl-2-pyrrolidone (CHP), dimethylacetamide (DMA) and dimethylformamide (DMF). In each case, the mixing parameters

DOI: 10.1038/NMAT3944

were: V=2000 mL, D=32 mm, Ci=50 g/L and N=4000 rpm. Dispersions were produced for a range of mixing times and the concentrations measured optically. The concentrations of graphene in DMA and DMF were extremely low. This can be explained by the fact that their surface energies (~66 mJ/m^2 equivalent to surface tension[7] ~36 mJ/m^2) are too low to give the small flakes retained by the centrifuge regime used here (see section 8.4). The concentration of exfoliated graphene in CHP was well above that achieved for NMP. This is consistent with the high viscosity of CHP (η=0.0115 Pa·s, see section 8.4). We note that, like NMP, the time exponent for CHP dispersions was close to 0.66 (figure S4.4).

However, we note that there are some disadvantages associated with CHP. Its high boiling point may make it difficult to remove from the graphene while its toxicity and cost may be an issue. Further work is required to identify the ideal solvent for use in shear exfoliation.

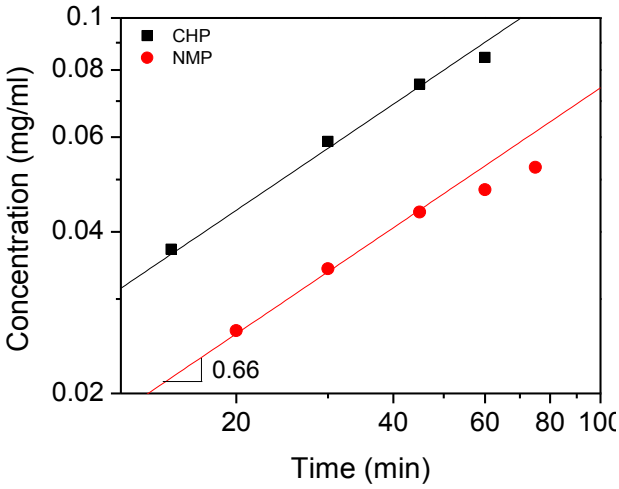

Figure S4.4: Concentrations of liquid phase exfoliated graphene/NMP and graphene/CHP dispersions prepared in shear mixer

S4.6 Surfactant and polymer solutions

One way to illustrate the versatility of shear mixing for graphene production would be to demonstrate that it can exfoliate graphite not only in solvents but also using surfactant or polymer solutions as stabilisers. To test this, graphite was mixed in an aqueous surfactant solution in the same way as for NMP dispersions described above. A surfactant solution was prepared by dissolving 7.5 g sodium cholate (Sigma Aldrich) in 1500 mL of deionised water.[14]

This was then added to the beaker in which 75 g of graphite (Sigma Aldrich) had been added. The mixing head was then lowered and the rotor speed slowly increased to the set speed.

Similarly for dispersions in PVA solutions, a solution of 30 g of PVA in 1500 mL of deionised water was prepared at 50 °C. This was then used as the mixing liquid in the same way as for NMP and sodium cholate solutions as described above.

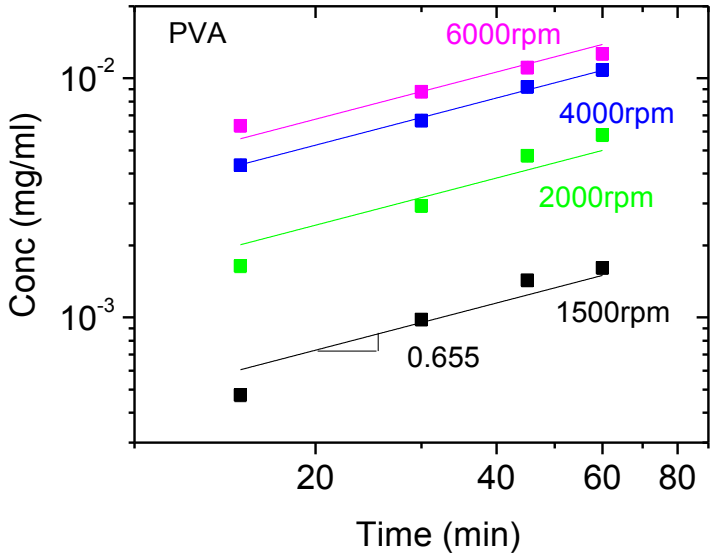

Figure S4.5: Concentration vs. mixing time for all mixing experiments in PVA solutions.

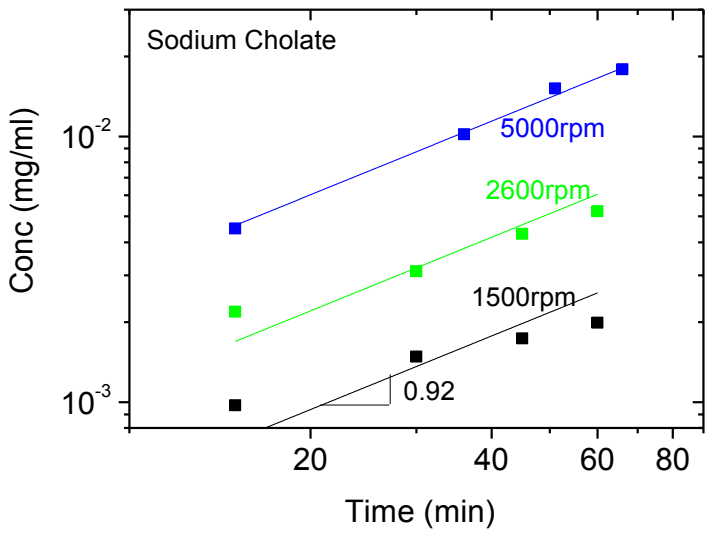

Figure S4.6: Concentration vs. mixing time for all mixing experiments sodium cholate solutions.

DOI: 10.1038/NMAT3944

Shown in figures S4.5 and S4.6 are examples of data for dispersed graphene concentration as a function of mixing time in both surfactant (sodium cholate/water) and polymer (polyvinylalcohol/water) solutions. We note that control experiments show that graphene cannot be exfoliated by application of shear in water alone (i.e. in the absence of surfactant or polymer). For the PVA stabilised dispersions we see the dispersed concentration scaling as $C \propto t^{\tau} N^{n}$ with τ=0.66 and n=0.92. We note that the value of τ is identical to that found for NMP based dispersions while the value of n is slightly below that found for NMP dispersions. We note that we did not perform enough measurements to determine the other exponents for PVA stabilised dispersions.

We studied the exfoliation of graphene in surfactant solutions in more detail. We exfoliated two types of graphite, purchased from Sigma-Aldrich and FutureCarbon Gmbh, Germany (SGN18) in water and sodium cholate. We mixed the graphite in surfactant solutions for a number of combinations of mixing parameters (V=600 mL-2.5 L, t=10-60 min, N=2000-6000 rpm, C_i=10-100 g/L, D=12-32 mm). We used a simple algorithm to estimate the scaling exponents relating the concentration to the mixing parameters ($C \propto C_i^{\chi} t^{\tau} N^{n} D^{d} V^{v}$). This gave the combination τ=1.08, v=-0.47, n=2.54 and d=3.34 (χ was fixed at 1 for the fitting procedure) for both types of graphite (figure S4.7). We note that these exponents are in general somewhat larger than the NMP mixing exponents. The reasons for this difference are unclear but may be related to the fact that the stabilisation mechanisms for solvent and surfactant stabilised graphene are different (see section S1.3).

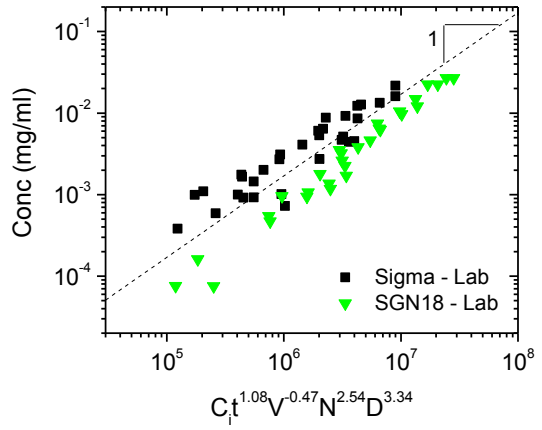

Figure S4.7: Concentration of two types of graphite, exfoliated by shear mixing in surfactant, as a function of the appropriate scaling factor.

S4.7 Sediment recycling

As shown in the main paper, the yield of exfoliated graphene (i.e. $Y=C/C_i$) is very low, never greater than 2×10^{-3}. This makes this process potentially very wasteful. However, such waste can be avoided, if the sediment that is removed by centrifugation can be recycled to increase the yield.

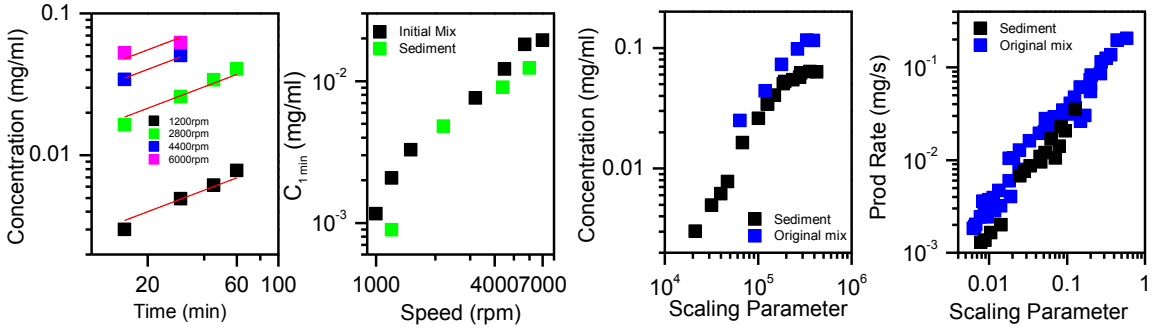

Figure S4.8: a) Concentration vs. time, b) $C_{1\,min}$ vs. time, c) Conc., & d) PR vs. scaling parameter for recycled graphene/NMP dispersions.

In order to demonstrate graphite sediment can be recycled, we mixed sediment in NMP varying both N and time of mixing. After centrifuging the dispersions for 150 min at 1500 rpm, the recycled graphene/NMP samples were analysed by optical absorption, TEM and Raman spectroscopy. Measurement of concentration (figure S4.8) shows that graphene from recycled sediment generally follow the same scaling laws as those shown in figure 2 (main paper). TEM reveals that there are no obvious differences between graphene produced from fresh graphite, and that produced from the sediment (figure S4.9). Thin flat graphene flakes along with some folded are visible from micrographs. Flakes were qualitatively observed to be larger in samples from recycled sediment than under the same conditions from original graphite. Typical Raman spectra of recycled graphene samples are shown in figure S4.10. It is worth noting that I_D/I_G is lower compared with initial mix graphene films, suggesting that the flakes exfoliated from the recycled sediment are larger than those initially. This supports the qualitative observations from TEM.

DOI: 10.1038/NMAT3944

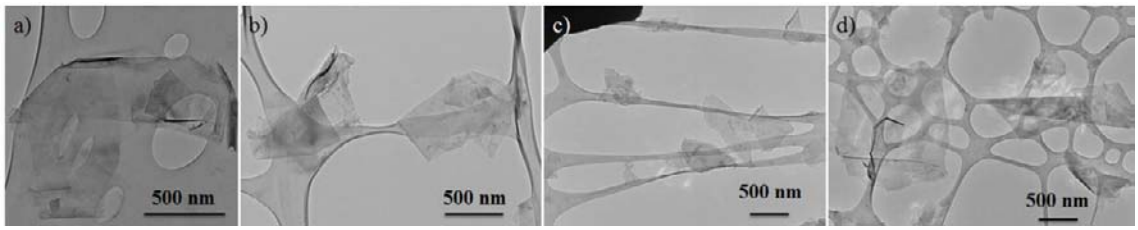

Figure S4.9: Transmission electron micrographs of recycled graphene flakes (after CF), shear mixed for 30 min at a) 1200 rpm, b) 2800 rpm, c) 4400 rpm and d) 6000 rpm.

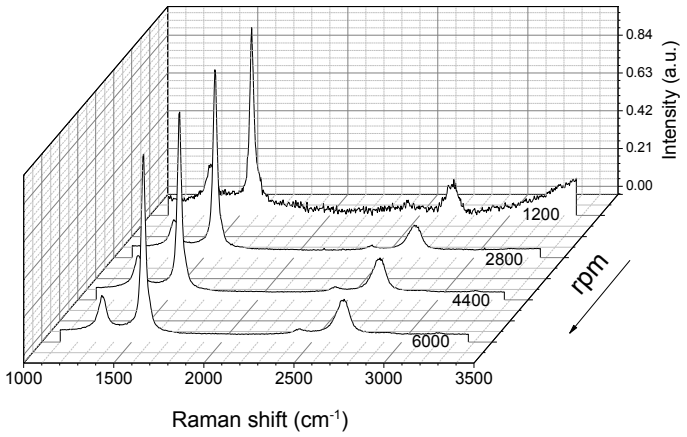

Figure S4.10: Raman spectra of recycled graphene films

The ability to achieve multiple sediment recycling steps was tested using the water/surfactant system. An initial mixture of 50g of graphite (Sigma) in 500 mL water-sodium cholate solution (2g/L) was prepared, and mixed for 20 min using the 32 mm rotor at 6000 rpm. The top 400 mL of the resulting dispersion was decanted (some settling occurred during this step) and centrifuged at 1500 rpm for 40 min. The top 320 mL of the supernatant was removed and retained for analysis, while the sediment and remaining 80 mL was returned to the mixing beaker with the 100 mL left after the mixing. A further 320 mL of fresh surfactant solution was added and the mixing repeated as for the initial exfoliation step, and the process repeated for a total of 33 cycles. The cumulative yield (mass of graphene recovered divided by starting graphite mass) is shown as a function of recylcling run number in figure S4.11. This curve is initially linear (0.15% recovered per run) but turns over after ~10 runs before following a new linear curve with reduced slope (0.07% recovered per run). A total of 1.67 g of graphene was exfoliated giving a yield of 3.35%.

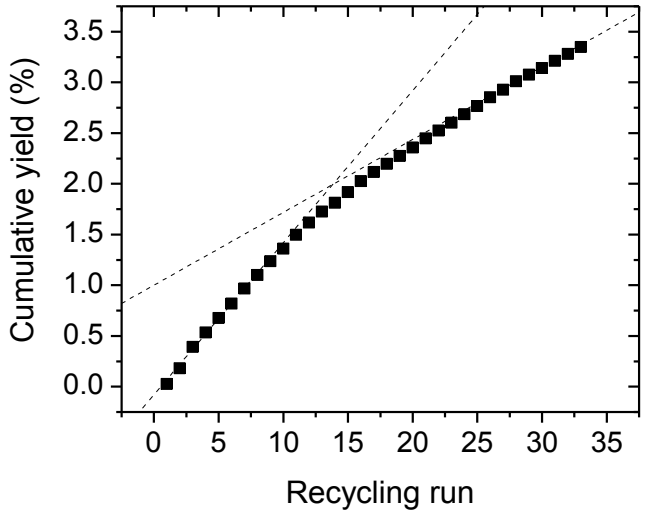

Figure S4.11: Cumulative yield *versus* recycling run for shear-exfoliated graphene

S4.9 Other mixers?

Scale up is more likely to be successful if the exfoliation process is relatively insensitive to the details of the mixer. Because we have demonstrated exfoliation to be controlled by the shear rate (see main text and SI, section 7), any mixer that can generate the required shear rates (i.e. $\dot{\gamma}_{min}$ >10^4 s^{-1}) is likely to successfully exfoliate graphite.

To test this, we performed trials using a relatively crude mixer type – a standard kitchen blender. We purchased a Kenwood kitchen blender (Kenwood Limited, UK, BL370 series) in a high street shop (figure S4.12A). Because the blender was predominately made of plastic, we chose to exfoliate graphite in a surfactant solution, rather than using NMP. To emphasise the insensitivity of the exfoliation to the details of the procedure, we chose to use a household dishwashing fluid (Fairy Liquid) rather than an industrial surfactant. We performed a number of trials typically using V=500 mL, 20≤C_i≤100 g/L, 10≤t≤30 min and a ratio of surfactant to graphite concentrations of C_i/C_{FL}~8.

Shown in figure S4.12B, is a photo of the blender during one of these trials. One disadvantage of using household detergent is the amount of foam generated. Shown in figure S4.12C is a TEM image of a graphene nanosheet produced in this way. Raman spectroscopy on a filtered film (figure S4.12D) shows the flakes to have a D band consistent with edge defects implying that, like the Silverson mixer, shear exfoliation does not introduce basal plane defects

DOI: 10.1038/NMAT3944

(see figure S3.16). In addition, the shape of the 2D band is consistent with few-layer graphene.[19] We can use the Raman thickness metric described in section S3.7 (eg equation 3.5) to estimate the thickness of blender exfoliated flakes to be N_G=4-5 layers. This is slightly thinner than the flakes produced by the Silverson mixer. This clearly shows that even very crude mixers can produce well exfoliated graphene. Shown in figure S4.12E is a graph of graphene concentration plotted *versus* initial graphite concentration for three mixing times showing that the yields achieved here are comparable to those obtained using the Silverson mixer.

These results clearly show that shear exfoliation of graphite is not limited to a specific mixer type but can be achieved by even the crudest mixer. This is more evidence that this process can be scaled up successfully.

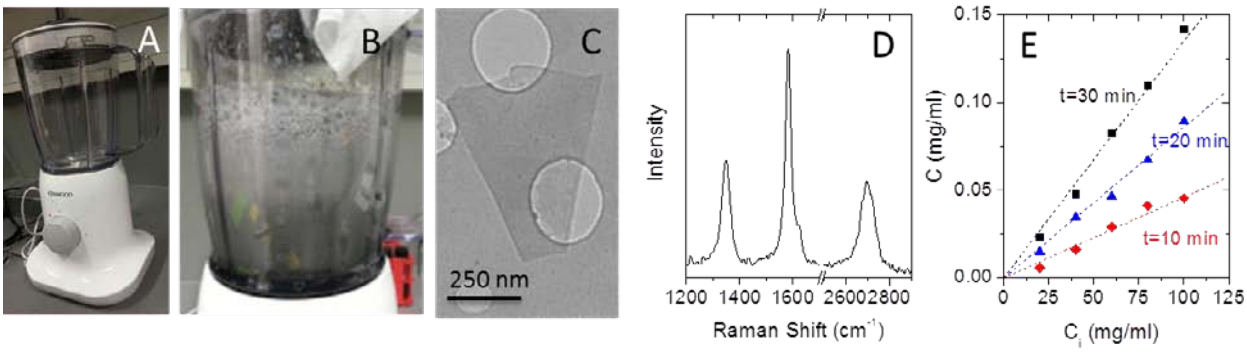

Figure S4.12: Shear exfoliation of graphite in a kitchen blender using a household detergent. A) The Kenwood blender used here. B) A photograph of the mixing process. C) A TEM image of a graphene flake produced by shear exfoliation in a blender. D) Typical Raman spectrum of blender exfoliated graphene. E) Concentration of exfoliated graphene plotted *versus* graphite concentration for three different mixing times.

It might seem surprising that a mixer as crude as a kitchen blender can be used to produce graphene. However, it can be explained as follows. In a rotating blade mixer, turbulence is produced which will result in the presence of locally high turbulent shear rates.[28] The Reynolds number (Re) associated with the rotating blade[26] is $\mathrm{Re}_{Blade} = ND^2\rho/\eta$, where ρ and η are the liquid density (1000 kg/m^3) and viscosity (0.001 Pa s) respectively. When N is at its maximum value (18 krpm for the Kenwood blender), then $\mathrm{Re}_{Blade} = 10^6$, far above the value of $\mathrm{Re}_{Blade} \sim 10^4$ where turbulence becomes fully developed.[29]

Turbulent motion results in strong spatial and temporal variation of the local shear rate.[28,30] However, the mean turbulent shear rate is controlled by the energy dissipation rate (per unit mass), ε,[30-32]

$$\dot{\gamma}_t = \sqrt{\varepsilon\rho/\eta}\,. \qquad [4.10]$$

Assuming that all of the inputted power, P, is dissipated via turbulence (i.e. $\varepsilon \approx P/\rho V$)[31] allows us to write

$$\dot{\gamma}_t \approx \sqrt{P/V\eta} \qquad [4.11]$$

Then, at maximum blade speed, P=400 W and if V=0.5 L, $\dot{\gamma}_t \approx 2.8\times10^4$ s^{-1}, well above the threshold of $\dot{\gamma}_c \sim 10^4$ s^{-1} for graphene production.

This shows that even a simple kitchen blender, so long as the power is high enough, can generate enough turbulence to give local shear rates which are high enough to produce graphene. Using equation 4.11, we estimate that, when mixing in an aqueous environment, the minimum shear rate of 10^4 s^{-1} will be exceeded, and so graphene produced, once the power density is greater than roughly $P/V \sim 100$ W/L, easily achievable in most kitchen blenders.

It is important to compare the exfoliation mechanisms in the blender v the Silverson rotor-stator mixer. As mentioned above, the blender generates high shear via turbulence throughout the vessel. In contrast, the rotor-stator mixer generates high shear in the rotor-stator gap. It is worth considering can the Silverson mixer generate turbulent shear rates throughout the vessel which are high enough to exfoliate graphite (i.e. $\dot{\gamma}_t \geq 10^4 s^{-1}$). The power inputted to the liquid by the Silverson mixer given by $P = N_P \rho N^3 D^5$ where N_P=2 and ρ is the solvent density.[29] Then using eq 4.11, the mean turbulent shear rate in the bulk of the liquid is

$$\dot{\gamma}_t \approx \sqrt{N_P \rho N^3 D^5 / V\eta} \qquad [4.12]$$

Using this, we can plot the relationship between n and D which gives $\dot{\gamma}_t = 10^4 s^{-1}$. We superimpose this line (red) on the graph reproduced from figure 2A (main text) showing the combinations of N and D which give good exfoliation. Turbulent shear rates above 10^4 s^{-1} are only produced for N>10^4 rpm for all rotors used, speeds that are inaccessible to this mixer. This data clearly shows that the Silverson mixer does not supply enough power to generate high

DOI: 10.1038/NMAT3944

enough turbulent shear to result in exfoliation throughout the bulk of the liquid. Furthermore, this confirms the high shear in the rotor stator gap to be responsible for exfoliation.

However, this figure provides one important suggestion for scale-up. For large rotors, with D>10 cm, $\dot{\gamma}_t = 10^4 s^{-1}$ can be achieved for N~1000 rpm, a speed that is achievable. This means that large rotors should be able to achieve exfoliation both through high shear rates in the rotor-stator gaps and via high turbulent shear rates in the bulk of the liquid. This might significantly increase the production rate.

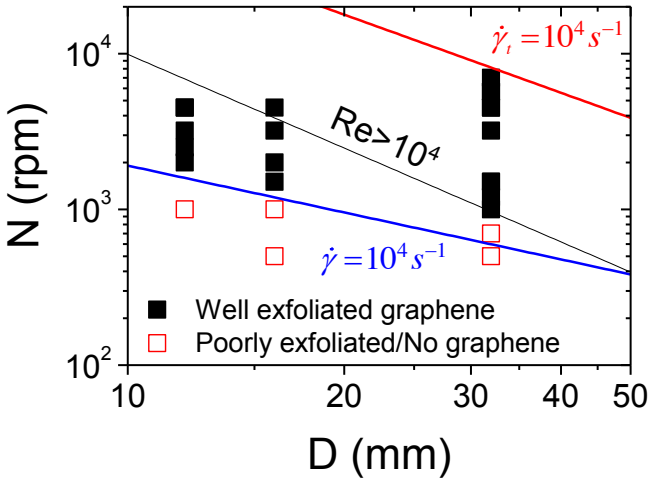

Figure S4.13: Phase diagram of rotor speed, N, *versus* diameter, D, for dispersions prepared in the Silverson mixer that show good exfoliation according to TEM (black symbols). The region above the black line represents fully developed turbulence *i.e.* Re>10^4. The region above the red line represents the scenarios when mean turbulent shear rates in the bulk liquid are above $\dot{\gamma}_t$>10^4 s^{-1}. The region above the blue line represents the scenarios when average shear rate in the rotor-stator gap is above $\dot{\gamma}$>10^4 s^{-1}.

S5 Shear exfoliation of MoS_2 and other layered compounds

Graphite is just one of a wide range of layered compounds. A number of such compounds, notably BN and the transition metal chalcogenides have been exfoliated by sonication in solvents.[4] It is important to ascertain whether such exfoliation processes can be scaled up using shear mixing.

We performed shear mixing on a range of layered materials such as boron nitride (BN), molybdenum disulphide (MoS_2), tungsten disulphide (WS_2), molybdenum selenide ($MoSe_2$) and molybdenum telluride ($MoTe_2$) in the organic solvent, N-methyl-2-pyrrolidone (NMP). We note that NMP is not necessarily the optimum solvent for all of these materials.[4,5] However, we use it in the interests of consistency.

We have carried out a full parameter dependent study for MoS_2 dispersions, varying time of mixing (t), rotor diameter (D), rotations per minute (N), initial concentration (C_i) and volume (V). After mixing, the MoS_2/NMP dispersions were centrifuged for 40 min at 1500 rpm to remove the unexfoliated MoS_2. The supernatant was collected and its absorption spectrum measured.

Since a scattering background is known to contribute to the MoS_2 absorbance in dispersions,[4] we have examined a series of samples and measured concentration by two different methods: vacuum filtration, and optical absorption measurements. In the former case, dispersions were filtered through alumina membranes (Anodisc, 20 nm pore) and the films dried in a vacuum oven. The concentration was then derived from the mass of the film and the volume of dispersion filtered. In the latter case, the concentration was derived from Beer-Lambert's law ($A/l=\alpha C$). The absorption is taken at the MoS_2 absorption peak at 679 nm. By plotting the resulting A/l values against concentration measured by mass for 20 samples, a value of 1827 $(g/L)^{-1}\cdot m^{-1}$ has been measured. This was then used to measure the concentration of subsequent MoS_2 dispersions.

The concentration of MoS_2 follows power laws in all processing parameters, giving an overall scaling parameter of $C_{MoS_2} \propto t^{0.56} C_i^{0.7} D^{1.8} V^{-0.5} N^{1.3}$ (figure 5.1). We note that as shown in the main paper (figure 3 H), the concentration also scales reasonably well with the scaling parameter found for graphene. In addition, the yield also scales well with the square root of energy density (figure S5.1-G) as shown in the main paper (figure 3A) for the graphene NMP dispersions. This produces flakes of reasonable quality (figure S5.2).

DOI: 10.1038/NMAT3944

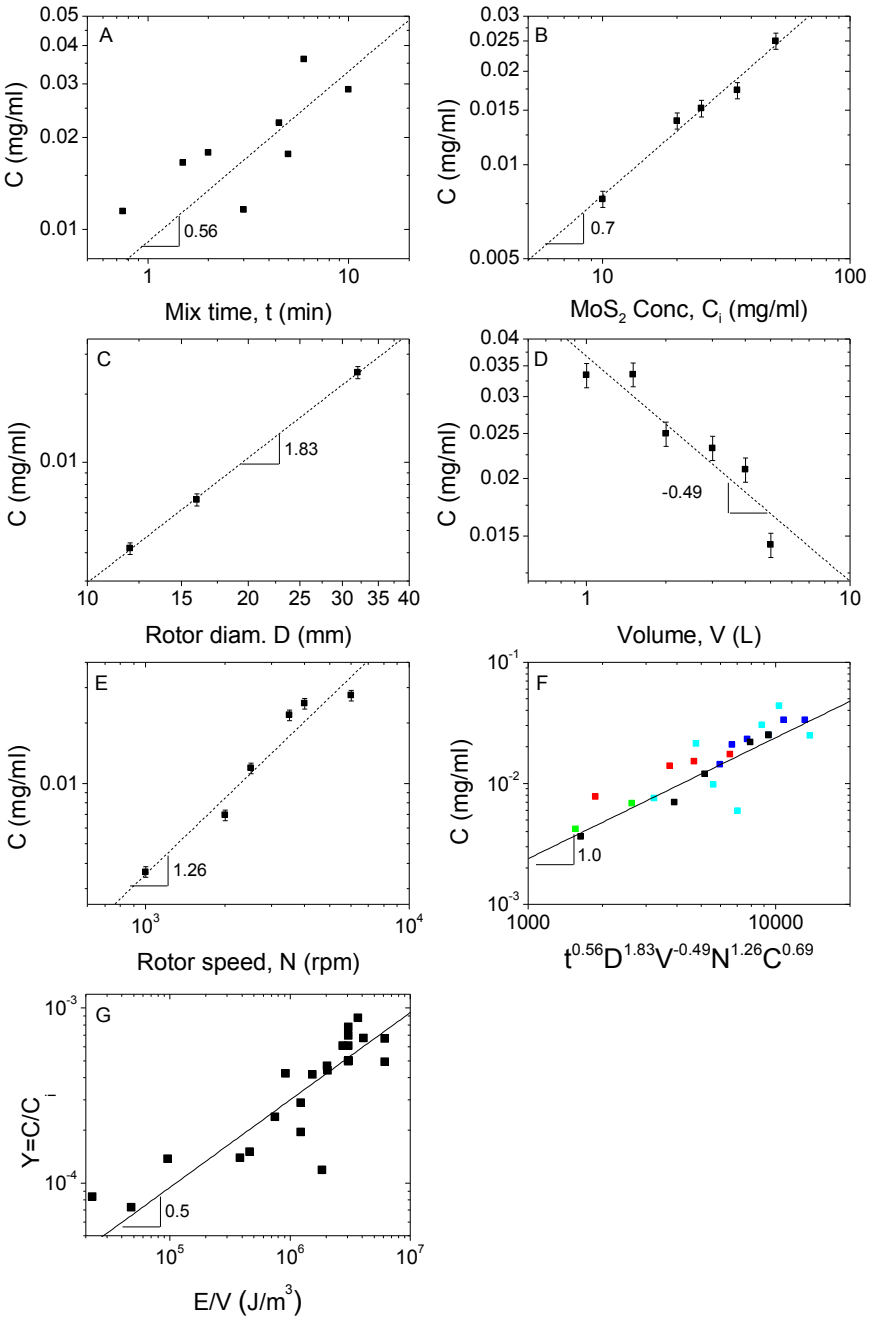

Figure S5.1: Concentration of exfoliated MoS_2 in NMP, plotted *versus*, (A-E) t, C_i, D, V, and N. F) The concentration plotted *versus* the resultant scaling parameter $t^{0.56}C_i^{0.69}D^{1.83}V^{-0.49}N^{1.26}$. G) Yield ($Y=C/C_i$) plotted *versus* energy density. The line represents square root behaviour.

Finally, we also demonstrated BN, WS_2, $MoSe_2$ and $MoTe_2$ can be exfoliated in NMP by preparing one sample for each material (C_i=25 g/L, N=4000 rpm, V=1000 mL, D=32 mm, t=5

min), measuring absorbance data and flake size by TEM (figure S5.3). Typical absorption spectra of BN, WS_2, $MoSe_2$ and $MoTe_2$ are shown in figure S5.4, which agree with reported literature.[4,5] Concentrations for these dispersions were measured by the filtration method described above, due to problems with subtracting the scattering background (see figure 3 H, main paper).

Material	**Supplier and Product**	**Particle size**[a]	**Assay**[a]
MoS_2	Sigma Aldrich, 69860-500G	~6 μm (max. 40 μm)	~98.5 %
BN	Sigma Aldrich, 255475-50G	~1 μm	~98 %
WS_2	Sigma Aldrich, 243639-50G	~2 μm	~ 99 %
$MoSe_2$	Materion, M-1102	-325 mesh	~99 %
$MoTe_2$	Materion, M-1105	<10 μm	~99 %

Table S5.1: Information on starting material for inorganic layered compound exfoliation. [a.] Supplier's specification.

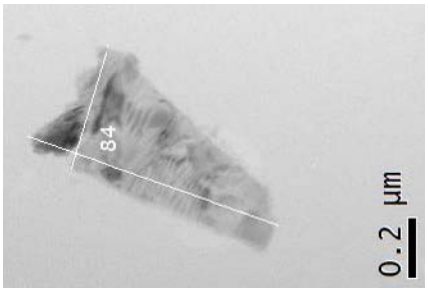

Figure S5.2: TEM image of shear exfoliated MoS_2

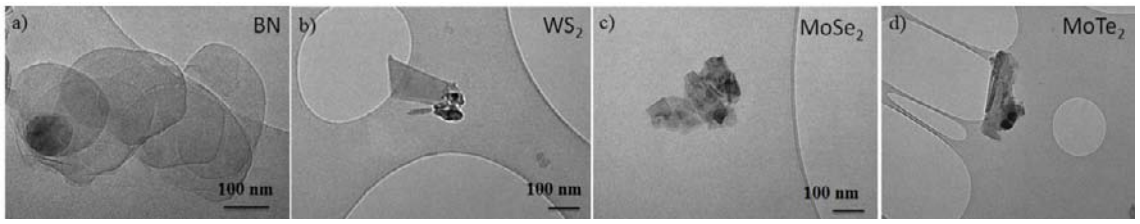

Figure S5.3: Transmission electron micrographs of nanolayered A) boron nitride (BN) and transition metal chalcogenides (TMDs) such as B) WS_2, C) $MoSe_2$ and D) $MoTe_2$ obtained by shear mixing.

DOI: 10.1038/NMAT3944

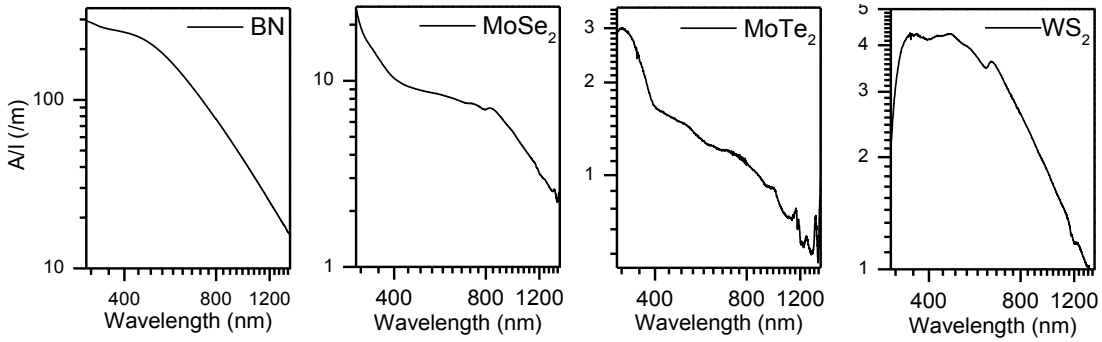

Figure S5.4: Absorption spectra of dispersions of layered materials in NMP after shear mixing.

S6 Large scale trial

In order to test the process at a pilot scale, three experiments were carried out using the test facilities at Silverson Machines Ltd. in the UK. The experimental conditions used in each experiment are summarised in table S6.1 below, along with the mixer used. In all cases the graphite was exfoliated in aqueous surfactant solutions.

Run	Graphite Source	Mixer	Type	C_i (g/L)	D (mm)	N (rpm)	V (L)	C_{surf} (g/L)	Max P_R (g/hr)
1	Sigma	275LS	In-line	10	70	3000	50	0.4	0.1
2	Sigma	DX	Batch	10	98	3000	100	0.4	0.4
3	SGN18	450LS	In-line	100	110	3000	300	2	5.3

Table S6.1: Experimental conditions used for large-scale trials.

In all three runs, the mixing time was 4 hr, with ~50 mL samples taken at regular intervals. No cooling of the vessel was used, and a maximum temperature of ~38 °C was measured after 4 h mixing. This was not thought to have affected the exfoliation process significantly. All three mixers were fitted with square-hole high shear screen. The in-line mixers are self-pumping, and no restrictions were made to the flow-rate in the pipes. Liquid was drawn from the bottom of the vessel and returned to the top, with the return pipe positioned to ensure adequate bulk circulation.

The large scale trials resulted in production of very large quantities of exfoliated graphene. TEM and Raman characterisation showed the material produced to be well exfoliated and of good quality (figure S6.1). Raman characterisation of films prepared from the 300 L dispersion shows a D/G ratio of 0.18 (averaged over 100 spectra).

The concentration scaled with time in a manner identical to the samples produced at smaller scales. The maximum measured graphene concentration was 0.07 g/L (figure S6.3). For the SGN18 graphite in both lab-scale and large-scale trials, the concentration scales as $C = 10^{-9} C_i t^{1.08} N^{2.54} D^{3.34} V^{-0.47}$.

DOI: 10.1038/NMAT3944

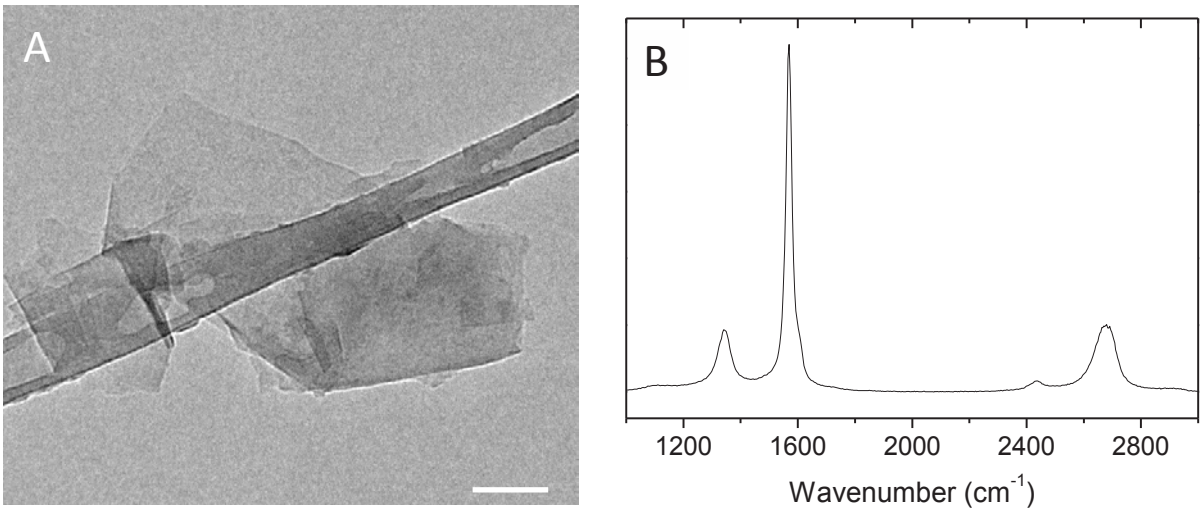

Figure S6.1: A) TEM and B) Raman of graphene prepared in 300 L shear mixing trial.

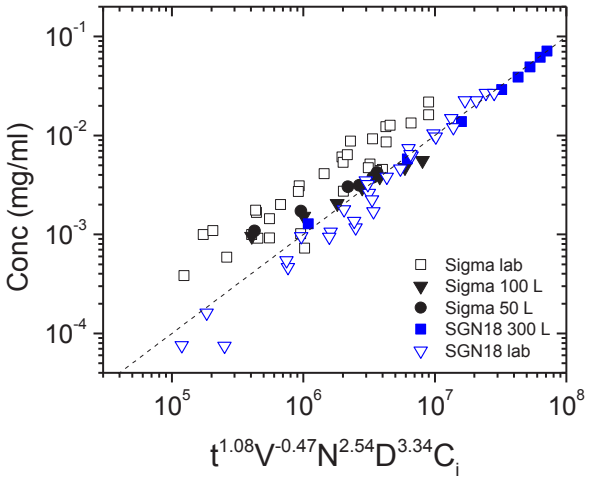

Figure S6.2: Concentration as a function of mixing time for graphite exfoliated in aqueous surfactant solutions. Two types of graphite were used, purchased from Sigma-Aldrich and SGN18 graphite, purchased from FutureCarbon. The open symbols represent lab-scale trials (V<5 L) while the closed symbols represent large scale trials (V up to 300 L).

The production rate can be calculated as $P_R = VC/t$. The production rates were much higher than the lab-scale dispersions, reaching 5.3 g/h for the 300 L batch process. Using the scaling equation above, amd the dashed fit line in figure S6.2, the production rate scaled as

$$P_R = 10^{-9} C_i t^{0.08} N^{2.54} D^{3.34} V^{0.53} \approx 10^{-9} C_i N^{2.54} D^{3.34} V^{0.53} \quad [6.1]$$

In this case, the production rate is independent of t and the analysis is simpler than that given in section 4.3. Assuming $D = k_3 V^{1/3}$ and k_3=0.325 (see section S4.3), then

$$P_R \approx 2.3\times10^{-11} C_i N^{2.54} V^{1.64} \quad [6.2]$$

This can be used to estimate the production rate using surfactant on scale-up to V=10 m^3. Taking C_i=100 g/L and N=3000 rpm, gives 7.5 kg/h, significantly larger than the 0.1 kg/h estimated for NMP exfoliation (section S4.3).

However, if there are limitations to the speed of such large rotors (for V=10 m^3, $D = k_3 V^{1/3}$ implies D=0.7 m) such that N=5/D (section 4.3), then

$$P_R \approx 2.4\times10^{-8} C_i V^{0.8} \quad [6.3]$$

Giving P_R=54 g/h, considerably smaller than the 100 g/h estimated for NMP (section S4.3).

However, we note that under the constraint that N=5/D, the production rate grows faster for surfactant exfoliation (equation 6.3) than NMP exfoliation ($P_R(V) = 6.4\times10^{-6} V^{0.59}$, section S4.3). This means that for very large tanks V>100 m^3, surfactant exfoliation becomes more efficient (figure S6.3).

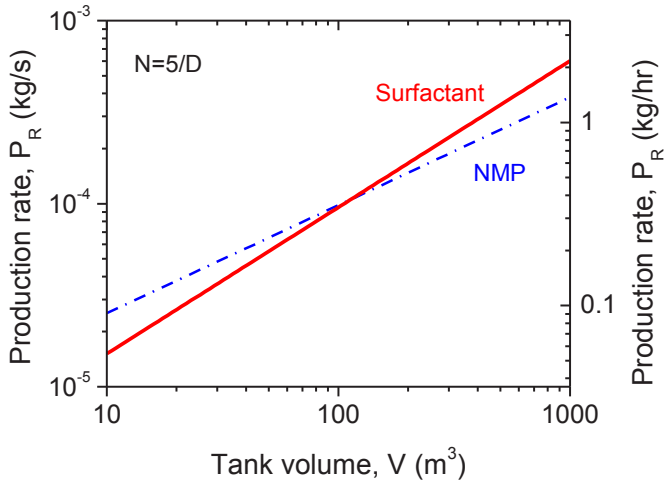

Figure S6.3: Production rate of graphene in both surfactant and NMP plotted against tank volume under the conditions that $D = 0.325 V^{1/3}$ and N=5/D.

DOI: 10.1038/NMAT3944

S7 Rheology: is turbulence required?

When assessing the mechanism of exfoliation, it is important to know whether turbulence is required for shear induced exfoliation. It is well known that fully developed turbulence exists in rotor/stator mixers such as that used here when the effective Reynolds number is above 10,000 ($Re>10^4$).[29] In rotor-stator mixers, the Reynolds number is generally taken as[29]

$$\mathrm{Re}_{Mixer} = \frac{\rho N D^2}{\eta} \qquad [7.1a]$$

Thus, to assess the importance of turbulence, it is important to ascertain the range of mixing conditions (i.e. combinations of N and D) under which graphene can be made. To do this, we performed TEM analysis on dispersions produced for a range of combinations of N and D. The samples studied were those prepared for the initial mixing study (see above), the flake length measurement study (see below) and a number of other samples produced to extend the N-D space explored. Shown in figure S7.1 is a map of N-D parameter space showing (squares) the samples analysed by TEM. The samples were either designated as well exfoliated (filled squares) or poorly exfoliated i.e. containing many thick, black, electron opaque flakes or clearly aggregated flakes or no flakes observed (open squares). It is clear from this data that good exfoliation occurs for all D so long as N is high enough.

Fully developed turbulence occurs in our mixer for $Re_{Mixer}>10^4$ and from eqn [7.1a], this is the case so long as

$$N > \frac{10^4 \eta}{\rho D^2} \qquad [7.2]$$

We have plotted this condition on figure 7.1 as the upper dashed line. It is clear from this graph that graphene is being produced at Reynolds numbers significantly below 10^4 and so fully developed turbulence is not required for graphene production.

This begs the question: can graphene be produced in a laminar flow environment if the shear rate is high enough? In order to test this in an environment where the shear rate was very well defined, we attempted to exfoliate graphite in NMP in a Couette cell attached to a rheometer. This type of cell consists of a small gap between two concentric cylinders, one solid and one hollow. Shear is applied when one of the cylinders rotates at a controlled angular velocity.

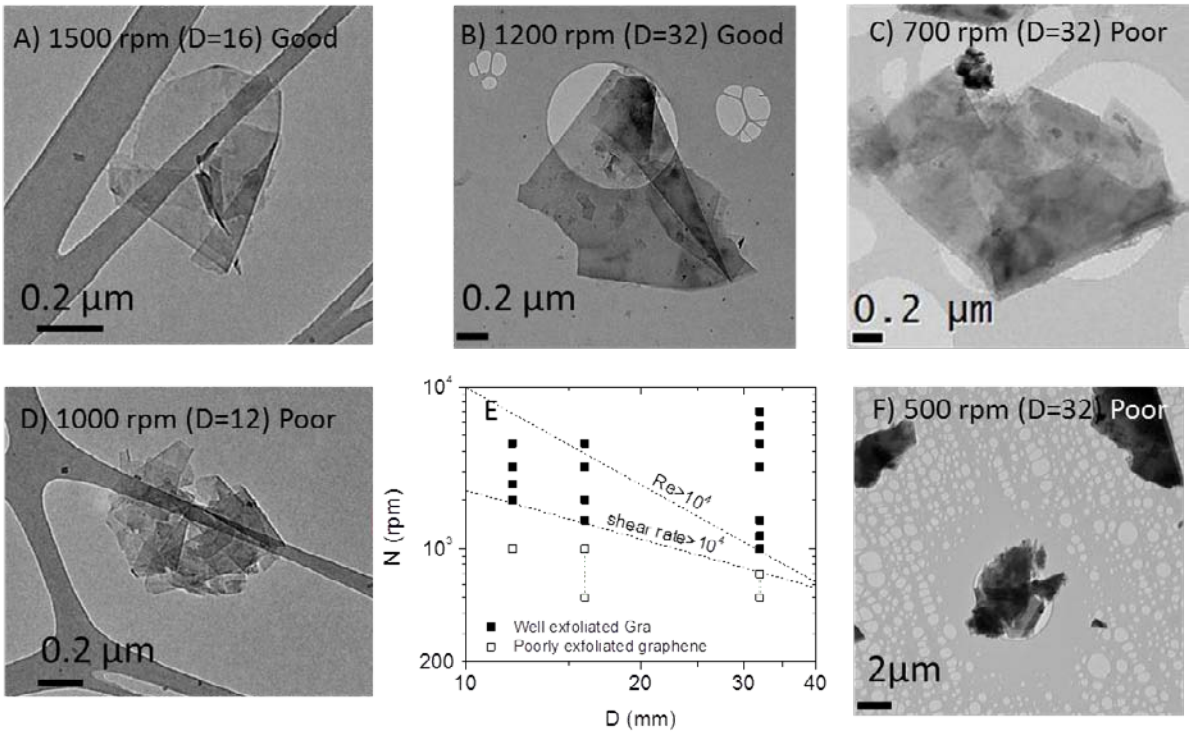

Figure S7.1: TEM images showing well and poorly exfoliated graphene. Map showing positions of samples analysed by TEM on an (N, D) co-ordinate system (N and D are rotor speed and diameter). Samples which appear well exfoliated are marked as black squares and samples which are poorly exfoliated are marked as open squares. Samples are considered poorly exfoliated if TEM shows large numbers of black, electron opaque flakes. Also shown are two dashed lines. The upper one represents the scenario where the Reynolds number, $Re=10^4$, the criterion for fully developed turbulence in rotor/stator mixers like these. The lower line represents the scenario where the effective shear rate in the rotor stator gap is $\dot{\gamma} = 10^4\ s^{-1}$. The regions of the map above these lines represent mixing conditions of $Re>10^4$ and $\dot{\gamma} > 10^4\ s^{-1}$ respectively.

S7.1 Rheological measurements

The measurements in the Couette geometry were performed with the MCR 301 Rheometer from Anton Paar. The radius of the inner cylinder is R=14.36 mm with a length of 15 mm. The gap between the inner and outer cylinder is d=100 μm. Shear is applied by rotating the inner cylinder at angular frequency ω while the outer one is stationary. These conditions ensure an almost perfectly uniform shear rate within the gap and allow us to reach shear rates of up to 45 271 s^{-1} at 3000 rpm, which is the maximum rotation rate of the rheometer. This maximum shear rate

DOI: 10.1038/NMAT3944

corresponds to a Taylor number of around 440 which is well below the critical value of 1700 at which the Taylor instability sets in (the Taylor instability represents the transition from laminar to periodic secondary flow in a Couette).[33]

The Reynolds number in a Couette is

$$\mathrm{Re}_{Couette} = \frac{R\omega d\rho}{\eta} = \frac{\dot{\gamma} d^2 \rho}{\eta} \qquad [7.1b]$$

The maximum shear rate corresponds to Reynolds number of $\mathrm{Re}_{Couette}$=275. We note that in this geometry, one report has suggested a Taylor-like instability at $\mathrm{Re}_{Couette}$ =128, even though this is below Ta=1700.[34] Thus, while we expect the flow to be laminar, we cannot completely exclude the presence of any secondary flow (i.e. the Taylor instability) at shear rates above 2.1×10^4 s^{-1} (i.e. $\mathrm{Re}_{Couette}$=128). However, at all shear rates accessible to this machine, we are very far from fully developed turbulence (as we do not see a significant increase of the apparent viscosity with shear rate for the pure solvent).

The rheometer contains a reservoir below the narrow gap such that the total volume (reservoir and gap) is 25 mL. Into this reservoir was placed 1.25 g of sieved graphite powder. To this, 25 mL of NMP was added, such that the initial graphite concentration was C_i=50 g/L. The Couette was then rotated at a well-defined speed (and so shear rate) for a pre-determined time. The liquid was then removed from the Couette, centrifuged (2000 rpm for 45 minutes) and the supernatant collected. Supernatants were generally dark, indicating the presence of dispersed graphitic material. The concentration of dispersed material was measured by absorption spectroscopy (see above). In general, TEM (see main paper, fig 3 C) and Raman spectroscopy (figure S7.2) showed the dispersed material to be few-layer graphene. This procedure was performed a number of times, rotating at 3000 rpm ($\dot{\gamma}$ = 45 271 s^{-1}) for various times from 10 to 120 minutes.

In a second set of experiments, the Couette was rotated for 60 minutes at various rotational speeds from 3000 rpm to 33 rpm. The results are plotted in figures 3 C and 3 D (main paper) as C vs. t and $\dot{\gamma}$. These results show that the concentration of graphene produced under laminar flow in the Couette scales with time as a power law with exponent 0.69. This is very similar to the exponent of close to 0.66 observed in the shear mixer for all mixing parameters. This suggests the exfoliation method to be similar for mixing under laminar, intermediate and fully developed

turbulent flow conditions. In addition, the results show the existence of a minimum shear rate, $\dot{\gamma} \approx 10^4$ s^{-1}, below which the concentration of exfoliated material is very low. Above this critical shear rate, the concentration increases rapidly with shear rate. We note that we have shown that graphene is definitely produced in the Couette for $10^4 \leq \dot{\gamma} \leq 2.1\times10^4$ s^{-1}. As described above, flow in this regime is expected to be laminar.

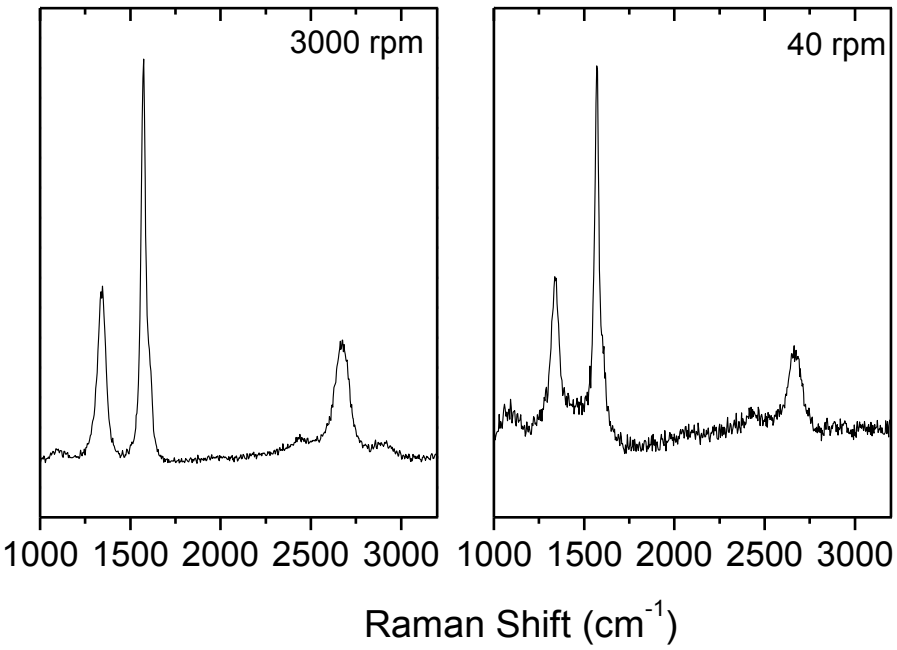

Figure S7.2: Raman spectra of material extracted from the Couette for two rotation speeds (after centrifugation). Left: After rotating at 3000 rpm for 60 minutes and Right: After rotating at 40 rpm for 60 minutes.

We note that the mixer (shear mixer not couette) data shown in figure 2 F implies a minimum value of N. We can transform N to an approximate shear rate in the rotor stator gap using

$$\dot{\gamma} = \frac{v_{tip}}{\Delta R} = \frac{\pi DN}{\Delta R} \qquad [7.3]$$

where ΔR is the rotor-stator gap. We note that when plotted against shear rate (rather than N), the mixer data (figure 3 E, main paper) also show evidence for a minimum shear rate close to 10^4 s^{-1}. We also note that the data in figure S7.1 are consistent with good exfoliation only occurring for

DOI: 10.1038/NMAT3944

combinations of N and D such that $\dot{\gamma} \geq 10^4$ s^{-1} (i.e. $\dot{\gamma} = \pi DN / \Delta R > 10^4$ so $N > 10^4 \Delta R / \pi D$ see lower dashed line).

This combination of data from the Couette and the shear mixer show clearly that graphene is not produced in any meaningful quantities unless the local shear rate is $\dot{\gamma} > 10^4$ s^{-1}. In order to understand this presence of a minimum shear rate for exfoliation, it will be necessary to develop a simple model for exfoliation due to shear.

S7.2 Shear exfoliation model

The data for graphene concentration as a function of shear rate clearly show a minimum shear rate below which very little graphene is formed. We can understand this by developing a simple model to describe the shear exfoliation of graphene.

Consider two square platelets, dimensions L×L, weakly bound and initially stacked on top of each other, being placed in a flowing fluid with non-zero shear rate. The velocity differential between the top and bottom of the sheets will result in an induced shear stress, σ. This may result in shear delamination.

The induced stress can be related to the induced force, F, by $F = \sigma L^2$. For Newtonian fluids, the applied stress is related to the shear rate by Newton's law: $\sigma = \eta\dot{\gamma}$ giving $F = \eta\dot{\gamma}L^2$ or

$$\dot{\gamma} = F / \eta L^2 \qquad [7.4]$$

To assess the force, we need to consider the energetics of the delamination process. Initially, the platelets are stacked on top of each other (figure S7.3, left). The force induces relative sliding (middle figure shows sliding at arbitrary point where overlap distance is *x*). Finally delamination is complete (right figure). We can analyse this situation in terms of the interfacial energies which can be broken into three types: liquid-liquid (LL), liquid-platelet (LP) and platelet-platelet (PP).

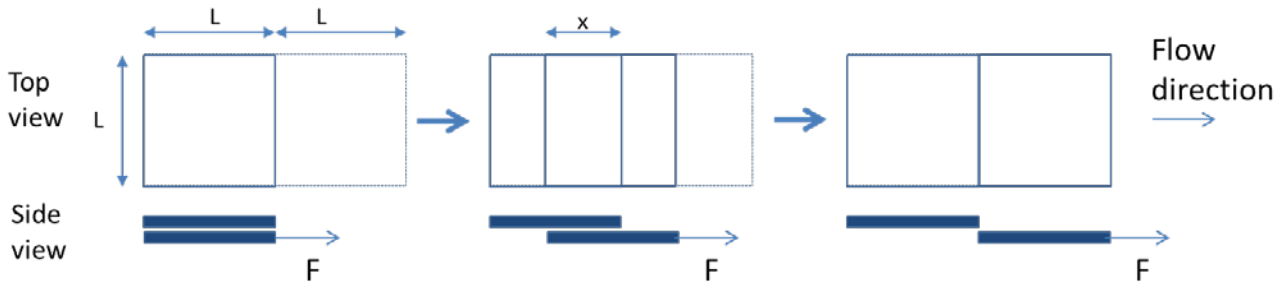

Figure S7.3: Schematic representing the shear exfoliation process.

In the initial scenario (left), within the dashed box (2L×L), there are PP and PL interactions at the relative interfaces. However, we must also consider LL interactions in the plane of the platelet-platelet interface in the region where the sheared platelet will subsequently move into. Thus the total energy (left) is:

$$E_{left} = -L^2\left[E_{LL} + E_{PP} + 2E_{LP}\right] \qquad [7.5]$$

where E_{LL}, E_{PL} and E_{PP} are areal interfacial bindings relating to the liquid-liquid, platelet-platelet and liquid-platelet interfaces respectively. The negative sign indicates that the interaction energies are negative, representing bound states. (E_{LL}, E_{PL} and E_{PP} are all positive quantities).

Similarly, in the scenario described by the middle figure, the energy is

$$E_{middle} = -L\left[xE_{LL} + 2(2L - x)E_{LP} + xE_{PP}\right] \qquad [7.6]$$

Finally, after delamination (right), the energy is

$$E_{right} = -L\left[4LE_{LP}\right] \qquad [7.7]$$

From this, we can estimate the energy change on delamination

$$\Delta E = E_{right} - E_{left} = -L^2\left[2E_{LP} - E_{LL} - E_{PP}\right] \qquad [7.8]$$

Using the geometric mean approximation,[8] $E_{LP} = \sqrt{E_{LL}E_{PP}}$, gives

$$\Delta E = L^2\left[\sqrt{E_{LL}} - \sqrt{E_{PP}}\right]^2 \qquad [7.9]$$

DOI: 10.1038/NMAT3944

Here use of the geometric mean approximation means the energy change is always positive i.e. energy needs to be supplied to result in delamination (except in the special case when $E_{LL} = E_{PP}$ and so $\Delta E = 0$).

More relevant, we can estimate the minimum applied force for delamination:

$$F_{\min} = -\partial E_{middle}(x) / \partial x \qquad [7.10]$$

$$F_{\min} = L\left[E_{LL} - 2E_{LP} + E_{PP}\right] \qquad [7.11]$$

Using the geometric mean approximation, $E_{LP} = \sqrt{E_{LL}E_{PP}}$, gives

$$F_{\min} = L\left[\sqrt{E_{LL}} - \sqrt{E_{PP}}\right]^2 \qquad [7.12]$$

This allows us to write an expression for a minimum shear rate for exfoliation of flakes of lateral size L

$$\dot{\gamma}_{\min} = \frac{\left[\sqrt{E_{PP}} - \sqrt{E_{LL}}\right]^2}{\eta L} \qquad [7.13]$$

Here E_{LL} and E_{PP} are identical to the surface energies of the liquid and the platelet. Thus, equation [7.13] can be rewritten as

$$\dot{\gamma}_{\min} = \frac{\left[\sqrt{E_{S,G}} - \sqrt{E_{S,L}}\right]^2}{\eta L} \qquad [7.14]$$

where $E_{S,G}$ and $E_{S,L}$ are the graphene and liquid surface energies.

The surface energy of the liquid must be distinguished from its surface tension. The liquid surface energy, E_{LL}, is related to the surface tension, Γ, by [35]

$$\Gamma = E_{LL} - TS_{LL} \qquad [7.15]$$

where S_{LL} is the liquid surface entropy. The surface entropy is a generic liquid property that tends to have values in the range 0.07-0.14 mJ/m^{2}K. Liquids of a given class tend to have very similar values of S_{LL}, with DMF and toluene for example shown to have values close to S_{LL}=0.11 mJ/m^{2}K [36]. Thus, we take the universal value to be ~0.1 mJ/m^{2}K. The surface tension of NMP is 40 mJ/m^2, which means the surface energy is 69 mJ/m^2 at room temperature.

From the data in figure 3-D, $\dot{\gamma}_{min} = 1\times10^4$ s^{-1}. As reported below, the size of flakes exfoliated in the mixer at this shear rate (N~800 rpm) is L~800 nm. TEM measurements in Couette exfoliated flakes showed similar dimensions. Applying, eqn [7.14], this is consistent with a surface energy of graphene of ~71 mJ/m^2 This is entirely consistent with the surface energy of graphene estimated from solvent exfoliation of graphite.[6,7]

We note that a similar but less complete model for shear exfoliation was proposed by Chen *et al*.[37]

DOI: 10.1038/NMAT3944

S8 Further mechanistic analysis

S8.1 Flake length measurements

We performed TEM experiments to determine how flake length depends on mixing parameters with the aim of using this data to help understand the mechanisms involved in shear exfoliation. We produced a large number of dispersions varying one parameter at a time while the other parameters took constant values from the following set: graphite concentration, C_i=50 g/L; mixing time, t=20 min; liquid volume, V=4.5 L; rotor speed, N=4500 rpm; rotor diameter, D=32 mm. For each of these dispersions, low resolution TEM micrographs (as discussed in section 3.1) were collected and the dimensions of 100 randomly chosen flakes were measured. We also note that the data may be slightly biased to larger flakes due to a portion of very small flakes falling through the holes in the TEM grid.

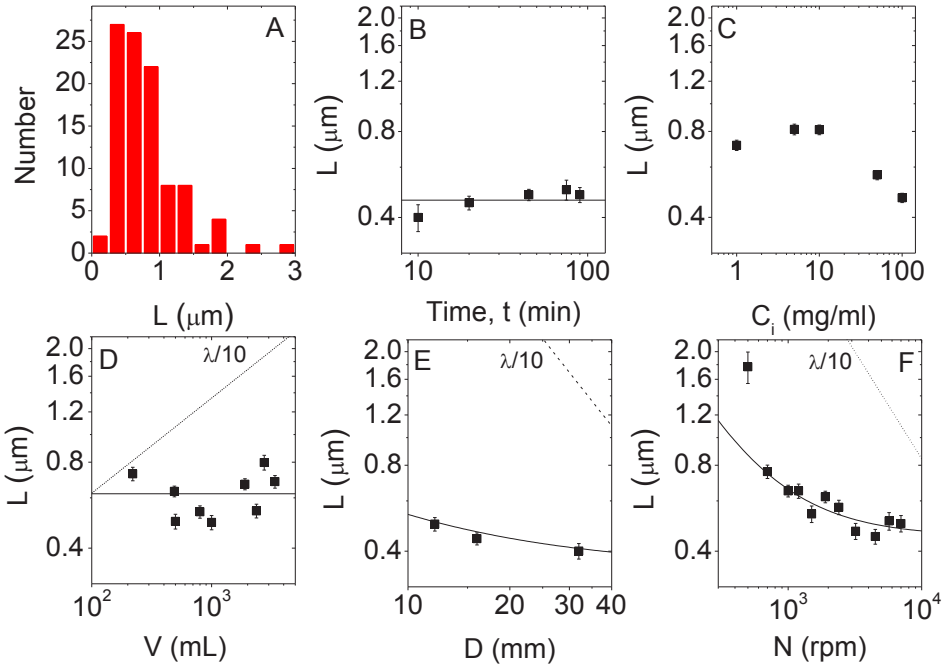

Figure S8.1: TEM measurement of flake lateral dimensions. We produced a large number of dispersions varying one parameter at a time while the other parameters took constant values from the following set: graphite concentration, C_i=50 g/L; mixing time, t=20 min; liquid volume, V=4.5 L; rotor speed, N=4500 rpm; rotor diameter, D=32 mm. A) Example of histogram of flake length measured by TEM. B-F) Mean flake length plotted *versus* B) mixing time, C) initial graphite concentration, D) liquid volume, E) rotor diameter, F) rotor speed. In B and D the solid line represents the mean of the process-independent flake length. In E and F the solid lines are

fits to equation [8.10] with fit parameters: E) E_{PP}=70.8 mJ/m^2 and L_{CF}=700 nm and F) E_{PP}=70.6 mJ/m^2 and L_{CF}=900 nm. We note that while the fit parameters are not identical, they are close. In addition, the values for L_{CF} are close to the value of L_{CF}≈1 μm suggested by the data in figure S8.3. In D, E and F, the dotted lines represent λ/10 where λ is the Kolmogorov length scale.

Shown in figure S8.1-A is an example of a flake length histogram. These histograms are generally broad with flake lengths varying from, ~100 nm to ~3000 nm. From these histograms, we calculated the mean flake length. These data are plotted *versus* processing parameter in figures S8.1-B – F. Despite the inevitable scatter, in most cases, the flake length is roughly independent of the processing parameter. The most obvious deviation from this behaviour is the data where N was varied (figure S8.2-F). Here, the flake length decreases with increasing N, appearing to saturate at L~500 nm for N>6000 rpm ($\dot{\gamma}$>7.5×10^4 s^{-1}). In addition, it is worth noting that for very low N, the exfoliation state is very poor (figure S8.2) but improves dramatically as N increases.

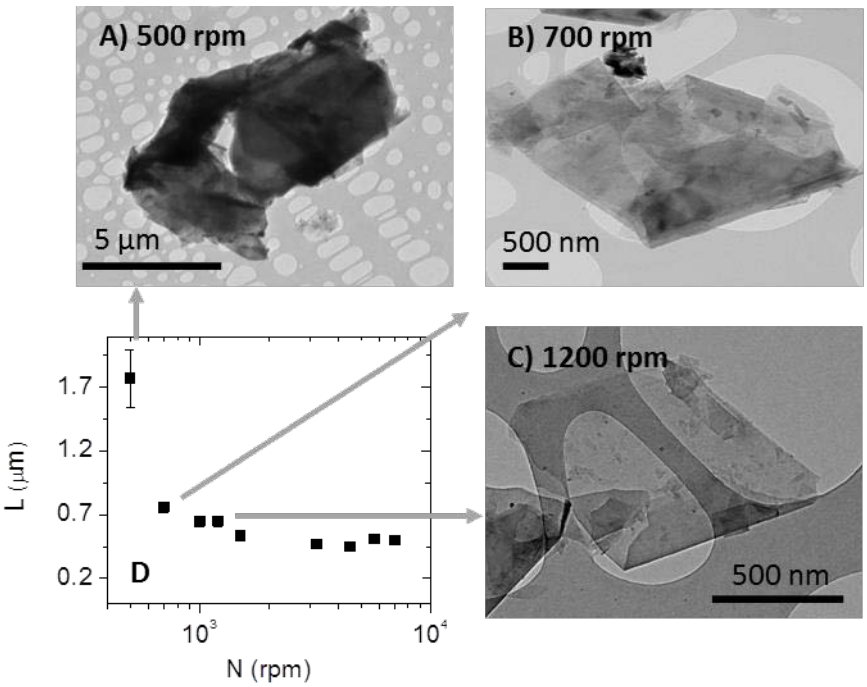

Figure S8.2: Graph illustrating the change in flake characteristics as N is decreased.

DOI: 10.1038/NMAT3944

In addition, there is a suggestion in figure S8.1-C that L may increase slightly with decreasing C_i. This might be explained by preferential aggregation of larger flakes, at high values of C_i (higher C_i – more aggregation –larger flakes more prone to aggregation). These aggregates would be removed in the centrifugation step leading to smaller the average flake size for samples prepared at higher C_i.

S8.2 Turbulent breakage?

Particle breakage under high shear is well known. In particular, particle breakage in turbulent flow has been well studied.[32] Usually, the final particle size is interpreted in relation to the Kolmogorov length scale, λ.[32,38] This is approximately the size of the smallest eddies in a turbulent system and is given by

$$\lambda = l\,\mathrm{Re}^{-3/4} \qquad [8.1]$$

where l is the length scale of the largest eddies (usually taken to be the size of the system) and Re is the Reynolds number associated with the system. For mixers, this is usually taken as

$$\mathrm{Re}_{Mixer} = \rho N D^2 / \eta \qquad [8.2]$$

where η and ρ are the liquid viscosity and density. We can approximate $l = V^{1/3}$ leading to

$$\lambda = \left(\frac{\rho}{\eta}\right)^{-3/4} V^{1/3} N^{-3/4} D^{-3/2} \qquad [8.3]$$

In turbulent mixing, the particles usually interact strongly with eddies roughly their own size. This interaction can result in breakage. The fragments then interact with smaller eddies resulting in breakage. This process continues until the particles are roughly the size of the smallest eddies (i.e. λ). By this stage there are no smaller eddies and breakage stops.[38] Thus, in this model, λ roughly represents the terminal particle size.

There are three problems with applying this model here. The first is that, as described in the main text and above, we do not always work with turbulent mixtures. Some of our dispersions (i.e. those prepared with low D and N, see figure 3-B (main text) and figure S7.1) were prepared under conditions where $\mathrm{Re}<10^4$. Under these circumstances, fully developed turbulence should not have occurred.[29] This means the cascade of eddies should not have fully developed and so breakage should not occur as described above. Secondly, even if this issue could be ignored, the

Kolmogorov length, as calculated by equation [8.1] is much larger than the size of the flakes measured by TEM (plotted on the graphs in figure S8.1 is $\lambda/10$ which is considerably larger than the observed flake length). Thirdly, graphene is the strongest material known to man with a breaking strength of 130 GPa.[39] Hydrodynamic stresses are usually used to break weakly bound agglomerates.[32] It is doubtful whether hydrodynamic stresses are able to break such a material. Thus, it is unlikely that the Kolmogorov length scale can explain the observed flake sizes.

S8.3 Mechanism controlling flake size

We believe the flake size is controlled by the mechanism described in section 7.2. Equation [7.14] describes the minimum shear rate required to exfoliate flakes of a given size. However, if there are graphite crystallites present of a range of lateral sizes, it can be interpreted as describing the minimum flake size which can be exfoliated at a given shear rate:

$$L_{\min} = \frac{\left[\sqrt{E_{LL}} - \sqrt{E_{PP}}\right]^2}{\eta\dot{\gamma}} \qquad [8.9]$$

Such a minimum size exists because a minimum flake area is required for enough force to be transferred to result in exfoliation. This means that shear exfoliation (fixed $\dot{\gamma}$) of graphite with a range of lateral crystallite sizes will result of exfoliation of crystallites above this minimum size. This means production of graphene flakes at a range of lateral sizes above L_{min}. However, after exfoliation the dispersions are centrifuged to remove any unexfoliated crystallites. We would expect this to remove both crystallites and exfoliated flakes above some cut-off size, L_{CF}. Obviously L_{CF} depends on centrifugation conditions. Thus after centrifugation, the remaining flakes exist in the range of lateral sizes: $L_{min} \leq L \leq L_{CF}$.

We can test this by examining the maximum and minimum flake size observed in the statistical data sets used to generate figure S8.1. However, care must be taken: small flakes are difficult to count and measure accurately in TEM. Some of them may fall through the grid while others may be hard to see and so be missed during image analysis. Because of this, a good deal of scatter is expected for any analysis involving minimum flakes size. Partly because of this and in an attempt to minimise the influence of outliers, we identified the 10^{th} smallest flake observed in the flake size data sets for each value of N. This value is then a proxy for the minimum flake size. Similarly we identified the 10^{th} largest flake observed in the flake size data sets for each value of

DOI: 10.1038/NMAT3944

N and used this value as a proxy for the maximum flake size. We then transformed N to shear rate (using $\dot{\gamma} \approx \pi ND / \Delta R$) and plotted both minimum and maximum flake size vs. $\dot{\gamma}$ in figure S8.3. Although the data is scattered this graph clearly shows the maximum flake size to be roughly invariant with $\dot{\gamma}$ at L_{CF}≈1000 nm. This invariance is expected for a quantity controlled by centrifugation rather than processing parameters. In addition, the minimum flake size falls off with increasing $\dot{\gamma}$ in a manner consistent with equation 8.9. This data suggests the surface energy of graphene to deviate from that of NMP by 1-2 mJ/m^2.

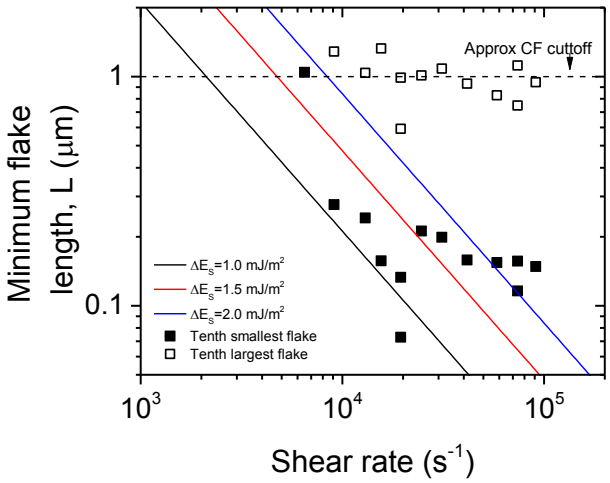

Figure S8.3: Plot of minimum flake length as a function of shear rate. Solid lines are predictions for minimum flake length, as calculated from equation 8.9. NB: ΔE_s is difference between solvent and platelet surface energies. The data represent the tenth largest and tenth smallest flakes observed in each sample (the nine largest and smallest were ignored to reduce the influence of outliers). The dashed line illustrates the fact that centrifugation (CF, 1500 rpm and 150 min) tends to remove flakes above a certain cut-off size.

As figure S8.3 confirms that the flake size exists in the range $L_{min} \leq L \leq L_{CF}$, we can approximate the mean flake size as $\langle L \rangle \approx (L_{\min} + L_{CF})/2$. Changing variable from $\dot{\gamma}$ to N gives

$$\langle L \rangle \approx \frac{\Delta R\left[\sqrt{E_{LL}} - \sqrt{E_{PP}}\right]^2}{2\eta\pi ND} + \frac{L_{CF}}{2} \qquad [8.10]$$

This is valid when $L_{\min} < L_{CF}$. As shown in figure S8.1, this data well describes the data for mean L vs. both N and D.

We can further simplify this equation by applying the approximation: $(\sqrt{x}-\sqrt{a})^2 \approx (x-a)^2/4a$ to give

$$\langle L \rangle \approx \frac{\Delta R\left[E_{LL}-E_{PP}\right]^2}{8E_{PP}\eta\pi ND} + \frac{L_{CF}}{2} = \frac{\Delta R \Delta E_s^2}{8E_{PP}\eta\pi ND} + \frac{L_{CF}}{2} \qquad [8.11]$$

where ΔE_s is the difference between solvent and platelet surface energies. This illustrates how the flake length is expected to be sensitive to the difference in surface energies between solvent and platelet.

Note equation 8.11 implies that the flake size can be controlled independently of mixing parameters by controlling L_{CF} which can be varied by varying the centrifugation rate. To test this, we prepared a dispersion using typical mixing parameters (C_i=100g/L, V=500mL, t=60min, D=32mm, N=5000rpm) and then centrifuged at different rates (centrifugation time 150 min). We then measured the graphene concentration and the mean nanosheet size (figure S8.4). We do indeed see a considerable dependence of nanosheet size on centrifugation rate. This will allow control of nanosheet size. However the concentration falls off with increasing rate as expected. This is because increasing rpm reduces L_{CF}, leaving fewer and fewer nanosheets dispersed after centrifugation.

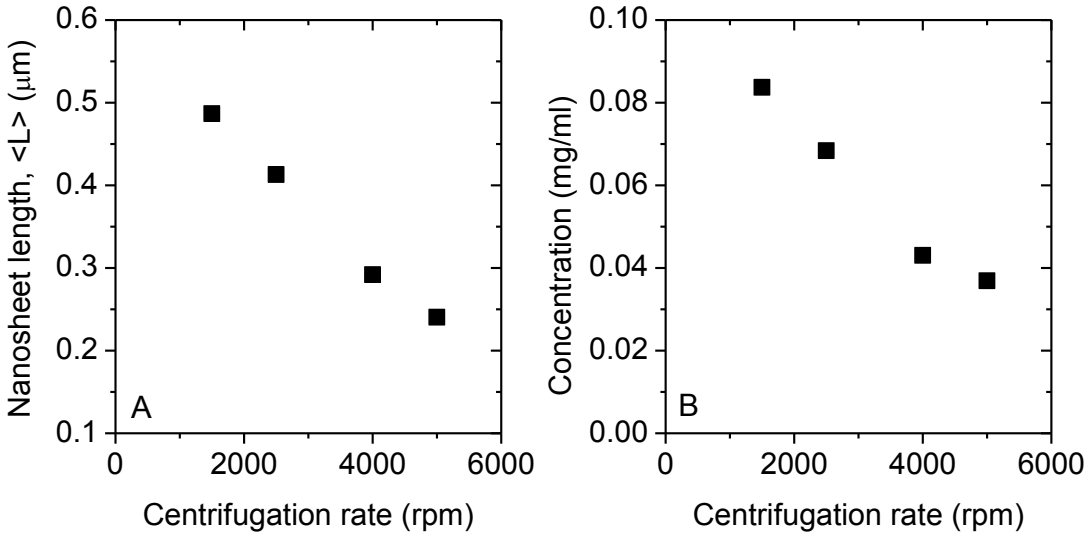

Figure S8.4: The effect of varying centrifugation rate on A) flake size and B) concentration.

DOI: 10.1038/NMAT3944

S8.4 Solvent limitations

The mechanism outlined above suggests a natural limit to graphene production in solvents. When $L_{\min} \geq L_{CF}$, all graphene flakes produced are big enough to be removed by centrifugation. This occurs when:

$$\frac{|\Delta E_s|}{\sqrt{\eta}} \geq \sqrt{\frac{4\pi L_{CF} E_{PP} N D}{\Delta R}} \qquad [8.12]$$

So, for lab scale exfoliation, assuming L_{CF}=1 μm, E_{PP}=70 mJ/m^2, N=6000 rpm (100 rps, $\dot{\gamma} \approx 7.5\times10^4$ s^{-1}) and D=32 mm (ΔR=135 μm), the limit of graphene production is at $\left(|\Delta E_s| / \sqrt{\eta}\right)_{Max}$=0.144. Taking η~0.002 Pa s, this gives a rough estimate of $|\Delta E_s|_{\max}$ = 7.5 mJ/m^2. This is a relatively narrow range, meaning relatively few solvents are suitable for shear exfoliation. However, it includes many of the solvents which can be used to exfoliate graphene[6,7] (or other layered compounds[4,5]).

S9 Comparison with other production methods

S9.1 Comparison with sonication

Much of the work in the literature (see below) to produce defect-free graphene involves sonicating graphite in solvents. However, we note that sonication is generally carried in small volumes from 10s to 100s of mL. As we have shown in this work however, shear mixing can be carried out in volumes up to 100s of L. In order to compare the efficacy of shear exfoliation *versus* sonication, we prepared graphene by sonication of the same starting graphite in NMP using an ultrasonic tip (Sonics and Materials, VCX750) fitted with a flat-head horn transducer. Sonication was operated using a cycle of 8 s on, 2 s off to prevent damage to the horn. Typical power outputs as given by the inbuilt power meter were 16-22 W.

In order to make an appropriate comparison, the graphite was sonicated in volumes similar to those used in the mixer (220-1000 mL) and for similar times (15-360 minutes). In all cases the dispersions were centrifuged and the concentration measured in the same way as for the mixer. From the concentration, we calculated the production rate ($P_R = VC/t$) and yield ($Y=C/C_i$). These three parameters are plotted *versus* the total energy input per unit volume. For the mixer, this was calculated from $E/V = tP/V$ where P is the power output of the mixer as given by $P = N_P \rho N^3 D^5$ where $N_P=2$ and ρ is the solvent density.[29] This gives

$$\frac{E}{V} = \frac{N_p \rho t N^3 D^5}{V} \qquad [8.13]$$

(N.B this means that $\sqrt{E/V} \propto t^{0.5} N^{1.5} D^{2.5} V^{-0.5}$). For the sonicator, E/V is calculated as for the mixer but where the power is taken from the reading of the built-in power meter.

The resultant data is shown in figure S9.1 and clearly shows the mixer to be far superior in all cases. For example, the graphene yield is ~10 times higher for the mixer than the sonicator for E/V= 100 MJ/m^3. Most importantly, the trends are such that the differential gets wider as E/V decreases. This is important as this is the regime that will be important on scale-up (large V). We note that at very high values of E/V (i.e. those found when sonicating small volumes) sonication may surpass shear mixing. However, such regimes are irrelevant for scale-up.

Essentially, we can sum up these results as follows. If high concentrations are required, then the best results will be achieved by sonicating at high energy density i.e. for long times in small volumes. However, this will give limited volumes and so limited production rates. However if

DOI: 10.1038/NMAT3944

high production rate is required, shear mixing is the only possible solution. High production rates are possible but at low yield. Nevertheless, these yields are much higher than would be achieved by sonication.

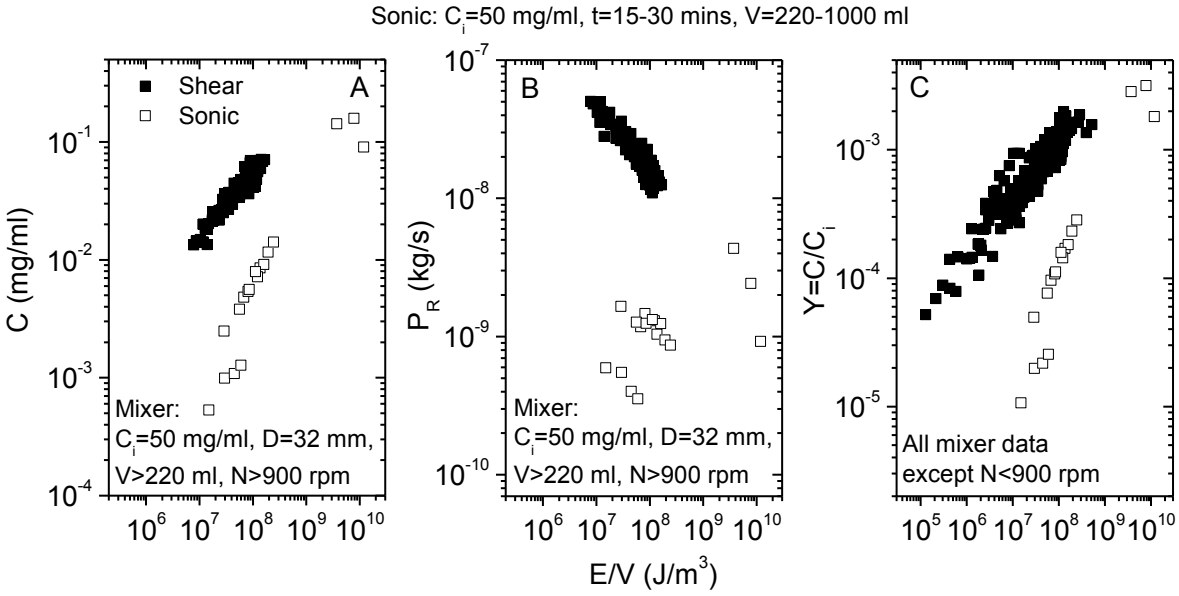

Figure S9.1: Comparison of A) graphene concentration, B) production rate and C) yield for both shear exfoliated graphene and graphene produced by sonication plotted *versus* the total inputted energy per volume. NB, In A) and B) we have limited the number of mixer data points as indicated in the panel. This is simply to avoid clutter.

S9.2 Comparison with the literature

We have analysed a number of papers which produce graphene in large quantities. In almost all cases these are liquid processing methods. The exception is the work described in ref [40]. While this described CVD growth it reports one of the largest production rates we could find. As such we thought it relevant to include. This data is summarised in table S9.1 and figure S9.2 and in all cases gives production rates far below those described here except for reference [41] which described a production rate of 1.5-2.5 g/h. However, this graphene had a relatively large Raman D:G ratio of 0.65, indicating that the flakes are very small of relatively defective. On the contrary, a number of papers report production of graphene with very small Raman ratios. However, for these papers, in no case is the production rate greater than 0.3 g/h.

Table S9.1: List of papers describing liquid exfoliation of graphene at reasonable production rates (PR). Abbreviations: GO: graphene oxide, r-GO reduced graphene oxide, GNR: graphene nanoribbon, GIC: graphite intercalation compound, son.: sonication, chem.: chemical, conc.: concentration, exf.: exfoliation, prod. Production.

Ref	**Method**	**Raman D/G**	**Oxidation state**	**Comment on production rate**	**Estimated max production rate**
This work	Shear exfoliation in solvent	0.17-0.37	None		5.3 g/h
[41]	Wet stirred media milling in the presence of SDS	~0.6-0.7 (532nm)	None: XPS C1S identical to feed material	Max c = 25 g/L, V = 0.6 L, t = 3 h (initial graphite conc. of 50 g/L). Assume beads take up ~50-75% of volume.	1.5-2.5 g/h
[40]	CVD from sodium ethoxide	~1 (532 nm)	Edge termination by -C(O)OH		~1 g/h
[42]	Intercalation with K (glovebox)	No Raman	Not discussed	Intercalation: m = 70 g, t = 3 d, PR refers to intercalation process without washing and redispersion	Intercalation: 0.9 g/h
[43]	Reduction of GO (produced by modified Hummer's method) by water	No Raman	16 % O according to XPS, 13 % according to EA	No yield given for dispersion of reduced GO, PR for GO preparation (assuming ~3 h per filtration step) and GO reduction (with 100 % yield)	GO: <0.6 g/h GO reduction: 0.45 g/h
[44]	Interlayer catalytic exfoliation with	0.1 (633 nm)	None: XPS C1S identical to feed material	Demonstrated for 10 g graphene in 5	0.4 g/h

DOI: 10.1038/NMAT3944

	$FeCl_3$ and H_2O_2 (glovebox)			L, overall process duration 26 h	
45	Reduction of GO by Na in liquid NH_3	~ 1.4 (514 nm)	O: 5.6 %, N: 0.9 % (XPS)	PR refers to reduction of GO (without GO production): m = 0.5 g, t ~ 1.5 h, V = 100 mL, assuming 100 % yield	GO reduction: 0.33 g/h
46	Exfoliation by chlorosulfonic acid and H_2O_2	0 (514 nm)	None: XPS C1S identical to feed material	Small scale proof of principle, no yield stated after redisperison of intercalated material, PR refers to dried powder	~0.25 g/h
47	Electrochemical charging and Li intercalation of a graphite electrode	<0.2 (532 nm)	None (XPS identical to feed material after washing)	m = 2 g, t ~ 12 h, (yield 70 % of dry FLG powder, 15 g demonstrated)	Powder: 0.12 g/h
48	GO reduction by hydroiodic and acetic acid	1.1 (514 nm)	O content 7.2% (XPS), C:O ratio 15.3	Reduction: m = 2.8 g, V = 1.5 L, t = 40 h (without GO formation, processing and dispersion)	GO reduction: 0.07 g/h
49	Oxidation of graphite by nitronium ions (microwave)	0.45 (785 nm)	C content 79 % (XPS)	c = 3 g/L, Oxidation: t = 30s, Dispersion t = 30 min, V assumed 10 mL	0.06 g/h
50	GO produced by modified Hummers' method	~ 1.3 (633 nm) after reduction	Ratio C-O to C-C in XPS C1s core level ~1.2:1 in GO	c = 12.5 g/L, V = 0.5 L, t ~ 5 d	GO: ~0.04 g/h
50	GO by Staudenmaier method. Never	~1 for GO, surfactant wrapped GO			0.04 g/h

	reduced, direct functionalisation	and two functionalised (514 nm)			
51	GO production (Brodie method)	~ 1.4, very broad (633 nm)	C-C and C=C: 78 % (XPS C1s core level fitting)	GO production: m = 1 g, t = 25 h, no yield given, PR assuming 70 %	GO production: 0.028 g/h
52	GO by modified Hummers' method	No Raman	$C_{3.62}$ $O_{3.10}$ $H_{1.94}$ (EA)	c = 2 g/L, V = 40 mL, t ~ 3 h (GO preparation and dispersion), m(GO) ~ 10 g	0.027 g/h
53	GO by Hummers' method	~ 1.4, very broad	Typical r-GO	Max c = 5 g/L, V = 100 mL, t = 21 h (GO preparation, delamination and reduction)	0.02 g/h
54	Sonication in pyrene surfactant (expanded graphite)	~0.33 (633 nm), starting powder , ~ 0.3 in starting powder	None suggested by Raman and TGA	c = 1 g/L, V = 20 mL, t = 1 h	0.02 g/h
10	Sonication in surfactant	~0.93 (514 nm) (reasonably broad D-band)	Not discussed,		0.018 g/h
55	Sonication in isopropanol	0.2-0.4 (633 nm)	XPS identical to feed material	c = 0.25 g/L, t = 20 min, no V given, PR estimated with V = 20 mL	~ 0.015 g/h
56	Intercalation by ternary KCl-NaCl–$ZnCl_2$ eutectic system (glovebox)	~0.15 (514 nm)	Very few: XPS 96.6% C, 2.9% O (similar to feed material)-	PR of preparation of intercalation compound: 0.02 g/h; 60 % yield after dispersion	~0.012 g/h
57	Grinding in ionic liquid	0.23 (514 nm)	3.6at%), c.f. 3.4at%O in starting graphite	(20wt% yield)	0.01 g/h
58	Sonication of GO	No Raman	C/O atomic ratio 2.3,	PR for dispersion	0.01 g/h

DOI: 10.1038/NMAT3944

	in solvents		Ratio C-O to C-C in XPS C1s core level ~1.4:1 (XPS)	(not GO production), max c = 1 g/L, V = 10 mL, t = 1 h	
59	Sonication and thermal treatment in NMP	< 0.15 (514 nm)	C-O < 6% (XPS)	m(initial) = 0.3 g, V = 50 mL, t = 15 h, no concentration given, PR calculated for yield 60 %	<0.01 g/h
60	Sonication in chloroform	No Raman	Not discussed	c = 0.5 g/L, V = 100 mL, t = 6 h (no centrifugation step)	$8.0x10^{-3}$ g/h
61	Sulfonation of GO to yield functionalized reduced GO	No Raman	S:C ratio 1:35, N:C ratio 1:31 (EA)	C = 2 g/L, Sulfonation and reduction process (not including GO prep.): t ~ 28 h, PR assuming V = 100 mL	$\sim 7x10^{-3}$ g/h
62	Sonication from Graphite. Surfactant, NMP and o-DCB	~1.5 (514 nm)	Not discussed	Not given. Final conc 0.18, 0.1 and 0.06 g/L for each solvent, after 3h, 6-9h and 6-9h (1.2wt% starting). Estimate rate assuming V = 100 mL	$\sim 6\times10^{-3}$ g/h
63	Mild sonication in the presence of gum arabic	~0.25 (633 nm), FLG (5-20 layers)	Discussed in terms of Raman, electrical characteristics and band gap, significantly less defectous than r-GO	Yield: 5-6%, Initial graphite conc. 10 g/L, PR with respect to stable FLG	$\sim 6\times10^{-3}$ g/h
64	Sonication in non-ionic polymeric surfactant	0.35	None-little suggested by Raman and XPS	m = 5.2 mg, V = 10 mL, t = 5 h, no yield given, PR refers to	$\sim 6x10^{-3}$ g/h

				60 % yield	
52	GO produced by modified Hummers' method followed by reduction and stabilization with *p*-phenylene diamine	0.65, but fluorescence background, very broad bands (514 nm)	81 % C after reduction (XPS)	GO (solid): m = 1 g, t = 6.5 h; Reduction and dispersion: m = 0.15 g, t ~ 25 h (no yield given, PR refers to 100 %)	GO solid: 0.15 g/h Red/disp: $5x10^{-3}$ g/h
14	Sonication in surfactants	0.25-0.6	Few basal plane defects according to Raman	Max c = 0.025 g/L, V = 100 mL, t = 30 min	$5x10^{-3}$ g/h
9	Sonication in NMP	~0.2-0.4 (633 nm)	Not discussed	Max c = 1.9 g/L after 270 h. V = 700 mL	$\sim 5\times10^{-3}$ g/h
65	GO and r-GO dispersion for inkjet printing	~ 0.9 (532 nm), D band broad	Typical GO and r-GO	Reduction and dispersion: initial GO c = 3.0 g/L, V = 5 mL, t ~ 2 h, no yield given, PR calculated for yield 60 %	$4.5x10^{-3}$ g/h
66	Dissolution in superacids (chlorosulphonic acid)	0.1-0.5 (514 nm; depending on centrifugation time)	XPS: increased S and O content ascribed to adsorbed/trapped acid not introduction of defects/functionalization	Conc. Graphene 2 g/L after stirring 2d, PR assumed for volume 100 mL	$\sim 4.2\times10^{-3}$ g/h
67	Exfoliation in tetraethylene glycol diacrylate by sonication	~0.15 (532 nm), 0.1 in powder	None suggested by Raman	Max c = 9.5 g/L, V = 10 mL, t = 24 h	$3.9x10^{-3}$ g/h
68	Sonication of nanoribbons in hypophosphorous acid	~0.4 (identical to GNR starting material)	Not discussed, P content 0.5 % (XPS)	c = 0.2 g/L, V = 100 mL, t estimated assuming 2 h per filtration cycle: t ~ 6 h	$\sim 3.3x10^{-3}$ g/h

DOI: 10.1038/NMAT3944

69	Exfoliation in organosilanes by sonication	0.65 (532 nm), 0.14 in powder	Little suggested by Raman	Max c = 8 g/L, V = 10mL, t = 24h	$3.3x10^{-3}$ g/h
70	Sonication in cyclohexanone	No Raman	Not discussed	m = 3 mg, t=1 h	$3 x10^{-3}$ g/h
11	Sonication in SDBS surfactant	0 on thick films (large FLG), ~ 0.4 on thin films (small flakes), 532 nm	Few basal plane defects according to Raman, IR and XPS (max. 14%)	Max c = 0.05 g/L, V = 25 mL, t = 30 min	$2.5x10^{-3}$ g/h
71	Grinding and mild sonication with ionic liquid (HMIH)	Estimated from spectra: 0.18 (532 nm)	Only addressed in terms of Raman (none suggested)	c = 5.33 g/L, V = 10 mL, sonication time 24 h (initial graphite conc. 25 g/L)	2.2×10^{-3} g/h
72	Exfoliation in vinylcaprolactam by sonication	~0.l4 (532 nm), 0.1 in powder	None-little suggested by Raman	Max c = 5 g/L, V = 10 mL, t = 24h	$2.1x10^{-3}$ g/h
73	Sonication in SC surfactant	0 (488 nm)	None suggested by Raman	c = 0.25 g/L, V = 100 mL, t = 12 h	$2 x10^{-3}$ g/h
74	High-shear mixing and sonication in ODCB	<0.3 (514 nm)	O content , 10 % (XPS)	Max c = 0.03 g/L, V = 100 mL, t = 1.5 h	$2.0x10^{-3}$ g/h
75	GO produced by modified Hummers' method	1.2-1.6 (488 nm)	Ratio C-O to C-C in XPS C1s core level ~1:1 in GO	Yield 4.3 wt%, m_i = 2 g, t ~ 2d	GO: $\sim1.8x10^{-3}$ g/h
76	Mild sonication in the presence of 1-pyrene carboxylic acid	~0.15 (532nm)	XPS: slight increase in C-O species, attributed to adsorbed surfactant	V = 250mL, t ~ 1.5 d, no yield given, dispersed graphene conc. estimated from absorbance (assuming abs_{660nm}=1/2 abs_{270nm}, α (graphene in aqu. surfactant)= 1390 mL $mg^{-1}m^{-1}$)	$<1.7\times10^{-3}$ g/h

77	Exfoliation in diisocyanates by sonication	0.2-0.3 (532 nm), 0.11 in powder	None-little suggested by Raman	Max c = 3.8 g/L, V = 10mL, t = 24 h	$1.6x10^{-3}$ g/h
78	Microwave irradiation of $FeCl_3$ and CH_3NO_2 co-intercalated graphite	0, but FLG (~ 5 layers)	Raman suggests none	GIC prepared by refluxing in nitromethane for 6 days, Exfoliation of GIC within seconds by microwave	GIC: 1.4×10^{-3} g/h Exfoliation of GIC: 1.2 g/h
21	Sonication in NMP	< 0.25 (633 nm) for bath, < 0.35 for tip (633 nm)	None suggested by Raman	c = 0.45 g/L, V = 500 mL, 168 h	$1.3x10^{-3}$ g/h
79	Sonication in NMP	0.25-2.5 (457, 514, 633 nm)	Not discussed	Volume not given, final conc 0.11 g/L after 9 h Estimate rate assuming V = 100 mL	~1.2×10^{-3} g/h
80	Sonication in surfactants	~0.9 (514 nm)	Not discussed	c = 0.7 g/L, no t and V given, PR assumed for V = 20 mL, t = 12 h	$1.2 x10^{-3}$ g/h
81	Sonication with non-ionic block copolymers	~0.45 (514 nm)	Not discussed	c = 0.07 g/L, V = 8 mL, sonication time 30 min, initial graphite concentration 75 g/L	1.1×10^{-3} g/h
82	Sonication of GO with triblock copolymer surfactant	No Raman	Not discussed	c = 16 g/L, t = 1 h, Volume not given, PR refers to 100 mL of stabilized GO produced acc. to ref[83]	GO prod: ~$1x10^{-3}$ g/h GO disp.: 1.6 g/h
83	GO by Staudenmaier	No Raman	C/H/O ratio is 86.4/0.8/11.3 after		~$1x10^{-3}$ g/h

DOI: 10.1038/NMAT3944

	method. Thermal reduction		reduction (elemental analysis), C/O ratio as low as 9.7 (XPS)		
84	Intercalation with ICl and IBr (to obtain bi-and trilayers)	<0.2 (633 nm)	None suggested by mapping large flakes in Raman	Graphite expansion: m = 0.05 g, t = 48 h (yield ~90%)	Expansion: $<1x10^{-3}$ g/h
85	Exfoliation in Ionic Liquid	0.17 (c.f. 0.05 for graphite)	XPS shows possible covalent bonding w/ IL	(0.95 g/L)	$9.5x10^{-4}$ g/h
86	Sonication in NMP	~0.36	Not discussed	Max c = 2.21 g/L, V = 10 mL, t = 24 h	$\sim 9\times10^{-4}$ g/h
87	r-GO dispersion in organic solvents	~ 1.4 (532 nm)	Typical GO and r-GO	GO dispersion and reduction: c = 0.3 g/L, V = 40 mL, t = 14 h	$8.6x10^{-4}$ g/h
88	Wet ball milling of graphene nanoribbons in DMF	0.34	Not discussed	No yield of exfoliated material given, PR refers to raw dispersion	$<7\times10^{-4}$ g/h
89	Sonication in water-acetone	0.25 (514 nm)	None: XPS C1S identical to feed material	Max c = 0.2 g/L, V = 30 mL, t = 12 h,	$5x10^{-4}$ g/h
90	Polymer stabilization of r-GO	No Raman	Typical GO and r-GO	c = 1.8 g/L, V = 12 mL, t = 48 h (dispersion process only)	$4.5x10^{-4}$ g/h
91	Oxidation followed by functionalization with alkylamine	No Raman	Not discussed	c = 0.5 g/L, t ~ 5.5 d, PR assuming V = 100 mL	$\sim 4x10^{-4}$ g/h
20	Sonication in low boiling point solvents	< 0.4 (633 nm); starting powder 0.14	None suggested by Raman	Max c = 0.5 g/L, V = 30 mL, t = 48 h	$3.1x10^{-4}$ g/h
12	Sonication in SC surfactant	0.57 (633 nm), up to 1.1 in slowly sedimenting	Few basal plane defects suggested (accumulated in slow sedimenting material)	Max c = 0.3 g/L, V = 400 mL, t = 400 h	$3x10^{-4}$ g/h

		components			
92	KC_8 GIC	Not given	None shown from XPS	(35% yield)	$2x10^{-4}$ g/h
7	Sonication in solvents	0 on thick films (large FLG), ~ 0.2 on thin films (small flakes), 633 nm	None suggested by Raman, XPS: contribution from residual solvent, no C-O peak	Max. c = 0.01 g/L, V = 10mL, t = 30 min (NMP)	$2x10^{-4}$ g/h
93	Sonication in CTAB/acetic acid	~ 0.2 (532 nm)	None-little suggested by Raman	Yield ~10 %, m(initial) = 0.1 g, t = 52 h	$1.9x10^{-4}$ g/h
6	Sonication in solvents	No Raman	Not discussed	Max. c = $8.5x10^{-3}$ g/L, V = 10 mL, t = 30 min (cyclopentanone)	$1.7x10^{-4}$ g/h
94	Two-step sonication in NMP	< 0.5 (633 nm)	None suggested by Raman	Max c = 63 g/L, V = 8 mL, t = 34 h	$1.5x10^{-4}$ g/h
95	Solvothermal reduction of chemically exfoliated graphene sheets	1 (633 nm)	Less defective than GO solvothermally reduced	Chemical exfoliation: V = 15 mL, t ~ 5 h, PR assumed with yield 70 % Reduction: c = 0.03 g/L, V = 20 mL, t = 12 h	Chem. exf: $1.4x10^{-5}$ g/h Reduction: $5x10^{-4}$ g/h
96	Sonication in surfactant	~1.3	Not discussed	Rate estimated from absorbance data	$\sim 7.6x10^{-6}$ g/h
97	Heating then sonication of expandable graphite (to obtain ribbons)	Poor spectrum shown, but no D-peak visible, though only shown to edge of D-peak wavenumber ($1350cm^{-1}$)	None claimed through XPS	No details. Yield ~0.5%	
98	GO by Hummers, reduction by	~1. Just under 1 before	Marked oxides content, as well as C-N peak.	No yields given	

DOI: 10.1038/NMAT3944

	hydrazine	reduction, just over 1 after reduction.	From XPS		
99	Li GIC	>1	XPS shows no oxides or Li (after rinsing procedure)	No details	
100	Mild GO & TBA intercalation	0.81-1.1 for annealed sheets	XPS gives best 92.1 % C-C after anneal	No details given	
101	Mild sonication with perylene bisimide surfactant	Estimated from spectra: 0.4-0.6 (532 nm)	Not discussed	No details given on graphene concentration or yield	
102	GO produced by modified Hummers' method	~ 1.7 (633 nm) before and after reduction	O content 8 % after reduction on substrate (XPS)	No details given	
103	GO produced by Hummers' method	1, but fluorescence background, very broad bands (514 nm)	High, but not quantified	No details given	
104	Thermal treatment of graphite-liquid crystal composite	~ 0 (633 nm)	Defect free suggested by Raman, XPS, XRD and FT-IR	No yield given on dispersion process after dry intercalation, no mass and V given, t= 1 h	

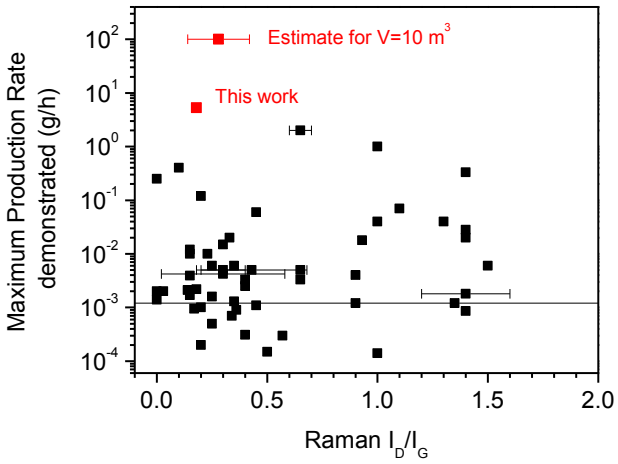

Figure S9.2: Plot of maximum production rate against Raman D:G intensity ratio for the graphene produced in the papers listed in table 9.1. Combinations of high quality (defect-free) graphene produced at high rate would be found in the top-left corner of this graph. Also shown is the maximum rate found in this work (surfactant exfoliation) and the lower limit for the production rate expected on scale-up to V=10 m^3 in NMP (see figure S4.3).

DOI: 10.1038/NMAT3944

S10 Applications of shear-exfoliated graphene

For shear-exfoliated graphene to be useful, it must be possible to apply it in the same applications as any other sort of liquid-exfoliated graphene with equivalent results. This has been demonstrated in figure 4 of the main paper. In this section we provide more information about sample preparation and measurements.

S10.1 Melt-processed composites

PET and PET/graphene nanocomposites were prepared by melt mixing at a temperature of 260 °C in a Brabender melt mixer. The melt mixing was performed by adding approximately half of the polymer quantity to the mixing bowl. Once the torque started to increase, finely ground graphene powder (produced by filtering a shear exfoliated graphene dispersion) was added to the mixing bowl. When the polymer melted and the torque started to diminish, the remaining polymer was gradually added to the mixer. Melt compounding was performed at an initial screw speed of 50 rpm for 4 minutes, then the screw speed was increased to 80 rpm within 1 minute and the melt mixing was conducted at this speed for another 5 minutes. The materials obtained via melt compounding were compression moulded at 280 °C on an electrically heated hydraulic press. The samples were quenched and then cut into 10 mm wide stripes in order to perform mechanical testing. The tensile tests were conducted on a Zwick Tensile Tester using a load cell of 2.5 kN and a speed of 5 mm/min. For both PET and 0.07 wt% composite, 5 strips were tested mechanically. In each case the resultant mechanical properties are given in table S10.1

	Modulus (GPa)	Strength (MPa)	Strain at break (%)
PET	0.81±0.04	52±8	8.4±1.0
0.07wt% Graphene in PET	0.92±0.01	73±5	10.1±2.0

Table S10.1: mechanical properties of PET and PET-graphene composites.

To put these results in context, we have performed a detailed literature analysis to assess the performance of composites of PET reinforced with a range of fillers. This information is shown in tables S10.2-5. This clearly shows that graphene performs much better than any other filler.

The relative change in mechanical properties is competitive with the best results in these tables. However, in our case, this reinforcement is obtained at much lower loading levels.

Matrix	Filler	Filler loading (wt%)	Fabrication process	% increase compared to neat polymer				Reference
				Tensile Strength (UTS)	Elastic modulus	Elongation at break	Stress at break	
PET	SWNT	0.03	Melt compounding	2	5	-3		[105]
		0.1		8	20	-8		
		0.3		8	26	-22		
		1		24	58	-31		
		3		30	60	-34		
PET	MWCNT (MD)	1	PET and PET/10 wt% MWCNT masterbatch were melt compounded on a co-rotating intermeshing twin-screw extruder Collin GmbH	7	13	~ -94		[106]
		2		16	29	~ -97		
		4		42	40	~ -97		
	MWCNT (TD)	1		11	10			
		2		16	21			
		4		30	42			

Table S10.2: Summary of previous work done on the mechanical properties of poly(ethylene terephthalate) /carbon nanotubes nanocomposites

Matrix	Filler	Filler loading (wt%)	Fabrication process	% increase compared to neat polymer				Reference
				Tensile Strength (UTS)	Elastic modulus	Elongation	Stress at break	
PET	Cloisite 15A	1	Co-rotating twin screw extruder	~27	~-3			[107]
		2		~16	~18			

DOI: 10.1038/NMAT3944

PET	organically-modified mica	0.5	Extrusion	24	12	-33		[108]
		1		2	14	-33		
		2		4	51	-33		
PET	Organic Montmorillonite (DK2)	1	Melt processing	~24		~ -37		[109]
		3		~ -13		~ -54		
		5		~ -36		~ -72		
PET	Organic modified Montmorillonite	3	Direct injection Moulded	-15	-2	-98	-15	[110]
		3	Extruded injection moulded	-11	-3	-93	-11	
PET	Rod-like silicate attapulgite	1	In situ polymerization	8	8	-79		[111]
		2		13	13	-		

Table S10.3: Summary of previous work done on the mechanical properties of poly(ethylene terephthalate) /clay nanocomposites

Matrix	Filler	Filler loading (wt%)	Fabrication process	% increase compared to neat polymer				Reference
				Tensile Strength (UTS)	Elastic modulus	Elongation at break	Stress at break	
PET	TiO_2	3	Direct injection Moulded	-33	-10	-99	-33	[110]
	SiO_2	3		-10	-3	-97	-10	
	TiO_2	3	Extruded injection moulded	-9	-3	-11	-9	
	SiO_2	3		-9	-3	-25	-9	
PET	Isooctyl POSS cage mixture	5	Melt processing	33	36	-53		[112]
	TriSilanol-	5		0	18	-25		

	Isooctyl-POSS							
	TriSilanol-Isooctyl-POSS	2.5	In situ polymerization	-17	-72	-25		

Table S10.4: Summary of previous work done on the mechanical properties of poly(ethylene terephthalate) /miscellaneous fillers composites

Matrix	Filler	Filler loading (wt%)	Fabrication process	% increase compared to neat polymer				Reference
				Tensile Strength (UTS)	Elastic modulus	Elongation	Stress at break	
PET	Glass Fiber	35	Melt compounding (without knit lines)	136		-67		[113]
PET		35		137		-69		
PET	Short Glass Fiber	10	Melt compounding	~20	~56	Reduces significantly		[114]
		20		~78	~152			
		30		~100	~248			
PET	Glass Fiber	23.3	Melt compounding	56		-50		[115]
PET	Glass Fiber	36		140		-96		[116]
PET	Glass Fiber	30		190				[117]
PET	SiO_2-MgO-CaO whiskers	1	in situ polymerization	~19	~82			[118]
		3		~52	~80			
		5		~52	~78			

Table S10.5: Summary of previous work done on the mechanical properties of poly(ethylene terephthalate) /glass fibers composites.

DOI: 10.1038/NMAT3944

S10.2 Dye-sensitised solar cells

To produce the dye-sensitised solar cells, TiO_2 on fluorine-doped tin oxide (FTO) coated glass was purchased from Solarprint Ltd. The electrode was then sintered in oxygen atmosphere at 450 °C for 30 minutes in a furnace to burn off the organic binder and other organic additives before being allowed to cool slowly to avoid cracking of the TiO_2 or glass. To stain the TiO_2 electrode, dye solution was prepared by dissolving dye N-719 (purchased from Dysole Ltd) in anhydrous ethanol at 3×10^{-4} M using a sonic bath for 2 h and then stirring overnight. The TiO_2 electrode was soaked in this dye solution for 72 h. After removing from the dye solution, it was rinsed with ethanol, dried under a light bulb and assembled immediately as described below.

The counter electrode consisted of a graphene film on a PET substrate. A graphene film (15 μm thick) was prepared by filtration onto a nylon membrane from a shear-exfoliated NMP dispersion as described previously.[9] This film was then peeled off the membrane and attached onto a PET substrate by hot pressing (70 kN, 290 °C, 5 minutes). A 1.5 × 2 cm section was cut from this for use as a counter electrode. For comparison, a standard platinum electrode was made by evaporating 20 nm Pt on FTO glass.

Just before assembling the cell, the TiO_2 electrode was rinsed in ethanol to remove any absorbed moisture or excess dye. Once the electrode was dried, a droplet of electrolyte (organic solvent based electrolyte - EL-HPE from Dysole Ltd) was placed on the TiO_2. To avoid shorting of the cell a thin plastic spacer (Meltonix 1170-25 Dysole Ltd) was inserted on top of the TiO_2 electrode. The counter electrode was then placed on top of the spacer.

I-V curves were measure using a Keithley 2400 and a Oriel Instrument 66902 solar simulator at 1 sun (AM1.5).

S10.3 Supercapacitors

We have prepared thin graphitic films by vacuum filtration of graphene-rich, surfactant stabilised dispersions. We have examined the potential of these films as electrodes in micro-supercapacitors by transferring them to ITO coated glass [76]. Electrochemical characterisation consisted electrochemical impedance spectroscopy using a three-electrode cell and Gamry

Reference 3000 potentiostat. Graphene electrodes were used as the working electrode with a carbon counter electrode and Ag/AgCl reference electrode. The supporting electrolyte used for all characterisation was 1.0 M Na_2SO_4.

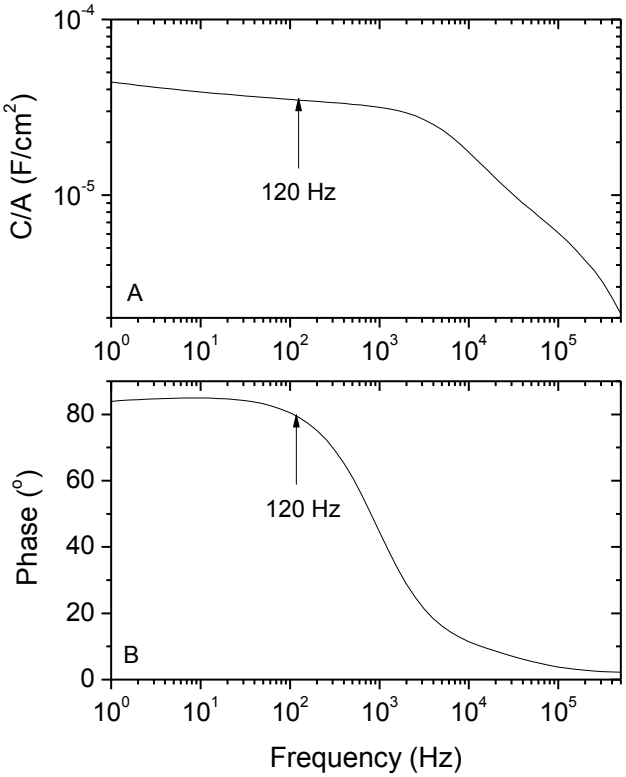

Figure S10.1: Areal capacitance and phase as a function of frequency for a 25 nm thick graphene electrode.

There is an increasing interest in the investigation of materials for supercapacitors capable of 120Hz ac line filtering [119,120]. Supercapacitors used in such applications must have high capacitance at 120 Hz (~mF for applications) and perform like pure capacitors at that frequency (rather than the more complicated equivalent circuit that more generally represents them). Thus, the phase angle at 120 Hz should be as close as possible to 90° [121]. By performing impedance measurements, we show that at 120 Hz, the impedance angle of the 25 nm graphene electrode is 79° (figure 10.1) which is comparable with thick (600 nm) graphene electrodes[119] and commercial aluminium electrolytic capacitors 83° (AECs) [120]. The areal capacitance as 0.35 mF/cm^2 (~280 F/g for a 25 nm thick film), which compares with thick (600 nm) graphene

DOI: 10.1038/NMAT3944

electrodes[119] and commercial aluminium electrolytic capacitors which displayed values of 0.088 and 0.3 mF/cm^2 respectively. We note that AECs are widely used for this purpose even though their bulk makes them among the largest components found in any electronic circuit. Because reasonable capacitance can be achieved with very thin electrodes of our graphene, mF capacitors could be built by stacking thin capacitors in a relatively small volume.

S10.4 Strain sensors

A *County Stationary No. 32* rubber band was placed in a beaker of toluene in a low power sonic bath for 3.5 hours. Under these circumstances, the band swells to approximately five times its initial volume. A dispersion of graphene in NMP was prepared by shear mixing. This was then vacuum filtered to form a film which was redispersed at high concentration by sonication (5 g/L).[94] To this was added water such that the final composition was NMP:water=20:80 by volume. The toluene-treated rubber band was then directly placed into this dispersion and stirred for 72 hours. After this treatment the rubber band was left to dry in a vacuum oven over night.

Samples for testing were prepared by cutting the band into 4 cm segments. Silver paint was applied to the ends of the band to allow for better contact with the conductive clamps holding the band in place. A Zwick Z0.5 ProLine Tensile Tester (100 N Load Cell) was used to apply dynamic strain to the band whilst a Keithley KE2601 source meter, controlled by LabView software, was used to measure the electrical resistance of the band as a function of time. Strain was applied to the band, during which resistance as a function of time, stress, and strain was recorded.

S11 References

1 Coleman, J. N. Liquid Exfoliation of Defect-Free Graphene. *Acc. Chem. Res.* **46**, 14-22, (2013).

2 Blake, P. *et al*. Graphene-based liquid crystal device. *Nano Lett.* **8**, 1704-1708, (2008).

3 Bourlinos, A. B., Georgakilas, V., Zboril, R., Steriotis, T. A. & Stubos, A. K. Liquid-Phase Exfoliation of Graphite Towards Solubilized Graphenes. *Small* **52**, 1841-1845, (2009).

4 Coleman, J. N. *et al*. Two-Dimensional Nanosheets Produced by Liquid Exfoliation of Layered Materials. *Science* **331**, 568-571, (2011).

5 Cunningham, G. *et al*. Solvent Exfoliation of Transition Metal Dichalcogenides: Dispersability of Exfoliated Nanosheets Varies only Weakly Between Compounds. *ACS Nano* **6**, 3468–3480, (2012).

6 Hernandez, Y., Lotya, M., Rickard, D., Bergin, S. D. & Coleman, J. N. Measurement of Multicomponent Solubility Parameters for Graphene Facilitates Solvent Discovery. *Langmuir* **26**, 3208-3213, (2010).

7 Hernandez, Y. *et al*. High-yield production of graphene by liquid-phase exfoliation of graphite. *Nat. Nanotechnol.* **3**, 563-568, (2008).

8 Hughes, J. M., Aherne, D. & Coleman, J. N. Generalizing solubility parameter theory to apply to one- and two-dimensional solutes and to incorporate dipolar interactions. *J. Appl. Polym. Sci.* **127**, 4483–4491, (2013).

9 Khan, U., O'Neill, A., Lotya, M., De, S. & Coleman, J. N. High-Concentration Solvent Exfoliation of Graphene. *Small* **6**, 864-871, (2010).

10 Green, A. A. & Hersam, M. C. Solution Phase Production of Graphene with Controlled Thickness via Density Differentiation. *Nano Lett.*, (2009).

11 Lotya, M. *et al*. Liquid Phase Production of Graphene by Exfoliation of Graphite in Surfactant/Water Solutions. *J. Am. Chem. Soc.* **131**, 3611-3620, (2009).

12 Lotya, M., King, P. J., Khan, U., De, S. & Coleman, J. N. High-Concentration, Surfactant-Stabilized Graphene Dispersions. *ACS Nano* **4**, 3155-3162, (2010).

13 Smith, R. J. *et al*. Large-Scale Exfoliation of Inorganic Layered Compounds in Aqueous Surfactant Solutions. *Adv. Mater. (Weinheim, Ger.)* **23**, 3944-3948, (2011).

14 Smith, R. J., Lotya, M. & Coleman, J. N. The importance of repulsive potential barriers for the dispersion of graphene using surfactants. *New Journal of Physics* **12**, (2010).

15 Bourlinos, A. B. *et al*. Aqueous-phase exfoliation of graphite in the presence of polyvinylpyrrolidone for the production of water-soluble graphenes. *Solid State Commun.* **149**, 2172-2176, (2009).

DOI: 10.1038/NMAT3944

16 May, P., Khan, U., Hughes, J. M. & Coleman, J. N. Role of Solubility Parameters in Understanding the Steric Stabilization of Exfoliated Two-Dimensional Nanosheets by Adsorbed Polymers. *J. Phys. Chem. C* **116**, 11393-11400, (2012).

17 Nemes-Incze, P., Osvath, Z., Kamaras, K. & Biro, L. P. Anomalies in thickness measurements of graphene and few layer graphite crystals by tapping mode atomic force microscopy. *Carbon* **46**, 1435-1442, (2008).

18 Ferrari, A. C. *et al*. Raman spectrum of graphene and graphene layers. *Phys. Rev. Lett.* **97**, 187401, (2006).

19 Yoon, D. *et al*. Variations in the Raman Spectrum as a Function of the Number of Graphene Layers. *Journal of the Korean Physical Society* **55**, 1299-1303, (2009).

20 O'Neill, A., Khan, U., Nirmalraj, P. N., Boland, J. & Coleman, J. N. Graphene Dispersion and Exfoliation in Low Boiling Point Solvents. *Journal of Physical Chemistry C* **115**, 5422-5428, (2011).

21 Khan, U. *et al*. Size selection of dispersed, exfoliated graphene flakes by controlled centrifugation. *Carbon* **50**, 470-475, (2012).

22 Eckmann, A. *et al*. Probing the Nature of Defects in Graphene by Raman Spectroscopy. *Nano Lett.* **12**, 3925-3930, (2012).

23 Malard, L. M., Pimenta, M. A., Dresselhaus, G. & Dresselhaus, M. S. Raman spectroscopy in graphene. *Physics Reports-Review Section of Physics Letters* **473**, 51-87, (2009).

24 Hanlon, D. *et al*. Production of Molybdenum Trioxide Nanosheets by Liquid Exfoliation and Their Application in High-Performance Supercapacitors. *Chem. Mater.*, (2014).

25 Dreyer, D. R., Park, S., Bielawski, C. W. & Ruoff, R. S. The chemistry of graphene oxide. *Chem. Soc. Rev.* **39**, 228-240, (2010).

26 Holland, F. A. & Chapman, F. S. *Liquid mixing and processing in stirred tanks*. (Reinhold Pub. Corp, 1966).

27 Holland, F. A. *Fluid Flow for Chemical Engineers* (Chemical Publishing Company, 1973).

28 Pope, S. B. *Turbulent Flows*. (Cambridge University Press, 2000).

29 Utomo, A. T., Baker, M. & Pacek, A. W. Flow pattern, periodicity and energy dissipation in a batch rotor-stator mixer. *Chem. Eng. Res. Des.* **86**, 1397-1409, (2008).

30 Marchisio, D. L., Soos, M., Sefcik, J. & Morbidelli, M. Role of turbulent shear rate distribution in aggregation and breakage processes. *AIChE J.* **52**, 158-173, (2006).

31 Boxall, J. A., Koh, C. A., Sloan, E. D., Sum, A. K. & Wu, D. T. Droplet Size Scaling of Water-in-Oil Emulsions under Turbulent Flow. *Langmuir* **28**, 104-110, (2012).

32 Wengeler, R. & Nirschl, H. Turbulent hydrodynamic stress induced dispersion and fragmentation of nanoscale agglomerates. *J. Colloid Interface Sci.* **306**, 262-273, (2007).

33 Drazin, P. G. & Reid, W. H. *Hydrodynamic stability*. 2nd edn, (Cambridge University Press, 2004).

34 Gollub, J. P. & Swinney, H. L. Onset of Turbulencein a Rotating Fluid. *Phys. Rev. Lett.* **35**, 927-930, (1975).

35 Lyklema, J. The surface tension of pure liquids - Thermodynamic components and corresponding states. *Colloids and Surfaces a-Physicochemical and Engineering Aspects* **156**, 413-421, (1999).

36 Tsierkezos, N. G. & Filippou, A. C. Thermodynamic investigation of N,N-dimethylformamide/toluene binary mixtures in the temperature range from 278.15 to 293.15 K. *J. Chem. Thermodyn.* **38**, 952-961, (2006).

37 Chen, X. J., Dobson, J. F. & Raston, C. L. Vortex fluidic exfoliation of graphite and boron nitride. *Chem. Commun. (Cambridge, U. K.)* **48**, 3703-3705, (2012).

38 Doran, P. M. *Bioprocess Engineering Principles*. (Academic Press, 1995).

39 Lee, C., Wei, X. D., Kysar, J. W. & Hone, J. Measurement of the elastic properties and intrinsic strength of monolayer graphene. *Science* **321**, 385-388, (2008).

40 Herron, C. R., Coleman, K. S., Edwards, R. S. & Mendis, B. G. Simple and scalable route for the 'bottom-up' synthesis of few-layer graphene platelets and thin films. *J. Mater. Chem.* **21**, 3378-3383, (2011).

41 Knieke, C. *et al*. Scalable production of graphene sheets by mechanical delamination. *Carbon* **48**, 3196-3204, (2010).

42 Viculis, L. M., Mack, J. J., Mayer, O. M., Hahn, H. T. & Kaner, R. B. Intercalation and exfoliation routes to graphite nanoplatelets. *J. Mater. Chem.* **15**, 974-978, (2005).

43 Liao, K.-H. *et al*. Aqueous Only Route toward Graphene from Graphite Oxide. *ACS Nano* **5**, 1253-1258, (2011).

44 Geng, X. *et al*. Interlayer catalytic exfoliation realizing scalable production of large-size pristine few-layer graphene. *Sci. Rep.* **3**, 1134, (2013).

45 Feng, H., Cheng, R., Zhao, X., Duan, X. & Li, J. A low-temperature method to produce highly reduced graphene oxide. *Nat Commun* **4**, 1539, (2013).

46 Lu, W. *et al*. High-yield, large-scale production of few-layer graphene flakes within seconds: using chlorosulfonic acid and H2O2 as exfoliating agents. *J. Mater. Chem.* **22**, 8775-8777, (2012).

DOI: 10.1038/NMAT3944

47 Wang, J., Manga, K. K., Bao, Q. & Loh, K. P. High-Yield Synthesis of Few-Layer Graphene Flakes through Electrochemical Expansion of Graphite in Propylene Carbonate Electrolyte. *J. Am. Chem. Soc.* **133**, 8888-8891, (2011).

48 Moon, I. K., Lee, J., Ruoff, R. S. & Lee, H. Reduced graphene oxide by chemical graphitization. *Nat Commun* **1**, 73, (2010).

49 Chiu, P. L. *et al*. Microwave- and Nitronium Ion-Enabled Rapid and Direct Production of Highly Conductive Low-Oxygen Graphene. *J. Am. Chem. Soc.* **134**, 5850-5856, (2012).

50 Lomeda, J. R., Doyle, C. D., Kosynkin, D. V., Hwang, W. F. & Tour, J. M. Diazonium Functionalization of Surfactant-Wrapped Chemically Converted Graphene Sheets. *J. Am. Chem. Soc.* **130**, 16201-16206, (2008).

51 Shin, H.-J. *et al*. Efficient Reduction of Graphite Oxide by Sodium Borohydride and Its Effect on Electrical Conductance. *Adv. Funct. Mater.* **19**, 1987-1992, (2009).

52 Chen, C. *et al*. Self-Assembled Free-Standing Graphite Oxide Membrane. *Adv. Mater. (Weinheim, Ger.)* **21**, 3007-3011, (2009).

53 Zhou, X. & Liu, Z. A scalable, solution-phase processing route to graphene oxide and graphene ultralarge sheets. *Chem. Commun. (Cambridge, U. K.)* **46**, 2611-2613, (2010).

54 Parviz, D. *et al*. Dispersions of Non-Covalently Functionalized Graphene with Minimal Stabilizer. *ACS Nano* **6**, 8857-8867, (2012).

55 Eun-Young, C., Won San, C., Young Boo, L. & Yong-Young, N. Production of graphene by exfoliation of graphite in a volatile organic solvent. *Nanotechnology* **22**, 365601, (2011).

56 Park, K. H. *et al*. Exfoliation of Non-Oxidized Graphene Flakes for Scalable Conductive Film. *Nano Lett.* **12**, 2871-2876, (2012).

57 Shang, N. G. *et al*. Controllable selective exfoliation of high-quality graphene nanosheets and nanodots by ionic liquid assisted grinding. *Chem. Commun. (Cambridge, U. K.)* **48**, 1877-1879, (2012).

58 Paredes, J. I., Villar-Rodil, S., Martínez-Alonso, A. & Tascón, J. M. D. Graphene Oxide Dispersions in Organic Solvents. *Langmuir* **24**, 10560-10564, (2008).

59 Oh, S. Y., Kim, S. H., Chi, Y. S. & Kang, T. J. Fabrication of oxide-free graphene suspension and transparent thin films using amide solvent and thermal treatment. *Appl. Surf. Sci.* **258**, 8837-8844, (2012).

60 Ghislandi, M., Tkalya, E., Schillinger, S., Koning, C. E. & de With, G. High performance graphene- and MWCNTs-based PS/PPO composites obtained via organic solvent dispersion. *Composites Science and Technology* **doi:j.compscitech.2013.03.006**, (2013).

61 Si, Y. & Samulski, E. T. Synthesis of Water Soluble Graphene. *Nano Lett.* **8**, 1679-1682, (2008).

62 Hasan, T. *et al*. Solution-phase exfoliation of graphite for ultrafast photonics. *Physica Status Solidi B-Basic Solid State Physics* **247**, 2953-2957, (2010).

63 Chabot, V., Kim, B., Sloper, B., Tzoganakis, C. & Yu, A. High yield production and purification of few layer graphene by Gum Arabic assisted physical sonication. *Sci. Rep.* **3**, 1378, (2013).

64 Kang, M. S., Kim, K. T., Lee, J. U. & Jo, W. H. Direct exfoliation of graphite using a non-ionic polymer surfactant for fabrication of transparent and conductive graphene films. *Journal of Materials Chemistry C* **1**, 1870-1875, (2013).

65 Dua, V. *et al*. All-Organic Vapor Sensor Using Inkjet-Printed Reduced Graphene Oxide. *Angewandte Chemie International Edition* **49**, 2154-2157, (2010).

66 Behabtu, N. *et al*. Spontaneous high-concentration dispersions and liquid crystals of graphene. *Nat Nano* **5**, 406-411, (2010).

67 Alzari, V. *et al*. In situ production of high filler content graphene-based polymer nanocomposites by reactive processing. *J. Mater. Chem.* **21**, 16544-16549, (2011).

68 Dimiev, A. M., Gizzatov, A., Wilson, L. J. & Tour, J. M. Stable aqueous colloidal solutions of intact surfactant-free graphene nanoribbons and related graphitic nanostructures. *Chem. Commun. (Cambridge, U. K.)* **49**, 2613-2615, (2013).

69 Nuvoli, D. *et al*. The production of concentrated dispersions of few-layer graphene by the direct exfoliation of graphite in organosilanes. *Nanoscale Research Letters* **7**, 674, (2012).

70 Yi, M., Shen, Z., Zhang, X. & Ma, S. Vessel diameter and liquid height dependent sonication-assisted production of few-layer graphene. *J. Mater. Sci.* **47**, 8234-8244, (2012).

71 Nuvoli, D. *et al*. High concentration few-layer graphene sheets obtained by liquid phase exfoliation of graphite in ionic liquid. *J. Mater. Chem.* **21**, 3428-3431, (2011).

72 Sanna, R. *et al*. Synthesis and characterization of graphene-containing thermoresponsive nanocomposite hydrogels of poly(N-vinylcaprolactam) prepared by frontal polymerization. *Journal of Polymer Science Part A: Polymer Chemistry* **50**, 4110-4118, (2012).

73 Shahil, K. M. F. & Balandin, A. A. Graphene–Multilayer Graphene Nanocomposites as Highly Efficient Thermal Interface Materials. *Nano Lett.* **12**, 861-867, (2012).

74 Hamilton, C. E., Lomeda, J. R., Sun, Z., Tour, J. M. & Barron, A. R. High-Yield Organic Dispersions of Unfunctionalized Graphene. *Nano Lett.* **9**, 3460-3462, (2009).

75 Su, C.-Y. *et al*. Electrical and Spectroscopic Characterizations of Ultra-Large Reduced Graphene Oxide Monolayers. *Chem. Mater.* **21**, 5674-5680, (2009).

76 De, S. *et al*. Flexible, Transparent, Conducting Films of Randomly Stacked Graphene from Surfactant-Stabilized, Oxide-Free Graphene Dispersions. *Small* **6**, 458-464, (2010).

DOI: 10.1038/NMAT3944

77 Scognamillo, S. *et al*. Synthesis and characterization of nanocomposites of thermoplastic polyurethane with both graphene and graphene nanoribbon fillers. *Polymer* **53**, 4019-4024, (2012).

78 Fu, W., Kiggans, J., Overbury, S. H., Schwartz, V. & Liang, C. Low-temperature exfoliation of multilayer-graphene material from FeCl3 and CH3NO2 co-intercalated graphite compound. *Chem. Commun. (Cambridge, U. K.)* **47**, 5265-5267, (2011).

79 Torrisi, F. *et al*. Inkjet-Printed Graphene Electronics. *ACS Nano* **6**, 2992-3006, (2012).

80 Buzaglo, M. *et al*. Critical parameters in exfoliating graphite into graphene. *Phys. Chem. Chem. Phys*. **15**, 4428-4435, (2013).

81 Seo, J.-W. T., Green, A. A., Antaris, A. L. & Hersam, M. C. High-Concentration Aqueous Dispersions of Graphene Using Nonionic, Biocompatible Block Copolymers. *The Journal of Physical Chemistry Letters* **2**, 1004-1008, (2011).

82 Korkut, S., Roy-Mayhew, J. D., Dabbs, D. M., Milius, D. L. & Aksay, I. A. High Surface Area Tapes Produced with Functionalized Graphene. *ACS Nano* **5**, 5214-5222, (2011).

83 Schniepp, H. C. *et al*. Functionalized Single Graphene Sheets Derived from Splitting Graphite Oxide. *The Journal of Physical Chemistry B* **110**, 8535-8539, (2006).

84 Shih, C.-J. *et al*. Bi- and trilayer graphene solutions. *Nat Nano* **6**, 439-445, (2011).

85 Wang, X. Q. *et al*. Direct exfoliation of natural graphite into micrometre size few layers graphene sheets using ionic liquids. *Chem. Commun. (Cambridge, U. K.)* **46**, 4487-4489, (2010).

86 Alzari, V. *et al*. Graphene-containing thermoresponsive nanocomposite hydrogels of poly(N-isopropylacrylamide) prepared by frontal polymerization. *J. Mater. Chem*. **21**, 8727-8733, (2011).

87 Park, S. *et al*. Colloidal Suspensions of Highly Reduced Graphene Oxide in a Wide Variety of Organic Solvents. *Nano Lett*. **9**, 1593-1597, (2009).

88 Zhao, W. *et al*. Preparation of graphene by exfoliation of graphite using wet ball milling. *J. Mater. Chem*. **20**, 5817-5819, (2010).

89 Min, Y., Zhigang, S., Xiaojing, Z. & Shulin, M. Achieving concentrated graphene dispersions in water/acetone mixtures by the strategy of tailoring Hansen solubility parameters. *J. Phys. D: Appl. Phys*. **46**, 025301, (2013).

90 Qi, X. *et al*. Amphiphilic Graphene Composites. *Angewandte Chemie International Edition* **49**, 9426-9429, (2010).

91 Niyogi, S. *et al*. Solution Properties of Graphite and Graphene. *J. Am. Chem. Soc*. **128**, 7720-7721, (2006).

92 Catheline, A. *et al*. Graphene solutions. *Chem. Commun. (Cambridge, U. K.)* **47**, 5470-5472, (2011).

93 Vadukumpully, S., Paul, J. & Valiyaveettil, S. Cationic surfactant mediated exfoliation of graphite into graphene flakes. *Carbon* **47**, 3288-3294, (2009).

94 Khan, U. *et al*. Solvent-Exfoliated Graphene at Extremely High Concentration. *Langmuir* **27**, 9077-9082, (2011).

95 Wang, H., Robinson, J. T., Li, X. & Dai, H. Solvothermal Reduction of Chemically Exfoliated Graphene Sheets. *J. Am. Chem. Soc.* **131**, 9910-9911, (2009).

96 Marago, O. M. *et al*. Brownian Motion of Graphene. *ACS Nano* **4**, 7515-7523, (2010).

97 Li, X. L., Wang, X. R., Zhang, L., Lee, S. W. & Dai, H. J. Chemically derived, ultrasmooth graphene nanoribbon semiconductors. *Science* **319**, 1229-1232, (2008).

98 Stankovich, S. *et al*. Synthesis of graphene-based nanosheets via chemical reduction of exfoliated graphite oxide. *Carbon* **45**, 1558-1565, (2007).

99 Valles, C. *et al*. Solutions of Negatively Charged Graphene Sheets and Ribbons. *J. Am. Chem. Soc.* **130**, 15802-+, (2008).

100 Ang, P. K., Wang, S., Bao, Q. L., Thong, J. T. L. & Loh, K. P. High-Throughput Synthesis of Graphene by Intercalation - Exfoliation of Graphite Oxide and Study of Ionic Screening in Graphene Transistor. *ACS Nano* **3**, 3587-3594, (2009).

101 Englert, J. M. *et al*. Soluble Graphene: Generation of Aqueous Graphene Solutions Aided by a Perylenebisimide-Based Bolaamphiphile. *Adv. Mater. (Weinheim, Ger.)* **21**, 4265-4269, (2009).

102 Mattevi, C. *et al*. Evolution of Electrical, Chemical, and Structural Properties of Transparent and Conducting Chemically Derived Graphene Thin Films. *Adv. Funct. Mater.* **19**, 2577-2583, (2009).

103 Gómez-Navarro, C. *et al*. Electronic Transport Properties of Individual Chemically Reduced Graphene Oxide Sheets. *Nano Lett.* **7**, 3499-3503, (2007).

104 Safavi, A., Tohidi, M., Mahyari, F. A. & Shahbaazi, H. One-pot synthesis of large scale graphene nanosheets from graphite-liquid crystal composite via thermal treatment. *J. Mater. Chem.* **22**, 3825-3831, (2012).

105 Anand, K. A., Agarwal, U. S. & Joseph, R. Carbon nanotubes-reinforced PET nanocomposite by melt-compounding. *J. Appl. Polym. Sci.* **104**, 3090-3095, (2007).

106 Nanni, F., Mayoral, B. L., Madau, F., Montesperelli, G. & McNally, T. Effect of MWCNT alignment on mechanical and self-monitoring properties of extruded PET–MWCNT nanocomposites. *Composites Science and Technology* **72**, 1140-1146, (2012).

107 Sanchez-Solis, A., Garcia-Rejon, A. & Manero, O. Production of nanocomposites of PET-montmorillonite clay by an extrusion process. *Macromol. Symp.* **192**, 281-292, (2003).

DOI: 10.1038/NMAT3944

108 Mun, M. K., Kim, J.-C. & Chang, J.-H. Preparation of poly(ethylene terephthalate) nanocomposite fibers incorporating a thermally stable organoclay. *Polym. Bull. (Berlin)* **57**, 797-804, (2006).

109 Wang, Y., Gao, J., Ma, Y. & Agarwal, U. S. Study on mechanical properties, thermal stability and crystallization behavior of PET/MMT nanocomposites. *Composites Part B: Engineering* **37**, 399-407, (2006).

110 Todorov, L. V. & Viana, J. C. Characterization of PET nanocomposites produced by different melt-based production methods. *J. Appl. Polym. Sci.* **106**, 1659-1669, (2007).

111 Chen, L., Liu, K., Jin, T. X., Chen, F. & Fu, Q. Rod like attapulgite/poly(ethylene terephthalate) nanocomposites with chemical bonding between the polymer chain and the filler. *Express Polymer Letters* **6**, 629-638, (2012).

112 Zeng, J., Kumar, S., Iyer, S., Schiraldi, D. A. & Gonzalez, R. I. Reinforcement of poly(ethylene terephthalate) fibers with polyhedral oligomeric silsesquioxanes (POSS). *High Perform. Polym.* **17**, 403-424, (2005).

113 Nadkarni, V. M. & Ayodhya, S. R. The influence of knit-lines on the tensile properties of fiberglass reinforced thermoplastics. *Polym. Eng. Sci.* **33**, 358-367, (1993).

114 Fung, K. L. & Li, R. K. Y. Mechanical properties of short glass fibre reinforced and functionalized rubber-toughened PET blends. *Polym. Test.* **25**, 923-931, (2006).

115 Abu-Isa, I. A., Jaynes, C. B. & Ogara, J. F. High-impact-strength poly(ethylene terephthalate) (PET) from virgin and recycled resins. *J. Appl. Polym. Sci.* **59**, 1957-1971, (1996).

116 Ashby, M. F. *et al*. *Engineering Materials and Processes Desk Reference*. 273 (Elsevier Science, 2009).

117 International, A. *Characterization and Failure Analysis of Plastics*. 20 (A S M International, 2003).

118 Li, N. *et al*. Preparation and properties of poly(ethylene terephthalate)/inorganic whiskers composites. *J. Appl. Polym. Sci.* **121**, 604-611, (2011).

119 Miller, J. R., Outlaw, R. A. & Holloway, B. C. Graphene Double-Layer Capacitor with ac Line-Filtering Performance. *Science* **329**, 1637-1639, (2010).

120 Lin, J. *et al*. 3-dimensional graphene carbon nanotube carpet-based microsupercapacitors with high electrochemical performance. *Nano Lett.* **13**, 72-78, (2013).

121 Sheng, K. X., Sun, Y. Q., Li, C., Yuan, W. J. & Shi, G. Q. Ultrahigh-rate supercapacitors based on eletrochemically reduced graphene oxide for ac line-filtering. *Scientific Reports* **2**, (2012).